Raman Spectroscopy Applied to Iron Oxide Pigments from Waste Materials and Earthenware Archaeological Objects

by

Malebogo Andries Legodi

Submitted in partial fulfillment of the degree

PHILOSOPHIAE DOCTOR

in

CHEMISTRY

in the faculty of Natural and Agricultural Sciences of the

UNIVERSITY OF PRETORIA
PRETORIA

Promoter: Prof. D. de Waal

2008

Declaration of oath

I, Malebogo Andries Legodi, the author of the present thesis entitled “Raman Spectroscopy Applied to Iron Oxides from Waste Materials and Earthenware Archaeological Objects” declare that the thesis contains only original work and that all the results included were generated by the author.

Signature:…… **Date:……**

Acknowledgements

The author wishes to express sincere gratitude to the following:

- Almighty GOD for giving me the capability, health and strength to complete the work
- Prof. D. de Waal (promoter) for her assistance, supervision and informed guidance. Thank you, also, for creating a conducive studying environment for me
- Annette Weitz and Monica van der Merwe for providing African clay pottery shards
- Prof. J. C. A. Boeyens for guidance and advice
- To the present and past research group members for the valuable discussions and advice
- Friends inside and outside the Department of Chemistry at UP for their invaluable advice and support
- My loving wife for her patience, encouragement and moral support
- NRF, Rolfes Pigments and University of Pretoria for the financial support

Summary

Raman spectroscopy is a vibrational spectroscopic technique. It gives a unique combination of non-destructive analysis, high spatial resolution and phase characterisation. In the current study Raman spectroscopy was used as the primary technique during the study of chemical components in archaeological earthenware samples (i.e. low temperature fired clay pottery) of South African and Chinese origin, and characterisation of iron oxides derived from mill scale.

One shard from each of the South African archaeological sites (Rooiwal, Lydenburg, Makahane and Graskop) was analysed by Raman spectroscopy, FT-IR spectroscopy, X-ray fluorescence (XRF) spectroscopy and X-ray diffractometry (XRD). The common features observed were montmorillonite ($Mg_3(Si,Al)_4(OH)_2.4.5H_2O[Mg]_{0.35}$), kaolin ($Al_2Si_2O_5(OH)_5$), quartz ($\alpha$-$SiO_2$), feldspar (K- and $NaAlSi_3O_8$), hematite (α-Fe_2O_3), calcium silicate ($CaSiO_3$) and illite ($KAl_4(Si_7AlO_{20})(OH)_4$). Gypsum ($CaSO_4.2H_2O$) and calcium carbonates ($CaCO_3$) were detected in Lydenburg, Makahane and Graskop shards. Amorphous carbon was observed in Lydenburg and Makahane shards while rutile appeared only in Makahane shard. The Lydenburg and Rooiwal shards showed the presence of anhydrite ($CaSO_4$).

The Chinese clay samples investigated by Raman spectroscopy were from the J A Van Tilburg museum at the University of Pretoria. The large red shard was recovered from the 1552 Portuguese shipwreck, São João, found around Port Edward, South Africa. Four other shards (two red and two gray) were recovered from the 1622 Portuguese shipwreck, the São João Baptista, found around Kenton-on-Sea off the South African coast. A 19th century Chinese teapot was also analysed. Hematite, kaolin, quartz, amorphous carbon and aluminosilicates were observed in all three red shards. All these components, except quartz, were also observed in the teapot. The gray shards showed the presence of quartz, kaolin, amorphous carbon and aluminosilicates. The pigments identified were hematite (in red samples) and black amorphous carbon (in all samples).

Magnetite and goethite were precipitated from mill scale-derived precursors in aqueous media. Hematite was then prepared from the calcination of goethite at 750 ^{o}C and maghemite from the thermal treatment of magnetite at 200 ^{o}C. The iron oxides were characterised by Raman spectroscopy, XRD, surface area determination and scanning electron microscopy (SEM). They were generally composed of very small sized particles showing high surface area values.

Samevatting

Raman spekroskopie is ‘n vibrasie spektroskopiese tegniek. Dit gee ‘n unieke kombinasie van nievernietigende analise, hoë ruimtelike resolusie en fase karakterisering. In die huidige studie was Raman spektroskopie gebruik as die primêre tegniek vir die bestudering van chemiese komponente van argeologiese erdewerk monsters (m.a.w. lae temperatuur gevuurde erdewerk) van Suid-Afrikaanse en Chinese afkoms, en karakterisering van ysteroksiedes verkry van meulskaal.

Een skerf van elk van die Suid-Afrikaanse argeologiese terreine (Rooiwal, Lydenburg, Makahane en Graskop) was geanaliseer met Raman, X-straal fluoressensie (XRF), X-straal diffraksie (XRD) en FT-IR spektroskopie. Die algemeenste kenmerke was illite ($KaI_4(Si_7AlO_{20})(OH)_4$), kaolien ($Al_2Si_2O_5(OH)_5$), kwarts ($\alpha$-$SiO_2$), veldspaat (K- en $NaAlSi_3O_8$), hematiet (α-Fe_2O_3), montmorilloniet $Mg_3(Si,Al)_4(OH)_2{\cdot}4.5H_2O[Mg]_{0.35}$), en kalsiumsilikaat ($CaSiO_3$). Gips ($CaSO_4{\cdot}2H_2O$) en kalsiumkarbonaat ($CaCO_3$) was waargeneem in die Lydenburg, Makahane en Graskop skerwe. Amorfe koolstof was waargeneem in die Lydenburg en Makahane skerwe, terwyl rutiel verskyn net in Makahane skerf. Die teenwoordigheid van anhidriet ($CaSO_4$) was ook waargeneem vir die Lydenburg en Rooiwal skerwe.

Die Chinese klei monsters wat vir Raman spektroskopie ondersoek gebruik was, was afkomstig uit die J A Van Tilburg museum van die Universiteit van Pretoria. Die groot rooi skerf was herwin van die São João, ‘n 1552 Portugese skeepswrak, gevind naby Port Edward, Suid-Afrika. Vier ander skerwe (twee rooi en twee grys) was herwin van die São João Baptista, ‘n Portugese wrak van 1622, gevind naby Kenton-on-sea, Suid-Afrika. ‘n 19de eeuse Chinese teepot was ook geanaliseer. Hematiet, kaolien, kwarts, amorfe koolstof en aluminosilikate was waargeneem in die teepot klei. Die grys skerwe het die teenwoordigheid van kwarts, kaolien, amorfe koolstof en aluminosilikate aangedui. Die pigmente wat geïdentifiseer is, was hematiet (in rooi monsters) en swart amorfe koolstof (in alle monsters).

Magnetiet en goethiet was gepresipiteer van meulskaal afkomstige voorgangers in waterige media. Hematiet was volgende voorberei deur goethiet te kalsineer by 750 ºC. Maghemiet was voorberei deur die termiese behandeling van magnetiet by 200 ºC. Al die ysteroksiedes was gekarakteriseer deur Raman spektroskopie, XRD, oppervlakte area bepalings en

aftaselektronmikroskopie (SEM). Die monsters was in die algemeen saamgestel uit baie klein partikels wat aanduidend is van hoë oppervlakte area waardes.

Table of contents

Chapter 1

Overall introduction

1.1. Background

There is continual interest in the development of new techniques and optimisation of existing ones for the non-destructive analysis of chemical components. The techniques are expected to give unambiguous information on all chemical components and if possible, their relative amounts. Such techniques as described above could find application in the study of archaeological earthenware objects and iron oxides, among other studies in chemistry.

1.2. Rationale for the study

1.2.1. Earthenware objects

The earthenware objects (referred to here as low temperature fired clay pottery) are often African domestic accessories and artefacts. These are the types of pottery that were produced below temperatures required for the melting and fusion of the raw aluminosilicates (e.g. clays, feldspar and quartz) into a glassy material in a process called vitrification. Vitrification is an integral part of Chinese ceramics production.

The low temperature fired red-brown and black pottery is common to Africa. The pottery shards have a coarse texture with open sponge-like internal structures and are visibly heterogeneous. This is contrary to the Asian ceramics, which are often white in colour, smooth textured and homogeneous. The Chinese potters are known for processing the clay minerals before pottery making, e.g. to reduce the iron oxide level. The Asian potters fire their clay wares at temperatures well in excess of 1100 ^{o}C [1]. The African pottery is not fired at high enough temperatures that are required for vitrification of the silicium and flux present in the clay [2]. No pre-treatment of clay minerals by African potters has been reported, but minerals were used as acquired [3]. Clay pots were used in cooking and in ritual context. In a settled culture, pottery became increasingly important for long-term storage of food and

liquids [4a]. The black coloured pottery without decorations was normally for daily use, e.g. cooking [2]. The decoration on pots can be ritualistic, cultural and reminders of etiquette of gender interactions [4b]. The brightly coloured (red and black) and most decorated pottery was used for storage and serving of food and drinks [2].

1.2.1.1. The standard procedure for making African clay pottery

The knowledge and understanding of raw materials, additives, processing of clay, decorating procedure, fuel and firing conditions used in pottery making aid in the full characterisation of components observed in the clay pots.

The quarried clay (either from riverbanks or the foot of a mountain) was initially broken into small pieces by hand. It was then powdered with wooden sticks as water was added in small portions to achieve a satisfactory level of working plasticity. Vessels were formed by a combined technique of modelling and coiling. The body, neck and shoulder were finished, complete with decoration, before the base was begun. Therefore, the making of clay vessels is a two-stage process [2]. Once the surface of the vessel was smoothed by hand and water, the pot was left to dry until firm but still workable. The surfaces of most pots were burnished with a smooth rounded river pebble until lustrous to varying degrees.

Some vessels were polished with fine graphite powder and further decorated and coloured with red ochre. Pots were left to dry for several days (~3). Firing occurred in oxidising atmospheres in either an open bonfire or shallow pit. Fuel used included cattle dung, tree bark and wood fuel stacked around the pot. The firing process was complete in about 40 minutes. After cooling, the exterior surfaces of the vessels were orange-red in colour, sometimes with dark gray or black patches. The dark gray or black colours are due to insufficient oxidation [2].

1.2.1.2. The significance of chemical phases that constitute museum clay artefacts

The information on chemical phase composition of valuable objects is even more relevant to the keepers and curators of clay items and artworks (e.g. of museum and private objects), because the origin, history, properties and full description of objects are closely linked to the chemical compositions.

Museums are the repositories of history, heritage, technology, culture, etc. Therefore, full characterisation of museum objects is essential to facilitate conservation, reconstruction, dating, discrimination and authentication, but the objects cannot be destroyed in the process. Objects of historical importance need to be preserved for the coming generations. Acceptable methods of preservation require full knowledge of the constituents of the preserved object. Reconstruction work is an integral part of every museum with clay products. For reconstruction of pottery the knowledge of the following is essential: raw materials (e.g. different types of clays), firing temperature, atmosphere of processing (i.e. oxidative or reductive atmosphere), special material applied to give the clay product unique properties and function of the product. For the museum record all objects are normally recorded with full description of shape, origin, size, markings, colours and decorations. The chemical compositions could provide an alternative and more reliable way of recording and characterising museum artefacts. Authentication is essential for discrimination between the genuine artefacts and imitations.

Most literature studies on earthenware objects (low temperature fired clay pottery) were of archaeological nature and concerned with the determination of various chemical species and their corresponding amounts. For instance, in provenance studies the assumption is often made that a link exists between the raw materials and the final clay products. The link is based on specific chemical species and their corresponding amounts. The results on chemical species obtained from the clay products are then compared with those obtained from the raw materials in the same area where the objects were found. The techniques often

used include neutron activation analysis (NAA), proton induced X-ray excitation (PIXE), petrography, infrared reflectance, X-ray fluorescence (XRF), etc [5, 6]. These techniques are used in conjunction with statistical clustering methods for grouping based on the amounts of chemical species. The results obtained are then used to define different groups of pottery, to identify foreign objects and to further retrace interactions and trade relations between different ancient communities. The techniques previously used to analyse these types of clay products are either destructive and/or give only elemental results. The valuable objects and those kept in museums cannot be analysed using the above techniques. Therefore, there is a need for a non-destructive technique that will give information on the chemical composition.

1.2.2. Iron oxides

The iron oxides are the largest sector of the inorganic pigment industry (including paint, ink, construction materials, etc), which are produced both chemically and from natural sources [7]. Pigments are fine powders used for colouring media and other powdery materials, e.g. metallic powders showing magnetic or anticorrosive properties that are intentionally dispersed (not dissolved) into media to increase value and to impart some special properties [8a]. The proportion of iron oxides as pigments will continue to rise as the construction activities increase and new markets are found as concern grows over the use of heavy metal pigments. The continually increasing importance of iron oxides is also based on their non-toxicity, chemical stability, durability, wide variety of colours and low costs. Therefore new and simple cost-effective methods for the preparation of iron oxides are required in order to meet the demands. With the development of new and cost-effective methods (including methods that use cheaper raw materials) arises the need for specific and sensitive techniques to maintain the required standard and quality levels.

As an additional work to the present study some of the pure iron oxides (namely, magnetite (Fe_3O_4, black), hematite (α-Fe_2O_3, red), maghemite (γ-Fe_2O_3, brown), goethite (α-FeOOH, yellow), and ferroxyhite (δ-FeOOH, dark brown)) were prepared and characterised (by Raman spectroscopy and X-ray diffraction) for use as standards during a separate study

involving the *in situ* micro-Raman spectroscopic analysis of the composition of passivation film on iron metal [9].

1.2.2.1. Theoretical background on inorganic pigments

The value of pigments results from their physical-optical properties. These are primarily determined by the pigment physical characteristics (crystal structure, particle size and distribution, particle shape, agglomeration, etc) and chemical properties (chemical composition, purity, stability, etc).

The two most important physical-optical assets of pigments are the ability to colour the environment in which they are dispersed and to make it opaque. Opacity of pigments prevents transmission of light and obscures the subject on which it is applied. The opacity of the pigment is a function of the pigment particle size and the difference between the pigment refractive index and that of the medium in which pigment particles are dispersed [8b]. Any agglomeration of pigment particles can affect their opacity. At a certain pigment loading/thickness the substrate becomes completely hidden and the pigment determines its colour [8b].

The most commonly measured pigment properties are elemental analysis, impurity content, crystal structure, particle size and distribution, shape, density and surface area. These parameters are measured so that pigment producers can better control production and set up meaningful physical and chemical pigment specifications.

The measured pigment colouristic properties include, colour, colour strength, opacity, lightfastness, weathering, heat stability, chemical stability and rheological properties [8b] and many of them are determined also by the dispersing media and processing conditions. The particle size and distributions affect the colour, colour strength, hiding power (the ability of a coating to hide the substrate [8c]) and rheological properties (related to the deformation and flow of dispersed pigment under the influence of applied stress) [10]. For inorganic pigments to be useful in most applications, they must have an average particle size between 0.1 and

10 µm [8d]. However, for smaller particles the granulating agents are added for intentional agglomeration (to form granules) in order to prevent powder dusting and make handling easier.

The surface area and porosity of the pigment affect its oil absorption ability, such that the higher the surface area the greater the oil absorption [8d].

Different shades are controlled primarily by the oxide particle size, shape and surface properties [8e]. If the surface area value is higher than expected (e.g. higher than that of literature and commercial product) then the particle surfaces are porous [11]. Uniformity of particle shape is essential, if quality hiding power is to be achieved [12]. Hiding power of a uniform coating is expressed as the area of substrate that can be hidden by unit volume of coating (m^2/L). It is expressed through the Lorentz-Lorenz equation:

$$HP = 0.16\ (n_p - n_m)^2$$

where n_p and n_m are the refractive indices of the pigment and medium, respectively [8c]. The ability of a pigment to change the colour of an opaque film is known as its tinting strength. Tinting strength is related to particle size, such that the increase in particle size results in decreases in tinting strength. The darker and more saturated colours yield deeper tints [13]. Elemental analysis, impurity content and stoichiometry are determined by chemical or instrumental analysis. Chemical analysis of principal components is carried out to determine pigment stoichiometry. The presence of undesirable elements, such as heavy metals, even in small amounts can make the pigment unusable for environmental reasons. A single-compound pigment can exist in several crystal structures not all of which have equal colouristic properties. A good pigment contains a colourant as a principal phase. Secondary phases determined by X-ray diffractometry might be present only to reduce colouristic properties [8c].

Many pigments can get darker, change their shade or lose colour saturation when exposed to high intensity light such as direct sunlight or UV lamp. Inorganic pigments, particularly

those containing ions that exist in several oxidation states, e.g. Fe, Pb, etc, usually get darker [8c]. Some colour changes can be reversible, while others are permanent. Lightfastness is measured by exposing pigment film to an artificial or natural light for a predetermined time [8f].

Weathering is the ability of the coloured system, i.e. coating, paint, etc, not the pigment alone, to resist light and environmental conditions. Colour and gloss changes are the main factors evaluated in weathering tests [8f].

Heat stability is expressed as the maximum temperature at which the colour of the system does not change. Chemical resistance can be determined by measuring colour changes of pigmented binder surfaces after exposure to various chemicals such as water-sulphur dioxide or water-sodium chloride systems [8f]. These systems imitate the environment to which the coloured articles could become exposed.

For more details on inorganic pigments, see reference [8].

1.2.2.2. Synthesis of iron oxides

In developing new methods (including the use of alternative starting materials) for the preparation of the desired products, a full investigation is often required in order to understand the processes taking place. The common aim of such an investigation is the determination of the reaction mechanism. The most important step in the investigation of the reaction mechanism involves the identification of as many reaction products as possible (irrespective of their amounts). The understanding of the reaction mechanism allows one to modify, control and optimise the process. The characterisation technique should be specific and sensitive enough to detect as many components present as possible.

Natural and synthetic iron oxides consist of well-defined compounds with known crystal structures [14, 15]. Chemically, these are oxides and oxyhydroxide compounds of iron. There are seven polymorphs of iron oxides with varying properties, namely, magnetite

(Fe_3O_4, black), hematite (α-Fe_2O_3, red), maghemite (γ-Fe_2O_3, brown), goethite (α-FeOOH, yellow), akaganeite (β-FeOOH, brown), lepidocrocite (γ-FeOOH, light brown) and ferroxyhite (δ-FeOOH, dark brown) [16, 17, 18]. Iron oxides are important compounds for pigments, catalysis, magnetic devices, adsorbents, batteries and corrosion of iron and steel [19, 20, 21].

The iron oxides can be prepared by either thermal treatment and/or precipitation from aqueous media. Hematite is the only thermally stable polymorph prepared by oxidative thermal treatment of iron salts [22, 23]. Magnetite is one of the most thermally unstable iron oxides. It turns first into maghemite around 200 ^{o}C, and then to hematite around 400 ^{o}C [24]. Therefore, hematite is a common contaminant of any iron oxide polymorph prepared under heat.

All the iron oxides can be prepared by precipitation methods. The precipitation of one iron oxide is often preceded by the formation of another, e.g. the hematite particles are formed from the akaganeite particles via dissolution/reprecipitation [25]. Depending on the reaction conditions several compounds may be formed as the final products, thus influencing the purity and properties of the desired products. The chemical phase composition and properties of the precipitate depend on the type of starting material, e.g. hydrolysis of $FeCl_3$ results in the formation of akaganeite and hematite only [16]. The presence of organic molecules (e.g. citrates), inorganic ions (e.g. phosphate, sulphate) or transition metal ions (e.g. Zn^{2+}, Cu^{2+}) in the precipitation medium influences the reaction mechanism and properties (e.g., colour, particle shapes and sizes) of the products [26, 27, 28].

The use of iron wastes as the starting material in the preparation of iron oxides has previously rendered the processes cost-effective [22, 23, 29]. However, the waste materials often contain the active substance together with some other undesired substances.

It is clear from the above information that the preparation of iron oxides either from pure starting materials or waste materials is often accompanied by contamination (including other iron oxide phases). The presence of undesired compounds may alter the phase of the

product and influence the reaction conditions (e.g. pH), mechanism and the properties of the desired product. The properties of iron oxides that are often influenced include the colour, crystallinity, particle characteristics, etc. These properties determine the use of iron oxides. Therefore, the preparation of iron oxides should be accompanied by the use of an analytical technique that could identify as many possible contaminants as possible, even in their amorphous form.

1.2.3. Raman spectroscopy

The literature shows that Raman spectroscopy has been studied extensively and applied widely. The unique properties of this technique involve non-destructive nature, no sample preparation, reliability, specificity and sensitivity [30, 31]. It is also amenable to *in situ* analysis [17, 32, 33]. Raman spectroscopy has been found to be particularly sensitive to coloured molecules [34]. This technique is most effective in structural characterisation, identification and detection [34]. Therefore, Raman spectroscopy can distinguish between structural forms of the same compounds, even in their amorphous form.

From the comparison of the properties of Raman spectroscopy (as given above) and those required by the types of samples under investigation, Raman spectroscopy appears to be the potential analytical technique required for the analysis of both low temperature fired clay pottery and iron oxides.

1.3. Aims and objectives

The chemical phase study of valuable clay products (e.g. ancient ceramic pottery) and iron oxides requires the application of a technique, which is amenable to *in situ* analysis, non-destructive, sensitive, specific and gives chemical phase results.

Raman spectroscopy seems to be an appropriate technique for the types of samples mentioned above (clay products and iron oxides). This technique can detect crystalline and amorphous chemical phases and can be connected to a microscope thus making it possible

to detect phases in micrometre scale while reducing fluorescence. It has been found to be sensitive and specific. It is also amenable to *in situ* and non-destructive analysis. The measurement times could be short.

The overall aims and objectives of the current study are to demonstrate the effectiveness of dispersive Raman spectroscopy as applied to the chemical phase determination of clay products and iron oxides. These have been previously difficult to analyse by this and other techniques. Two main studies were chosen for this purpose: a) the determination of the chemical composition of low temperature fired clay pottery (earthenware) and b) the evaluation of synthetic iron oxides.

1.4. Outline of the remaining chapters

The current study is divided into two major sections: a) the analysis of the low temperature fired clay pottery shards, and b) the preparation of iron oxides from mill scale iron waste.

Chapter 2 contains a literature review of the two major sections included in this study. This chapter outlines the developments and prospects in each section.

In Chapter 3 Raman spectroscopic theory and instrumentation are presented. Since this technique is applied in all the subsequent sections of the current study, it is appropriate that it be presented and described fully at this early stage. The theory of Raman spectroscopy, description of the different components and their uses and the operational parameters are outlined.

The main purpose of Chapter 4 was to determine the chemical components that constitute low temperature fired clay pottery using Raman spectroscopy. In this section a selected number of clay pottery shards from different locations in South Africa were analysed by Raman spectroscopy. The results were then compared with and complemented by those obtained when the same samples were analysed by X-ray diffractometry (XRD), FT-IR spectroscopy and X-ray fluorescence (XRF).

In Chapter 5 the results obtained when the chemical components in the low temperature clay pottery shards and clay pot of Chinese origin were analysed non-destructively using Raman spectroscopy are discussed.

The results obtained when iron waste materials were used in the preparation of various iron oxides are presented in Chapter 6. In this study magnetite, goethite, maghemite and hematite for pigment purposes were prepared from mill scale (iron waste). Magnetite and goethite were prepared directly from mill scale. Maghemite and hematite were then derived from thermal treatment of magnetite and goethite, respectively. The primary characterisation technique was Raman spectroscopy, while complementary techniques involved X-ray diffractometry (XRD), scanning electron microscopy (SEM) and surface area determinations.

The overall conclusions of the current study are then presented in Chapter 7. Finally, the Appendix section outlines the status of the core chapters (chapters 4 – 6) in the international peer review journals.

1.5. References

1. N. Palmgren, W. S. Steger and N. Sindius, Sung sherds, Almovist & Wilksell, Stockholm, a: p. 100; b: p. 387; c: p. 385. (1963).
2. A. Lindahl and E. Matenga, *Present and past ceramics and homesteads.* In: Ethnoarchaelogical project in the Buher district, Zimbabwe. Uppsala University Press, Uppsala, p. 11 (1995).
3. D. D. Rosenstein, *Ceramic production as a reflection of technological and social complexity in the late iron age of South Africa. An ethnographic and petrographic study*. Thesis, George Washington University Press, Washington DC, p. 17 (2002).

4. S. Hall, *A consideration of gender relations in the late iron age. Sotho sequence of the western highveld, South Africa*. In: Gender in African history ed. By Suzan Kent, Altamira Press, Walnut Creek, CA; a: p. 3; b: pp. 235 – 258 (1998).
5. J. Poblome, P. Degryse, W. Viaene, R. Ottenburgs, M. Waelkans, R. Degeest and J. Noud, J. Archaeol. Sci. **29**, 873 (2002).
6. C. A. Bollang, J. C. Vogel, L. Jacobson, W. A. van der Westhuizen and C. G. Sampson, J. Archaeol. Sci. **20**, 41 (1983).
7. G. Buxbaum, Industrial Inorganic Pigments, VCH Publishers, New York and Weinheim, p. 86 (1993).
8. J. A. Kroschwitz and M. Howegrant, *Pigments to powders handling.* In: Encyclopedia of chemical technology, John Wiley & sons, New York, Vol. 19, 4th ed., a: pp. 1 - 3; b: p. 24; c: p. 26; d: p. 25; e: p. 23; f: p. 8 (1996).
9 . M. K. Nieuwoudt, J. D. Comins, I. Cukrowski, D. de Waal and M. Legodi, Proc. 2nd Int. Conf. African Mater. Res. Soc., eds. Y. Ballim, A.G. Every, S. Luyckx and D. C. Levendis, Wits University Press, Johannesburg, pp. 57 – 58 (2003).
10. P. P. Hsu and Matijeć, Appl. Opt. **24**, 1623 (1985).
11. S. J. Gregg and K. S. W. Sing, Adsorption surface area and porosity, Academic Press, London, p. 49 (1967).
12. G. P. A. Turner, Introduction to paint chemistry and principles of paint technology, 2nd Edn. Chapman and Hall, London, pp. 95-107 (1980).
13. H. G. Völz, Prog. Org. Coat. **15**, 99 (1987).
14. I. Watson, Ind. Miner. **143**, 43 (1979).
15. U. Schwertmann and R. M. Cornell, *Preparation and characterization*. In: Iron oxides in the laboratory; VCH Verlagsgesellschaft, Weinheim, (1991) and ref. therein.
16. A. Šaric, S. Music, K. Nomura and S. Popovic, Croat. Chem. Acta **71**, 1019 (1998).
17. N. Boucherit, A. Hugot-Le Goff and S. Joiret, Corros. Sci. **32**, 497 (1991).
18. G. Nauer, P. Stretcha, N. Brinda-Konopik and G. Liptay, J. Thermal Anal. **30**, 183 (1985).
19. K. M. Parida and J. Das, J. Mater. Sci. **31**, 2199 (1996).

20. A. A. Kamner, B. B. Ezhov, N. S. Kopeler, Y. M. Kisselev and Y. D. Perfilyer, Electrochim. Acta, **36**, 1253 (1991).
21. T. Misawa, T. Kyuno, W. Suëtaka and S. Shimodaira, Corros. Sci. **11**, 35 (1971).
22. H. M. Ismail, N. E. Fouad, M. I. Zaki and M. N. Magar, Powder Technol. **70**, 183 (1992).
23. N. E. Fouad, H. M. Ismail and M. I. Zaki, J. Mater. Sci. Lett. **7**, 27 (1998).
24. Y. Goto, Jpn. J. Appl. Phys. **3**, 741 (1964).
25. J. K. Bailey and M. L. Mecartney, Colloid Surf. **63**, 151 (1992).
26. G. W. Bruemmer, J. Gerth and K. G. Tiller, J. Soil Sci. **39**, 37 (1988).
27. K. J. Farley, D. A. Dzombak and F. M. M. Morel, J. Colloid and Interf. Sci. **106**, 226 (1985).
28. C. C. Ainsworth, J. L. Pilon, P. L. Gassman and W. G. van der Sluys, Soil Sci. Soc. Amer. **58,** 1615 (1994).
29. B. T. Ousnam and D. Erasmus, US Patent 5,738,717 (1998) (to Corveagh Ltd)
30. N. Q. Liem, G. Sagon, V. X. Quang, H. van Tan and P. Colomban, J. Raman Spectrosc. **31**, 933 (2000).
31. P. Colomban and F. Treppoz, J. Raman Spectrosc. **32**, 93 (2001).
32. R. J. Thibeau, C. W. Brown and R. H. Heidersbach, Appl. Spectrosc. **32**, 523 (1978).
33. D. L. A. de Faria, S. V. Silva and M. T. de Oliviera, J. Raman Spectrosc. **28**, 873 (1997).
34. G. Dent, *Vibrational spectroscopy of colors, dyes and pigments.* In: Handbook of vibrational spectroscopy, eds. J. M. Chalmers and P. R. Griffiths, John Wiley & Sons Inc., Chichester, Vol. 4, pp. 2911 – 2912 (2002).

Chapter 2

Literature review

The literature presented in this section involves the studies related to the chemical components of clay products (including earthenware objects) and preparation of a selected number of iron oxides

2.1. Clay products

The literature covered in this section highlights the studies done on characterisation and investigation of thermal decomposition of clay minerals and related compounds often present in clay products. Furthermore, the clay compounds and some inorganic minerals (essential to the chemical characterisation of clay pottery) analysed by Raman spectroscopy are outlined.

2.1.1. Origin of clays

Clays are secondary minerals formed by weathering or hydrothermal alteration of rocks [1]. They are often found in rocks undergoing alterations. Therefore, clays often occur as several types mixed together and composed of rock-forming minerals such as carbonates, phosphates, feldspar, oxides, sulphates, etc. Types of clay minerals include smectite ($(Mg_3(Si,Al)_4(OH)_2.4.5H_2O[Mg]_{0.35}$), mica ($KAl_2(AlSi_3O_{10})(OH)_2$), kaolins ($Al_2Si_2O_5(OH)_4$), etc. Kaolin clay minerals include kaolinite, halloysite, nacrite and dickite [2]. They all have the same chemical formula $Al_2Si_2O_5(OH)_4$, but different structures [3]. Clays high in kaolinite content are suitable for earthenware pottery and binders in refractory material production [4]. Clays are often medium to brownish gray [1]. Mica gives a yellowish-brown colour to many other clay minerals [4]. Clay products result from the firing of clays and related compound at high temperatures. An example of the group of smectite clays is montmorillonite, which is one of the common clays often identified in the clay mixtures used in earthenware objects [1,2].

2.1.2. Types of clay ceramics

There are three major types of ceramics: porcelains, earthenware and stoneware. Earthenware objects are clay products manufactured at lower temperatures (≤ 900 ^{o}C). They are often red, brown, gray or black in colour. They are commonly African domestic pottery, but are also found in other parts of the world (e.g. China and Europe). The raw materials of earthenware objects are often not processed but are used as acquired [5]. Raman studies of earthenware objects are very rare.

Porcelain is characterised by a very low porosity (2% open porosity). It is white in colour (due to low iron content) and shows signs of a well-developed reaction between components [6a]. They are clay products (ceramics), which are prepared at higher temperatures (~1200 ^{o}C). The raw materials used in making porcelain are often similar to those used in making earthenware objects. Porcelains are widely studied by Raman spectroscopy. The application of Raman spectroscopy in archaelogical porcelain samples often included the analysis of pigments [7]. The majority of porcelain studies by Raman spectroscopy involves the use of FT-Raman [3, 8, 9] or higher laser excitation [10, 11].

Stoneware objects are made under similar conditions (e.g. higher temperature) as porcelains. They are much denser with low porosity and often occur in various colours other than white [6b].

2.1.3. Thermal evolution of clay minerals

The knowledge of the decomposition products of the clay minerals and raw material mixtures used in pottery making is important for chemical characterisation of objects, determination of raw materials and processing conditions (e.g. temperature). Materials identified in archaeological artefacts can be classified as primary minerals, firing minerals and secondary minerals [12]. Primary minerals are those present in raw materials, like quartz, which do not undergo reaction over a wide range of temperatures. Firing minerals, like rutile (TiO_2), are the products of thermally induced reactions, i.e. they are formed during firing. Secondary

minerals are those formed after production of wares (for instance, during use and burial) as a result of transformation of metastable firing minerals or infiltration of any solution [13]. The chemical components of clays are often analysed by X-ray diffractometry (XRD) in combination with other analytical techniques such as infrared (IR), thermogravimetry (TG) and X-ray fluorescence (XRF) [12, 14, 15]. However, these techniques have shown some drawbacks such as long analysis time, inability to give information on amorphous phases and are destructive.

During the firing of clay minerals and accompanying minerals such as quartz, feldspar, calcite, limestone, hematite, etc, a series of transformations occur which determine the final properties of the ceramic products [16, 17]. These crystalline structures gradually decompose and simultaneously others are formed [18]. For example, the thermal decomposition of kaolinite mineral has shown the formation of metakaolin ($Al_2O_3.4SiO_2$) at 550 ^oC, spinel-type phase ($Al_2O_3.3SiO_2$) at 950 ^oC, mullite-like phase ($Al_2O_3.2SiO_2$) at 1100 ^oC and mullite ($Al_2O_3.\frac{4}{3}SiO_2$) at 1400 ^oC [19, 6b].

The decomposition of the kaolinite rich in calcium carbonate results in anorthite ($CaAl_2Si_2O_8$) at 200 ^oC, gehlenite ($Ca_2Al_2SiO_7$) and plagioclase at higher temperatures in excess of 800 ^oC [20, 21, 22]. Illite decomposes at 800 ^oC to form spinel-type phase while $CaCO_3$ forms CaO in the same temperature region [9, 15]. Alia et al. [9] observed the presence of albite at 900 ^oC ($NaAlSi_3O_8$). Gehlenite and wollanstonite (α-$CaSiO_3$) form when calcium oxide (CaO) reacts with quartz around 600 – 700 ^oC. The decomposition of separate raw clays at 800 ^oC revealed that chlorite and kaolinite structures were completely destroyed. When the temperature is raised further and the modification of tetrahedral layer of clay minerals occurs then the intensities of the Raman bands weaken until the bands disappear completely. Bhatnagar and Goel [23] studied the thermal evolution of clay mixtures, e.g. kandite/mica, muscovite/mica, during brick making, in the temperature range 700 – 1100 ^oC. Dehydroxylation of clay mixtures was observed at 850 ^oC. The skeletal structure of muscovite/mica was still observed at 900 ^oC. Other compounds including spinel-type, e.g. olivine and enstatine, crystallise around 900 ^oC from micaceous structures. The final collapse of the illite skeletal structure also occurs around 850 ^oC – 900 ^oC [23, 24]. At elevated

temperatures the strength development and reduction in porosity of the clay products were observed during enhanced vitrification (≥ 1100 ^{o}C) [6a]. Vitrification of clay minerals involves the dissolution of alumina, hematite and spinel and their reaction with fused silica to form mullite, which progressively increases both in quantity and crystallinity, and finally dissolves in the liquid phase in excess of 1400 ^{o}C [6c]. The vitrification of illite and micaceous clays were observed around 1050 ^{o}C [9].

Minerals that have been identified in ceramic objects using other techniques include quartz, feldspar, calcite, gypsum, clay minerals, hematite, etc [4, 25]. The decomposition of various clay minerals and related compounds, e.g. illite, kaolinite, smectite, etc have been studied by techniques such as XRD, FT-IR, XRF, SEM and TG and their decomposition products at different temperatures have been identified [4, 12, 19, 23].

2.1.4. Raman spectroscopic analysis of clay minerals

There is a scarcity of data relating to the Raman spectroscopic study of chemical molecules that constitute low temperature fired ceramics (earthenware). For a chemical substance to give a Raman spectrum, the vibrations of its bonds and angles have to result in polarisability change. The aluminosilicates that form an integral part of clay pottery are composed mainly of Si-O and Si=O bands [26]. The polarisability changes in the above bonds are negligible. These compounds also have low scattering cross-section and therefore result in weak Raman bands. The Raman spectra of clays and related products are often accompanied by fluorescence and give broad bands due to the presence of amorphous aluminosilicates. The fluorescence in clay minerals is often due to organic substances that occur in soil and the presence of $Fe(OH)_3$ [14].

Clay minerals have also been studied by Raman spectroscopy using Fourier transform (FT) spectral acquisition and high wavelength excitation lasers (e.g. 632.8 nm). The clay minerals studied include kaolin clays (kaolinite, halloysite, nacrite and dickite) [3, 27], montmorillonite [28, 29], illite [9, 30], etc. Kaolinite appears to be the most studied of all clay minerals by Raman spectroscopy. Despite the use of FT-Raman spectroscopy, long recording times were

required [3, 31]. Therefore, the Raman spectra and the assignments of the above clay minerals and related compounds (quartz, rutile, anatase, mullite, etc) are known and available in the literature for reference [14].

The Raman spectroscopic characterisation of clay products is not possible without the full Raman characterisation of inorganic minerals (e.g. sulphates, carbonates and phosphates). A comprehensive Raman study on various inorganic minerals is beneficial for the complete characterisation of clay products [26, 32, 33]. The spectra of these minerals give intense and well-defined Raman bands due to the presence of high polarisability groups with substantial M-O π-bonding, where M is a metal ion [7, 26, 34].

2.1.5. Conclusion

Typical components that constitute raw materials of clay products and the processed objects have been identified using various destructive but robust techniques, such as XRD, FT-IR, SEM, etc. The thermal evolution of clay minerals and related compounds has also been studied. Studies show that there is often a gradual distortion from the original crystalline structure to some other amorphous forms (e.g. metakaolin) before a new phase (e.g. mullite) crystallises. Furthermore, clay minerals and other inorganic minerals common in nature have been characterised separately by Raman spectroscopy. Some clay objects are valuable pieces of art or have been manufactured in ancient times, therefore are kept in museums as heritage. These objects however, cannot be characterised on the basis of their chemical or mineralogical components because the analytical techniques applied at present are often destructive or cannot detect components of poor crystallinity. Therefore, there is a need for the application of a non-destructive technique to the clay products, which is sensitive, specific and amenable to *in situ* analysis.

2.2. Synthesis of iron oxides

The literature on iron oxides in this section deals with the preparation of hematite, magnetite, goethite and maghemite for pigment purposes, because these are the focus of the current study. The pigment properties are determined by the chemical phases and particle

morphology. Therefore, the synthesis methods presented are those concerned with the structure, particle shape or size.

It has long been known that varying colours of iron oxides are determined by average particle size rather than by variation in the chemical structure [35]. Heating temperature duration and atmosphere affect the iron particle characteristics, namely size, shape, specific gravity, sintering and surface area. The pigment properties influenced by the above characteristics are colour, tinting strength, hiding power and oil absorption [36].

2.2.1. Red iron oxide (hematite, α-Fe_2O_3)

The earlier workers were mainly concerned with the structural formation of the products and the applied aspects of the process. Therefore, most of the results brought forward have been documented inaccessibly in the patent literature [37- 42]. Hematite can be prepared by both thermal treatment of Fe (II) salts and precipitation from iron (III) salts in aqueous media.

2.2.1.1. Synthesis using thermal methods

The most common starting material for thermal treatment is steel pickling chemical waste (97.3% $FeSO_4.7H_2O$, 1% free H_2SO_4, 1% water and 0.7% unidentifiable impurities referred to here as SPW), $FeCl_2.H_2O$, Fe_3O_4 and α-FeOOH [43]. Hematite is the most thermally stable phase of all iron oxides. All other iron oxide phases turn into hematite under heat treatment. Due to the economic needs and environmental demands, SPW was used to prepare hematite. SPW is a waste formed during the final phase of steel manufacturing process called steel pickling. The decomposition of SPW in the temperature range 700 – 900 ^oC gave hematite of particle sizes 0.61 – 1.29 μm [43] in air and oxygen (O_2) atmospheres. When the reaction was carried out under dry nitrogen (N_2) atmosphere the formation of α-Fe_2O_3 of 1.76 – 3 μm began at 500 ^oC [44]. The increase in temperature and the use of N_2 atmosphere resulted in the increase in particle size and loss of colour and consequently loss in tinting strength. The thermal decomposition of pure $FeSO_4.7H_2O$ also results in red iron oxides [45]. High quality copperas reds are obtained by thermal decomposition of $FeSO_4.7H_2O$ in a

multistage process that includes the reduction of sulphates with carbon-containing compounds [37]. Thermal decomposition of $FeCl_3$ in air at high temperatures yielded low quality iron oxide pigments [39]. Micaceous red iron oxides were obtained when iron (III) chlorides and iron metal react at 500 – 1000 ^oC in an oxidising atmosphere in a tubular reactor. Micaceous iron oxide is a crystalline plate-like compound [46].

Black, brown and yellow iron oxides have been calcined at low temperatures in oxidising atmosphere under counter current flow to produce a wide range of different red shades [47a]. For instance, hematite has been observed when goethite (yellow) and magnetite (black) were decomposed separately [48]. When maghemite (brown) was heated at 400 ^oC pure red iron oxide was formed [49]. The calcinations of other iron oxide phases result in pure red hematite of high tinting strength. Thermal decomposition of jarosite compounds (e.g. hydrogen jarosite, sodium jarosite) at 900 ^oC yielded red iron oxides of particle sizes 20 – 60 μm [50, 51, 52]. Bye et al. [53] prepared acicular α-Fe_2O_3 with high tinting power by heating goethite to 500 ^oC. Yellow iron oxides (goethite) were acicular in shape.

2.2.1.2. Synthesis using precipitation methods

The work of Matijevic and Scheiner [54] demonstrated that iron oxide and oxyhydroxide particles could be controlled using precise control of reaction environment. The precipitation methods are often used in order to control the chemical phase formed and the particle characteristics. For a powdery material to show good pigment properties 85% of the particles must have sizes < 10 μm, have regular shapes and be uniform [55].

One of the earliest methods for the preparation of hematite involved the slow precipitation from solution in the presence of oxygen and metallic iron powder [56, 57]. The starting material often used in the preparation of hematite was ferric chloride. Other ferric salts such as nitrates were also used. The precipitation of hematite involves the hydrolysis of ferric ion in the presence of an alkali (e.g. NaOH). Various particle shapes have been prepared.

A gel-sol method involving phase transformation starting from highly condensed ferric hydroxide gel with excess of ferric ions yielded 2 μm pseudocubic, ellipsoidal, peanut-like and plate-like hematite [58 - 61]. Spindle-type hematite of particle size 1.90 μm was prepared by ageing dilute solution of ferric chloride in the presence of phosphate ions [61, 62]. Spherical and pseudocubic particles of α-Fe_2O_3 were prepared by ageing concentrated solution of ferric chloride at 100 ^oC [63, 64]. Diamandescu et al. [65] prepared hematite powders with distinct morphology (acicular, polyhedra, plate-like, spherical, hexagonal, etc) and dimensions 0.1 – 3 μm by hydrothermal synthesis using goethite and ferric hydroxides.

Atkins et al. [66] aged solutions of ferric nitrate at 100 ^oC for 18 days in the presence of NaOH to give hematite of particle size range 0.05 - 0.8 μm. The short time ageing using lower temperatures showed the presence of both goethite and hematite. The commonly proposed mechanism for the precipitation of hematite involves the formation of $Fe(OH)_3$, which then transforms into β-FeOOH. Hematite of particle size 0.25 – 2 μm results from dissolution and reprecipitation of the β-FeOOH [50, 67]. Uniform single crystal particles of α-Fe_2O_3 in the crystalline form and particle size range 0.35 – 0.41 μm were prepared by a highly condensed suspension of β-FeOOH particles doped with PO_4^{3-} ions in a solution of HCl and $NaNO_3$ [68]. Hydrous ferric oxide (HFO) was transformed into hematite in the presence of Zn (II) or Mn (II) at pH 6.5 and 65 ^oC [69].

2.2.2. Yellow iron oxide (goethite, α-FeOOH)

2.2.2.1. Synthesis using precipitation methods

Goethite is only prepared by precipitation methods. This compound shows only acicular and spindle-type (needle shaped) particle shapes [47b, 47c]. Atkins et al. [66] aged solution of ferric nitrate at room temperature for 24 hours to produce acicular goethite particles of 0.02 – 0.8 μm. Jang et al. [69] observed the formation of goethite in the presence of chloride. Yellow pigments have been prepared using oxidation of iron (II) hydroxide solution and oxidation of iron (II) salt solutions [70]. The oxidation of iron salt solutions is basically the Pennimann-Zoph process, which includes the use of metallic iron and FeOOH seed crystals to catalyse

oxyhydroxide formation [71]. Leskéla and Leskéla [45] and Tamaura [72] studied and prepared the yellow α-FeOOH pigments from iron (II) sulphate solution by alkali precipitation and gas oxidation methods. High quality yellow pigments (goethite) have been prepared during the reduction of nitrobenzene with iron in the presence of aluminium chloride [40]. Gallagher and Phillips [73] prepared crystalline goethite by hydrolysis of ferric oxalate solution in the presence of $NaHCO_3$. Goethite can also be prepared by the hydrolysis of ferric chloride [74, 75].

2.2.3. Brown iron oxide (maghemite, γ-Fe_2O_3)

2.2.3.1. Synthesis using thermal methods

Maghemite can be prepared by both thermal and precipitation methods. Goto [49] has shown that maghemite forms around 200 ^oC during the thermal treatment of magnetite. The single-phase brown maghemite has been prepared by the controlled oxidation of Fe_3O_4 at ca. 500 ^oC [41]. The calcinations of organic iron salts like ferrous oxalate [76], ferrous hydrazine carboxylate [77] and ferrous acetate [78] yield maghemite in a single step. Narasimhan et al. [79] showed that the direct thermal decomposition of ferrous carbonate gives maghemite. The thermal decomposition of lepidocrocite (γ-FeOOH) also results in maghemite [48].

2.2.3.2. Synthesis using precipitation methods

Itoh and Sugimoto [68] carried out the oxidation in air stream at 240 ^oC. The particle properties of the prepared maghemite can be controlled [80]. For instance, acicular gamma ferric oxide is prepared by first producing acicular particle of alpha ferric oxide (hematite) from alkali precipitation of ferrous salts followed by its tapotactic reduction to magnetite which is then oxidised under controlled conditions [81]. Jing and Wu [82] prepared acicular shaped γ-Fe_2O_3 particles using a molar ratio of lauric acid to iron nitrate of 2:1 at 300 – 400 ^oC. The molar ratio determined the particle sizes and thermal stability of maghemite.

2.2.4. Black iron oxide (magnetite, Fe_3O_4)

2.2.4.1. Synthesis using thermal methods

Black iron oxide pigment with a high tinting strength can be prepared by thermal decomposition of iron salts under reducing conditions [47d]. However, this process is not often used because of the furnace gases. It has also been reported that the thermal decomposition of red iron oxides at temperatures in excess of 1200 ^oC results in grayish black magnetite [11].

2.2.4.2. Synthesis using precipitation methods

The earliest method of preparing magnetite is the Laux process. During this process an aromatic nitro-compound, e.g. nitrobenzene is reduced with antimony or iron in the presence of iron (II) chloride or aluminium chloride, sulphuric acid and phosphorous acid [40]. When iron (II) chloride is added during the reduction of nitrobenzene with iron, a black pigment (magnetite) with very high tinting strength is produced. The raw materials for the Laux process are mainly by-products from other industries, e.g. steel scrap obtained from deep drawing, grinding from cast iron, $FeCl_2$ from steel-pickling [47d].

Feitknecht [83] first reported the formation of Fe_3O_4 by air oxidation of $Fe(OH)_2$ suspension. Kiyama [84] indicated that Fe_3O_4 is formed readily from $Fe(OH)_2$ suspensions at temperatures above 60 ^oC in the pH range 7 – 10. Tamaura et al. [85] showed that the reaction mixture of γ-FeOOH transforms into stoichiometric Fe_3O_4 at 25 ^oC when the pH was raised from 5 to 9. Ueda et al. [86] developed a method for the preparation of crystalline Fe_3O_4 involving the ageing of a solution containing low concentration of Fe^{2+} ions at room temperature. The particle sizes were less than 1 μm. Duboise et al. [87] prepared magnetite particles of fine octahedral morphology and 1 μm size by solvothermal method using FeOOH precursor and a mixture of water and ethanol (with reducing properties). The hydrolysis of $FeCl_3$ and $FeSO_4$ solutions containing urea at 90 – 95 ^oC resulted in Fe_3O_4 nano disks with average diameters of 40 – 50 μm and lengths of up to 1 μm [88]. Itoh and Sugimoto [68]

prepared magnetite by reduction of hematite in a H_2 stream at 330 ^oC. Magnetite particles grow from goethite when hydrous ferrous oxide is aged with Cu (II) and Fe (II) at pH 8.5 and room temperature [69].

2.2.5. Conclusion

The literature on the synthesis of certain iron oxides has been presented. Magnetite, hematite, goethite and maghemite of different particle sizes and shapes can be prepared by either thermal treatment of iron salts or precipitation from iron salts in aqueous media. The chemical phase and properties of the final products strongly depend on the reaction environment. Furthermore, the raw materials (type of iron salts) determine the product phase and particle characteristics. The resulting product often retains the particle characteristics. Iron oxides of various particle shapes (cubic, spherical, spindle-type, ellipsoidal, etc) and small sizes (< 1 μm) have been prepared. Therefore, iron oxides of particular properties can be tailor-made for a specific application. Many procedures showed that the preparation of one iron oxide phase might first involve the formation or phase transformation of another. Therefore, there is a possibility of contamination of one iron oxide phase by another. The presence of contaminants affects the properties of the products (e.g. colour, crystallinity). The preparation of iron oxides requires the use of analytical techniques that are sensitive to various structures, specific and able to detect amorphous compounds. However, most techniques used cannot detect amorphous compounds or compounds at very low levels, e.g. XRD. The preparation methods available are costly because they make use of pure starting materials, involve many complicated steps or give pigments of poor quality. Therefore, there is a need for simple, yet effective methods that may use cheaper raw materials (iron wastes) and analytical techniques that are sensitive to various structures, specific and capable of detecting amorphous compounds.

2.3. Raman spectroscopic analysis of iron oxides

The iron oxide polymorphs (including oxyhydroxides) occur as corrosion products and pigments, while they also find use in archaeological objects, novel/specialised materials (e.g. magnetic materials) and catalysis, among other applications.

The iron oxides, main products of iron corrosion, strongly absorb infrared radiation but are usually poor light scatterers [89]. Pure Fe_3O_4, FeO, $Fe(OH)_3$, $Fe(OH)_2$, α-Fe_2O_3, γ-Fe_2O_3, α-FeOOH, γ-FeOOH, β-FeOOH and δ-FeOOH, for use as reference materials in the study of iron corrosion, have been characterised by Raman spectroscopy and their spectra assigned [90 - 97]. Raman spectroscopy has further been used to confirm the presence of all the above-mentioned iron oxide polymorphs in samples obtained from the corrosion (under various conditions) of iron metal [90, 98, 99, 100].

The Raman spectra of natural iron oxide pigments such as haematite, Mars yellow (α-FeOOH), and Mars red (α-Fe_2O_3) have been recorded and assigned [10, 101, 102]. The Raman spectroscopic studies of the composition of archaeological objects (ceramics and other clay pottery) revealed that α-Fe_2O_3, Fe_3O_4, FeO and α-FeOOH were commonly used as pigments [10, 102, 103, 104, 105, 106].

The unique Raman spectrum of each iron oxide polymorph facilitates easy identification in mixtures and in the presence of other compounds, such as catalysts (α-Fe_2O_3, γ-Fe_2O_3) and novel/specialised materials (α-Fe_2O_3) [107,108].

The iron oxides and oxyhydroxides have been widely studied by Raman spectroscopy and their spectra fully assigned (see Table 2.1).

Table 2.1: Raman wavenumbers of all iron oxide polymorphs and their assignments as obtained from literature.

COMPOUND	WAVENUMBER (cm^{-1})	ASSIGNMENT	REFERENCES
Magnetite	298 319 540 668	t_{2g} (Fe-O asym. bend) e_g (Fe-O sym. bend) t_{2g} (Fe-o asym. bend) a_{1g} (Fe-O sym. str)	90, 97, 98, 99, 104
Goethite	299 400 550 1003	Fe-O sym. bending Fe-O-Fe / -OH sym. str Fe-OH asym. str Fe-OH asym. str	90, 91, 93, 98
Hematite	225 247 293 412 498 613	a_{1g} (Fe-O sym. str) e_g (Fe-O sym. bend) e_g and e_g (Fe-O sym.bend) e_g (Fe-O sym. bend) a_{1g} (Fe-O sym. str) e_g (Fe-O sym. bend)	94, 106, 107
Maghemite	344 390 507 665 721	e_g (Fe-O sym. str) t_{2g} (Fe-O asym. bend) t_{2g} (Fe-O asym. bend) a_{1g} (Fe-O sym. str) a_{1g} (Fe-O sym. str)	90, 94, 100, 105, 108
Akaganeite	300 415 745	Fe-O sym. bend Fe-O-Fe / -OH sym. str Fe-OH asym. str	90, 91, 94
Lepidocrocite	252 380 527 650 1307	Fe-O sym. bend Fe-O-Fe /-OH sym. str Fe-O asym. bend Fe-OH asym. str. Fe-OH asym. str.	90, 91, 94, 98
Feroxyhite	400 663 1322	Fe-O-Fe /-OH sym. str Fe-OH asym. str Fe-OH asym str	90, 91, 94

2.4. References

1. C. S. Hurlbut, Jr. and C. Klein, Manual of mineralogy, 19th Ed., John Wiley and Sons Inc, New York, pp. 77, 452 (1971).
2. M. J. Wilson, *Clay mineralogy*. In: Spectroscopic and chemical determinative methods, Chapman & Hall, London, pp. 18 – 20, (1994).
3. R.L. Frost, P.M. Fredericks and J.R. Bartlett, Spectrochim. Acta, Part A **49**, 667 (1993).
4. G. W. A. Nyakairu, H. Kurzwell and C. Koeber, J. African Earth Sci. **35**, 121 (2002).
5. A. Lindahl and E. Matenga, *Present and past ceramics and homesteads*. In: Ethnoarchaelogical project in the Buher district, Zimbabwe. Uppsala University Press, Uppsala, p. 11 (1995).
6. N. Palmgren, W. S. Steger and N. Sindius, Sung sherds, Almovist & Wilksell, Stockholm, a: p. 100; b: p. 387; c: p. 385. (1963).
7. R. J. H. Clark, Chem. Soc. Rev. **24**, 187 (1995).
8. H.G.M. Edwards, M. J. Falk, M. G. Sibley, J. Alvarez-Benedi and F. Rull, Spectrochim. Acta Part A **54**, 903 (1998).
9. J. M. Alia, H. G. M. Edwards, F. J. Garcia-Navaro, J. Parras-Armenteros and C. J. Sanchez-Jimenez, Talanta **50**, 291 (1991).
10. D. Bikiaris, S. Daniila, S. S. Sotiropoulou, O. Katsimbiri, E. Pavlidou, A. P. Moutsatsou and Y. Chryssoulakis, Spectrochim. Acta Part A **56**, 3 (1999).
11. J. Zuo, C. Xu, C. Wang and Z. Yushi, J. Raman Spectrosc. **30**, 1053 (1999).
12. G. E. Benedetto, R. Laviano, L. Sabbatini and P. G. Zambonin, J. Cultural Heritage, **3**, 177 (2002).
13. M. Maggetti, *Composition of Roman pottery from Lousonna (Switzerland)*. In: British museum occational paper 19, Chapman & Hall, London, pp 33 – 49 (1981).
14. N. Q. Liem, G. Sagon, V. X. Quang, H. van Tan and P. Colomban, J. Raman Spectrosc. **31**, 933 (2000).
15. M. M. Jordán, T. Sanfeliu and C. de la Fuente, Appl. Clay Sci. **20**, 87 (2001).

16. C. Real, *Análisis por difracción de rayos X de fases de alta temperature resultants de materias primas de interés industria*l. Tesis, Fac. Ciencias. Universidad de Sevilla (1977).
17. M. M. Jordán, T. Sanfeliu, C. de la Fuente, E. Ballbé, *Ceramic interest in weald clays from Castellon*. In: Third Euro-ceramics, vol. 2, Faenza Editrice Iberica, pp. 947 – 952 (1993).
18. M. M. Jordán, A. Boix, T. Sanfeliu and C. de la Fuente. Appl. Clay Sci. **14,** 225 (1999).
19. C. J.. McConville, W. E. Lee, J. H. Sharp, Brit. Ceram. Trans. **97**, 162 (1998).
20. J. Capel, F. Huertas and J. Laines, Mineral. Petrogr. Acta Part A **29**, 563 (1985).
21. F. González-Garcia, V. Romero-Acosta, R. G. Garcia and M. R. González, Appl. Clay Sci. **5**, 361 (1990).
22. J. V. Owen, J. Archaeol. Sci. **24**, 127 (1997).
23. J. M. Bhatnagar and R. K. Goel, Construct. Build. Mater. **16**, 113 (2002).
24. P. J. Michael and W. R. McWhinnie, Polyhedron **8**, 2709 (1989).
25. T. Rotunno, L. Sabbatini and M. Corrente, Archaeometry **39**, 343 (1997).
26. E. E. Coleyshaw, W. P. Griffith and R. J. Bowell, Spectrochim. Acta Part A **50**, 1909 (1994).
27. V. Pasjcini and P. Dhamelincourt, Appl. Spectroc. **48**, 638 (1994).
28. S. Akyuz, T. Akyuz and J. E. D. Davies, Vib. Spectrosc, **22**, 11 (2000).
29. R. L. Frost and L. Rintoul, Applied Clay Sci. **11**, 171 (1996).
30. W. Liu, Water Res. **35**, 4111 (2001).
31. K. H. Michaelin, S. L. Zhang, S. Yariv and I. Lapides, Appl. Clay Sci. **13**, 233 (1998).
32. I. A. Degen and G. A. Newman, Spectrochim. Acta Part A **49**, 859 (1993).
33. W. P. Griffith, *Advances in Raman and infrared spectroscopy*. In: Spectroscopy of inorganic based materials (Edited by R. J. H. Clark and R. E. Hester), Wiley, London, p. 119 (1987).
34. H. G. M. Edwards, E. M. Newton and J. Russ, J. Mol. Struct. **550 – 551**, 245 (2000).
35. G. P. A. Turner, Introduction to paint chemistry and principles of paint technology, 2nd Edn., Chapman & Hall, London, p. 95 (1980).
36. J. Gillan (ed.), *Pigments, dyestuffs and lakes*. In: Paint technology manuals, Chapman & Hall, London, Vol. VI (1966).

37. U. Schwertmann and R. M. Cornell, *Preparation and characterization*. In: Iron oxides in the laboratory; VCH Verlagsgesellschaft, Weinheim, (1991) and ref. therein
38. G.E. Noponen, US Pat. 2634193 (1947) (to Minnesota Mining & Manufacturing Co.).
39. H. Loevenstein, US Pat. 2592580, (1945) (to The Nitralloy Corp).
40. J. Laux, German Pat. DE 515758, (1925) (to I. G. Farbenind).
41. B. Krőckert, G. Buxbaum, A. Westerhaus, H. Brunn, German Patent, DE 3820499 (1988) (to Bayer).
42. J. Laux, German Patent, DE 463773 (1925) (to I. G. Farbenind).
43. H. M. Ismail, N. E. Fouad, M. I. Zaki and M. N. Magar, Powder Technology **70**, 183 (1992).
44. H. M. Ismail, M. I. Zaki, G. A. Hussein and M. N. Magar, Powder Technology **63**, 87 (1990).
45. T. Leskela, M. Leskela and L. Niinisto, Thermochim. Acta **72**, 229 (1984).
46. E. V. Carter, R. D. Laudon, J. Oil Colour Chem. Ass. **1**, 7 (1990).
47. G. Buxbaum, Industrial inorganic pigments, VCH publishers, New York and Weinheim, a: p.86; b: p. 84; c: p. 94, d: p. 87 (1993).
48. J. A. Kroschwitz and M. Howegrant, *Pigments to powders handling.* In: Encyclopedia of chemical technology, 4th ed, John Wiley & sons, New York, Vol. 19, p. 23 (1996).
49. Y. Goto, Jpn. J. Appl. Phys. **3**, 741 (1964).
50. A. Šaric, S. Music, K. Nomura and S. Popovic, Croat. Chem. Acta **71**, 1019 (1998).
51. J. Šubrt, T. Hanslik, A. Šolcova, V. Zapltál and J. Lipka, Chem. Průmysl, **36**/**61**, 637 (1986).
52. J. E. Dutrizac, Hydrometallurgy **42**, 293 (1996).
53. C. Bye and C. K. Howard, J. Appl. Chem. Biotechnol. **21**, 324 (1971).
54. E. Matijević and P. Scheiner, J. Colloid Interf. Sci. **63**, 509 (1978).
55. B. T. Ousnam and D. Erasmus, US Patent 5,738,717 (1998) (to Corveagh Ltd).
56. T. P. Prasad and B. R. Sant, Ind. Chem. J. **8**, 17 (1974).
57. K. R. Hancock, Iron oxide pigments, Reprint, Pfizer Inc. New York, p. 22 (1972).
58. T. Sugimoto, Y. Wang, H. Itoh and A. Muramatsu, Colloid Surface Part A **134**, 265 (1998).
59. T. Sugimoto and K. Sakata, J. Colloid Interf. Sci. **152**, 587 (1992).

60. T. Sugimoto, K. Sakata and A. Muramatsu, J. Colloid Interf Sci. **159**, 372 (1993).
61. T. Sugimoto, A. Muramatsu, K. Sakata and D. Shindo, J. Colloid Interf. Sci. **158**, 420 (1993).
62. M. Ozaki, S. Kratohvil and E. Matijević, J. Colloid Interf. Sci. **102**, 146 (1984).
63. E. K. De Blaco, M. A. Blesa and S. J. Liberman, React. Solids **1**, 189 (1986).
64. P. M. Morales, T. González-Carreno and C. J. Serna, J. Mater. Res. **7**, 2538 (1992).
65. L. Diamandescu, D. Mihaila-Torabasanu, N. Popescu-Pogroin, A. Totovina and I. Bibicu, Ceram. Int. **25**, 689 (1999).
66. R. J. Atkins, A. M. Posner and J. P. Quirk, J. Inorg. Nucl. Chem. **30**, 2371 (1968).
67. J. K. Bailey and M. L. Mecartney, Colloid Surface **63**, 151 (1992).
68. H. Itoh and T. Sugimoto, J. Colloid Interf. **265**, 283 (2003).
69. J. Jang, B. A. Dempsey, G. L. Catchen and W. D. Burgos, Colloid Surface Part A **221**, 55 (2003).
70. A. Suryanarayama, V. V. Ramasastry, T. P. Prasad and B. R. Sant, J. Sci. Ind. Res. **36**, 25 (1977).
71. R. S. Penniman and N. M. Zoph, US Pat. 1 327 061 (1917) (to West Coast Kalsomine Co.).
72. Y. Tamaura, P. V. Buduan and T. Katsura, J. Chem. Soc., Dalton Trans, 1807 (1981).
73. K. J. Gallagher and D. N. Phillips, Trans. Faraday Soc., **64**, 785 (1968).
74. U. Schwertmann and E. Murad. Clay Clay Miner. **31**, 277 (1983).
75. U. Schwertman and R. M. Taylor, Clay Clay Miner. **20**, 159 (1972).
76. V. Rao, A. L. Sashimohan and A. B. Biswas, J. Mater. Sci. **9**, 430 (1974).
77. P. Ravindranathan and K. C. Patil, J. Mater. Sci. Lett. **5**, 221 (1986).
78. B. R. V. Narasimhan, R. Srinivasan, P. Manorhar and F. D. Gnanam, Trans. Indian Ceram. Soc. **58**, 110 (1999).
79. B. R. V. Narasimhan, S. Prabhakar, P. Manohar and F. D. Gnanam, Mater. Lett. **52**, 295 (2002).
80. J. Mellor, A comprehensive treatise on inorganic and theoretical chemistry, Vol. XIII, Longman, London, p. 780 (1956).
81. G. Bate, In: E. P. Wohlfarth, Editor, Ferromagnetic materials, Vol. II, Amsterdam, p. 406 (1980).

82. Z. Jing and S. Wu, J. Solid State Chem. **17**, 1213 (2004).
83. W. Feitknecht, Z. Elektrochem. **63**, 34 (1959).
84. M. Kiyama, Bull. Chem. Soc. Jpn., **47**, 1646 (1974).
85. Y. Tamaura, K. Ito and T. Katsura, J. Chem. Soc., Dalton Trans., 189 (1983).
86. M. Ueda, S. Shimada and M. Inaga, J. European Ceram. Soc. **16**, 685 (1996).
87. T. Duboise and G. Demazeau, Mater. Lett. **19**, 38 (1994).
88. S. Lian, E. Wang, Z. Kang, Y. Bai, L. Gao, M. Jiang, C. Hu and L. Xu, Solid State Commun. **129**, 485 (2004).
89. U. R. Evans, The corrosion and oxidation of metals, E. Arnold, London, 1st supplementary volume, p. 185 (1968).
90. N. Boucherit, A. Hugot-Le Goff and S. Joiret, Corros. Sci. **32**, 497 (1991).
91. G. Nauer, P. Stretcha, N. Brinda-Konopik and G. Liptay, J. Thermal Anal. **30**, 183 (1985).
92. T. Misawa, T. Kyuno, W. Suëtaka and S. Shimodaira, Corros. Sci. **11**, 35 (1971).
93. R. J. Thibeau, C. W. Brown and R. H. Heidersbach, Appl. Spectrosc. **32**, 523 (1978).
94. D. L. A. de Faria, S. V. Silva and M. T. de Oliviera, J. Raman Spectrosc. **28**, 873 (1997).
95. D. Thierry, D. Persson, C. Leygraf, N. Boucherit and A. Hugot-Le Goff, Corros. Sci. **32**, 273 (1991).
96. T. R. Hart, S. B. Adams and H. Tempkin, Proc. 3rd Int. Conf. Light Scatter. Solid, eds M. Balkanski, R. Leite and S. Porto, Flamrion, Paris, pp. 254 and 259 (1976).
97. O. N. Shebanova and P. Lazer, J. Solid State Chem. **174**, 424 (2003).
98. J. Dűnnwald and A. Otto, Corr. Sci. **29**, 1167 (1989).
99. P. M. L. Bonin, M. S. Odziemkowski and G. W. Gillham, Corr. Sci. **42**, 1921 (2000).
100. S. J. Oh, D. C. Cook and H. E. Townsend, Corr. Sci. **41**, 1678 (1999).
101. L. Burgio and R. J. H. Clark, Spectrochim. Acta Part A **57**, 1491 (2001).
102. L. Burgio, R. J. H. Clark and K. Theodoraki, Spectrochim. Acta Part A **59**, 2371 (2003).
103. R. J. H. Clark and M. L. Curri, J. Mol. Struct. **440**, 105 (1998).
104. K. Witke, J. Gotze, R. Röβler, D. Dietrich and G. Marx, Spectrochim. Acta Part A **60**, 2903 (2004).
105. M. Ouyang and and H. Hiraoka, Mater. Research Bull. **32**, 1099 (1997).

106. P. S. Porto and R. S. Krishnan, J. Chem. Phys. **47**, 1009 (1967).

107. A. P. Kozlova, S. Sugiyama, A. I. Kozlov, K. Asakura and Y. Iwasawa, Catalysis **176**, 426 (1998).

108. Z. Wang and S. K. Saxena, Solid State Commun. **123**, 195 (2002).

Chapter 3

Raman spectroscopy

Spectroscopic techniques have been widely used by chemists for the investigations of atoms and molecules for many decades. The molecular spectra give information on molecular dimension, vibrational, rotational and electronic states.

3.1. Theory of Raman scattering

The basic principles of Raman spectroscopy are outlined in Figure 3.1, adapted from Merlin and Dele [1].

When a sample is illuminated with monochromatic light and scattering occurs various processes may take place. The electrons in an atom may be excited to virtual and excited states. When light scattering causes excitation to virtual states ($h\nu_o$, $h(\nu_o - \nu_m)$ and $h(\nu_o + \nu_m)$) there is nearly coincident de-excitation and a change in vibrational energy [2] (Figure 3.1). This process describes normal Raman scattering. In addition to elastic or Rayleigh scattering (scattering without wavenumber change), inelastic scattering occurs resulting in wavenumber change, $h(\nu_o \pm \nu_m)$, where $h(\nu_o - \nu_m)$ represents the Stokes lines and $h(\nu_o + \nu_m)$ the anti-Stokes lines. These lines are situated on either side of the Rayleigh line. The Stokes and anti-Stokes spectra contain the same frequency information, but as the anti-Stokes shifted spectrum is always weaker than the Stokes shifted spectrum, the Stokes spectrum is what is generally used in Raman spectroscopy.

When more energetic lasers are used for excitation a large number of electrons or molecules is excited by absorption of radiation, thus populating the excited state. A spontaneous radiant emission then occurs as the excited species loses all or part of the excess energy and returns to the ground state. The resulting radiant emission is of greater energy than that of light scattered during normal Raman scattering. This process is termed fluorescence and often swamps the Raman bands [3].

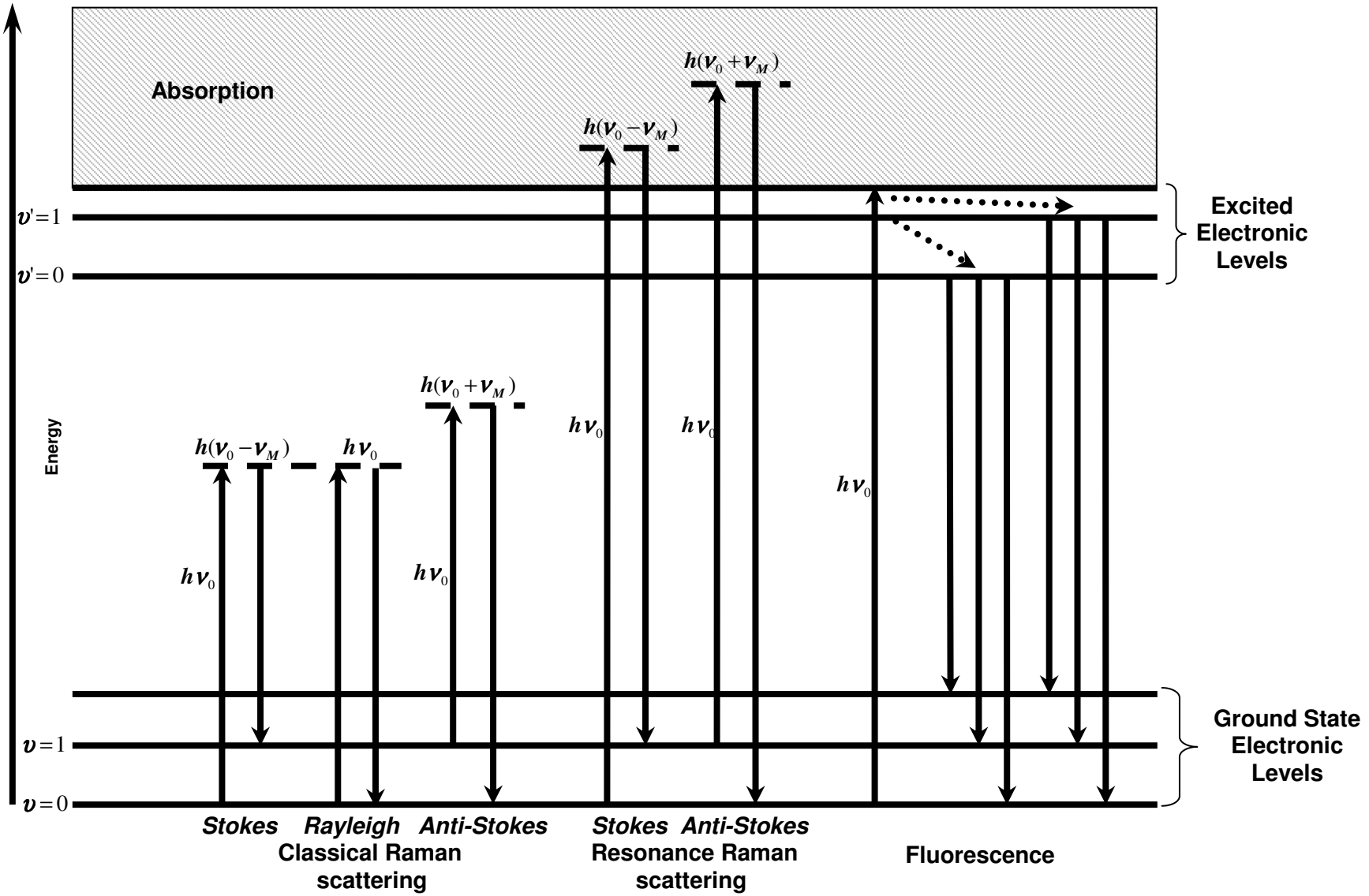

Figure 3.1: Energy levels and transition spectra originating from classical Raman and resonance Raman effect.

When the wavelength of the exciting visible radiation is close to or coincident with that of an electronic transition of the scattering species then a very large enhancement of the intensities of particular Raman bands, sometimes with the appearance of overtones and combination bands, occurs. This process is called resonance Raman spectroscopy (RRS) [4].

The energy difference between initial and final vibrational levels (ΔE) is calculated as follows [2]:

$$\Delta E = hc\left(\frac{1}{\lambda_{incident}} - \frac{1}{\lambda_{scattered}}\right) \qquad 3.1$$

where *h* is Planck's constant, *c* is the speed of light and *λ* is the wavelength [3]. The Raman shifts are normally expressed in wavenumber (cm^{-1}) and the wavenumber of the normal vibration ($\tilde{\nu}$) is then:

$$\tilde{\nu} = \frac{1}{\lambda_{incident}} - \frac{1}{\lambda_{scattered}} \qquad 3.2$$

where *λ* is the wavelength in cm.

When the energetics of the equation 3.1 are satisfied during light scattering, a spectrum unique to the molecule under investigation is obtained. The spectrum is usually represented as a plot of the Raman intensity against the wavenumber shift and a peak occurs whenever the conditions of equation 3.1 are satisfied.

3.2. Raman activity of vibration

Raman spectroscopy is a vibrational technique and thus each molecule has 3N-6 (3N-5 for linear molecules) potential vibrational motions, where N represents the number of atoms in the molecule, each band having a particular wavenumber, intensity and width [2]. Not all

normal modes of vibration will be observable as bands in the Raman spectrum. When a molecule is exposed to an electric field, a dipole moment is induced which is proportional to the electric field strength and to the molecular polarisability, α. A molecular vibration can only be observed in the Raman spectrum if it alters the molecular polarisability [5].

$$\frac{\partial \alpha}{\partial Q} \neq 0 \qquad 3.3$$

where *α* is the molecular polarisability and Q stands for the normal coordinate describing the motion of the atoms during a normal vibration. If the conditions of equation 3.3 above are fulfilled by symmetry, then vibrations are allowed or active in Raman spectra; if they are not fulfilled by the symmetry, they are forbidden or inactive. Group theoretical methods are used to determine the symmetries of the normal modes of vibration of molecules and crystal lattices [6, 7]. Character tables have been compiled to assist in determining the number of fundamental vibrations and the selection rules that govern Raman activity. The energy of a vibrational mode depends on molecular structure and environment.

The intensities of bands in the Raman spectrum of a compound are determined by the changes in polarisability, α, that occur during the vibrations. The intensity of a band in the Raman spectrum is given by the equation 3.4

$$I_{Raman} = KI_L(\tilde{\nu}_o - \tilde{\nu}_i)^4 (\frac{\partial \alpha}{\partial Q})^2 \qquad 3.4$$

where I_L is the power of the laser at the sample, $\tilde{\nu}_o - \tilde{\nu}_i$ is the wavenumber at which the band is measured and $\frac{\partial \alpha}{\partial Q}$ is the change in polarisability with the normal coordinate of the vibration [8]. The value of the constant of proportionality, *K*, is dependent on the efficiency at which Raman scattered light may be collected.

3.3. Raman instrumentation

The instrument type used in this study was a dispersive Raman spectrometer. The basic components of the Raman spectrometer include the light source, optical system, detector and signal amplifier. Figure 3.2 shows the organisation of components in relation to each other.

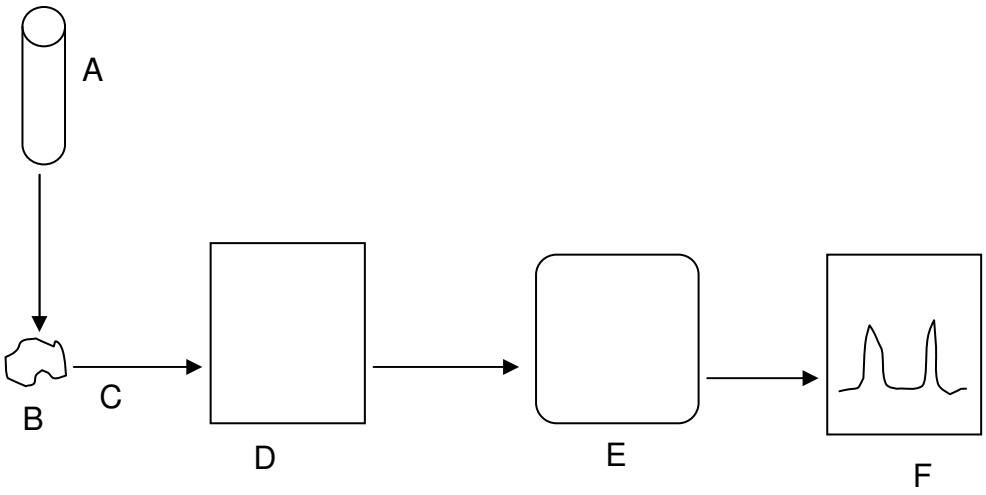

Figure 3.2: Schematic representation of the organisation of Raman components showing the path of the scattered light during recording. A, laser source; B, sample; C, scattered light; D, optical system (e.g. monochromator); E, detector (e.g. charge coupled detector) and F, signal amplifier.

Laser radiation is brought to focus on each grain in the sample via the microscope objective (x50 or x100). The scattered light is then collected and directed to the optical system (e.g. monochromator) and then to the detector. The data may then be processed and displayed on screen or a hard copy (Figure 3.2).

3.3.1. Light source

Due to the inherent weakness of the Raman scattering signal, the sources most often used are lasers. Lasers are high in intensity and are thus able to produce Raman scattering of sufficient intensity to be measured with reasonable signal-to-noise ratio. There are three types of lasers that operate in the ultraviolet (UV), visible and near-infrared regions. The

intensity of Raman scattering varies as the fourth power of the frequency of radiation [5]. Therefore, the order of sensitivity of lasers follows this trend: ultraviolet > visible > near-infrared. However, UV lasers are not commonly used.

The common lasers operating in the visible region are gas lasers, e.g. He-Ne (632.8 nm), Kr^+ (647.0 nm or 530.9 nm) and Ar^+ (488.0 or 514.5 nm). The use of short wavelength visible lasers for excitation of Raman spectra results in the high-energy photons inducing photon fluorescence. To reduce the problem of fluorescence, near-infrared (NIR) lasers are used to illuminate the sample [3]. The most commonly used NIR lasers are the diode lasers (782 or 830 nm) and the Nd/YAG laser (1074 nm). The light source for Fourier Transform Raman spectroscopy (FT-Raman) is the Nd/YAG laser. This technique was developed mainly to overcome fluorescence. However, the use of this type of laser results in weaker bands compared with visible lasers at the same power [8].

3.3.2. Optical system

Light collected from a sample needs to be processed in some way that wavenumbers and intensity information can be extracted from the detected signal. The component used for this purpose is the optical system. This component consists of filters, gratings and mirrors, which collectively select wavelength information to be sent to the detector. The optical system of the Raman spectrometer may be monochromators, polychromators and interferometers. Monochromators block all but a narrow spectral region from reaching the detector. Polychromators separate different wavelengths of light and deliver them to different detectors for simultaneous measurements. Spectra can be built up by measuring the transmitted intensity as the spectral region transmitted by the monochromator changes with time. Spectra from the polychromators can be built by making a histogram for signals from different detectors. Spectrometers (which include monochromators and polychromators) can be classified as dispersive and non-dispersive. Dispersive spectrometers deliver light to a position that varies continuously with wavelength. A dispersive polychromator is called a spectrograph. Non-dispersive spectrometers include anything else such as interferometers, dichroic beam splitters, optical filters and energy

selective detectors. The most common non-dispersive spectrometers use interferometers as their optical system and are called FT-Raman spectrometers [9].

3.3.3. Detector

Multichannel detectors are commonly used in Raman spectroscopy. These are transducers detecting multiple resolution elements at a time allowing spatial resolution in one or two dimensions [10]. The liquid N_2-cooled charged coupled device (CCD) was used in this study. The multichannel detectors are photodiode arrays, charge coupled devices (CCD), charge injection devices and non-silicate devices. An array detector is composed of an array of pixels, where each pixel is one resolution element of the array. The maximum amount of charge a pixel can hold is defined as a full well capacity (FWC), see Figure 3.3. Array detectors are integrative devices, collecting electrons as long as the detector is exposed to light. After exposure the device is sampled to read the signal. For instance, the CCD array is read by shifting the electrons from pixel to pixel across the chip into a register consisting of an analog amplifier and an analog-to-digital converter (ADC) converts the signal from the chip into a computer readable format [10], see Figure 3.4.

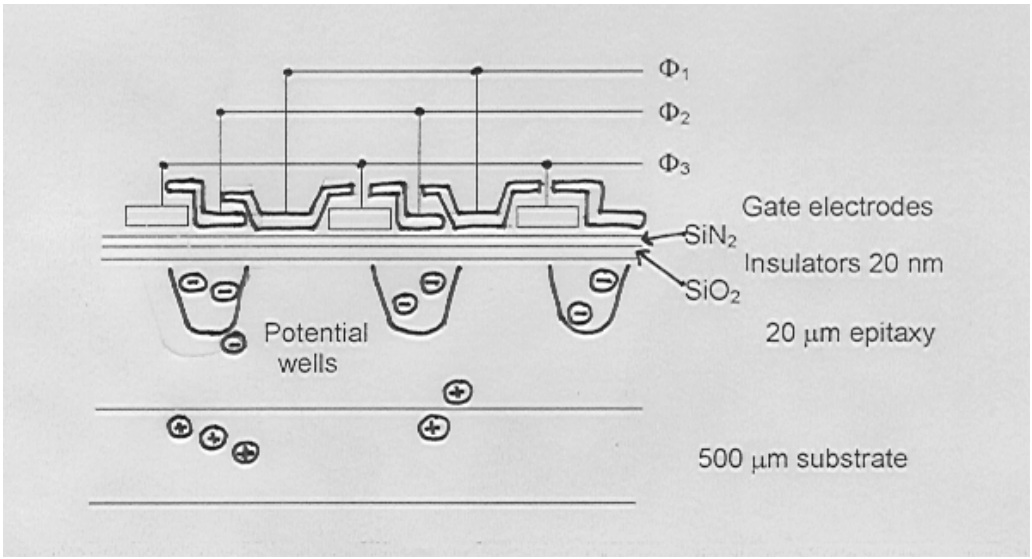

Figure 3.3: Cross-section of charge coupled detector (CCD), demonstrating the location of electrodes and the formation of potential wells. The locations of the electrons and holes in the diagram show where charge is collected.

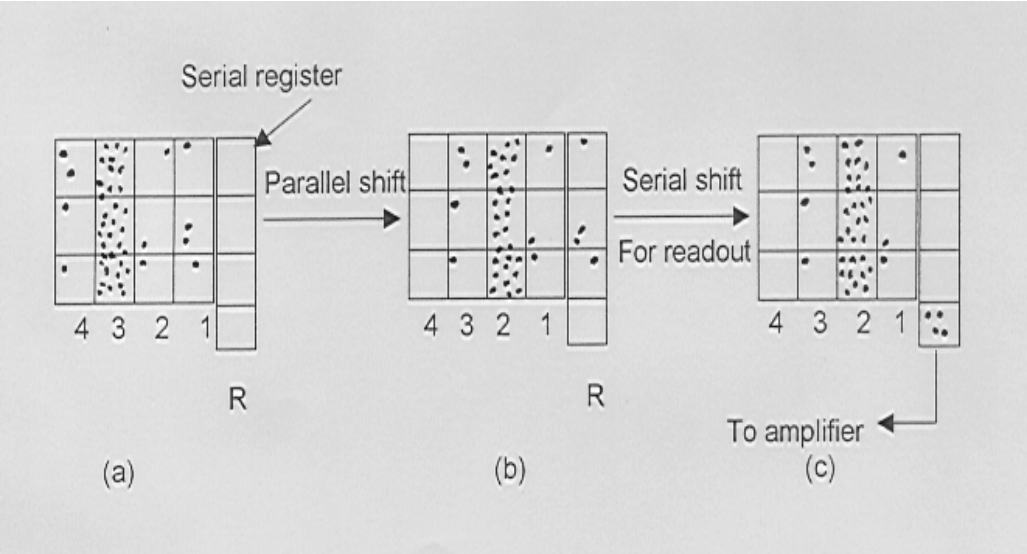

Figure 3.4: Illustration of charge readout on a CCD. (a) Charge collected on the CCD immediately following integration. (b) Readout begins - charge from columns in (a) are shifted one column towards the readout such that the charge from column 1 in (a) is moved to the readout in (b). (c) Charge in the readout is measured and the process is repeated until all columns have been read.

For more details on Raman instrumentation and its operations see ref. [9].

3.4. Operational parameters

There are a number of operational parameters that influence the quality of the Raman spectrum obtained from the sample which have been significant in the current study. These parameters include laser power, sample form, recording time, number of accumulations and confocal microscope.

3.4.1. Laser power

This parameter affects the shapes and intensities of the bands resulting from the sample under investigation. The increase in laser power may result in band broadening and shifts. These effects arise from local heating due to relatively high laser power, which enhances anharmonic interactions [11]. The increase in laser power may destroy the sample or

transform it into a different chemical phase. The laser power may range from a few milliwatts (0.1 mW) to several hundreds. For the heat sensitive compounds e.g. pigments, low laser powers (≤ 5 mW) are desirable in order to minimise the possibility of sample degradation [4]. Coloured molecules can be so strongly absorbing that they thermally degrade [12]. At lower laser power, no sample heating is observed but the spectrum is very weak. As the laser power is increased the Raman band intensities may increase but the baseline starts to increase at high Raman shift because of the effect of sample heating.

When laser power is increased to even higher values (several hundred milliwatts) the black body radiation may cause severe degradation of the spectrum. Black body radiation is continuum radiation produced when solids are so hot that they glow with heat [3]. It is produced by the innumerable atomic and molecular oscillations excited in the condensed solid by the thermal energy. The heat due to the increased laser power slowly changes the structure of the sample. Therefore, the operator must be careful to select the appropriate laser power to maximise the signal-to-noise ratio and minimise black-body radiation caused by the sample heating.

3.4.2. Sample form

Ways of diminishing sample heating include spinning the sample or diluting the sample in some matrix, e.g. oil, KBr, KCl, etc. The low concentration of the sample (often 2%) has the effect of diluting the colour and reducing thermal degradation [12]. This enables strong Raman spectra to be recorded where the bands due to the coloured component could predominate. The strong bands occur due to the molecule generating colour, most likely due to resonance Raman spectroscopy. Thermally stable samples can be analysed in their original form.

3.4.3. Sample recording time

Some compounds, e.g. silicates, are weak Raman scatterers and short time recordings may not yield any peaks. However, with longer recording times the results improve [13]. Therefore, the extension of recording time increases the efficiency and sensitivity of Raman spectroscopy. However, for heat sensitive samples degradation may occur as the recording time is lengthened.

3.4.4. Number of scan accumulations

The number of scan accumulations is closely linked to the recording time. When the sample recording is accompanied by more accumulations, there is an increase in efficiency and sensitivity. One distinct advantage that stems from the increased accumulations is the increase in the signal-to-noise ratio. The recordings using more accumulations result in more pronounced Raman peaks. However, increasing the number of accumulations can result in a different spectrum. This is a direct result of sample heating capacity and/or the heat capacity of its surroundings [14].

3.4.5. Confocal microscope

The use of Raman microscopy (Raman spectrometer coupled to a microscope) gives information on the microstructure of samples analysed and also improves the spatial resolution, the smallest physical distance between measured positions on the sample in single point mapping. When coupled to a confocally optical feature the samples buried in a matrix and at various depths can be analysed. A confocal optical set up occurs when an aperture is placed at the back-focal image plane, where only the radiation emitted laser focal volume will be collected [14]. A suitable choice of optical objectives and the hole for confocal microscope will enable the detection of structural phases existing in micrometre size and along with the depth of the sample, while reducing fluorescence. The use of a confocal hole of several tens of micrometres could give results on a volume < 1 μm^3 [15].

3.5 References

1. J. C. Merlin and M. L. Dele, Bull. Soc. Zool: Biophysique-Biochemie, **108**, 289 (1983).
2. L. C. Prinsloo, *Raman spectroscopic investigation of radiation damage in carbon implanted diamond*. Thesis, University of Pretoria, Pretoria, pp 6 – 8 (2001) and ref. therein.
3. D. A. Skoog, F. J. Holler and T. A. Nieman, Principles of instrumental analysis, 5th edn. Saunders College Publishing, New York, pp 148 and 435 (1998).
4. R. J. H. Clark, Chem. Soc. Rev. **24**, 187 (1995).
5. G. Keresztury, *Raman spectroscopy theory.* In: Handbook of vibrational spectroscopy, eds. J. Chalmers and P. R. Griffiths, John Wiley & Sons Inc., Chichester, Vol. 1, p. 76 (2002).
6. W. G. Fateley, F. R. Dollish, N. T. Dewitt and F. F. Bentley, *Infrared and Raman selection rules for molecular and lattice vibrations.* In: The Correlation method, John Wiley & Sons Inc., New York, (1972).
7. D. M. Adams and D. C. Newton, Tables for factor group and point group analysis, Beckmann-RIIC Ltd, London, (1970).
8. P. R. Griffiths, *Introduction to vibrational spectroscopy.* In: Handbook of vibrational spectroscopy, eds. J. Chalmers and P. R. Griffiths, John Wiley & Sons Inc., Chichester, Vol. 1, p. 36 (2002).
9. M. J. Pelletier, *Raman monochromators and polychromators.* In: Handbook of vibrational spectroscopy, eds. J. Chalmers and P. R. Griffiths, John Wiley & Sons Inc., Chichester, Vol. 1, p. 477 (2002).
10. C. J. S. Pommier, L. K. Watton, T. D. Ridder and M. B. Denton, *Array detectors for Raman spectroscopy.* In: Handbook of vibrational spectroscopy, eds. J. Chalmers and P. R. Griffiths, John Wiley & Sons Inc. Chichester, Vol. 1, p. 510 (2002).
11. D. L. A. de Faria, S. V. Silva and M. T. de Oliviera, J. Raman Spectrosc. **28**, 873 (1997).

12. G. Dent, *Vibrational spectroscopy of colors, dyes and pigments.* In: Handbook of vibrational spectroscopy, eds. J. Chalmers and P. R. Griffiths, John Wiley & Sons Inc., Chichester, Vol. 4, p. 2925 (2002).
13. R.L. Frost, P.M. Fredericks and J.R. Bartlett, Spectrochim. Acta, Part A **49**, 667 (1993).
14. B. T. Bowie, D. B. Chase, I. R. Lewis and P. R. Griffiths, *Anomalies and artifacts in Raman spectroscopy.* In: Handbook of vibrational spectroscopy, eds. J. Chalmers and P. R. Griffiths, John Wiley & Sons Inc., Chichester, Vol. 3, p. 2367 (2002).
15. N. Q. Liem, G. Sagon, V. X. Quang, H. van Tan and P. Colomban, J. Raman Spectrosc. **31**, 933 (2000).

Chapter 4

Raman spectroscopic study of ancient South African domestic clay pottery

Available online at www.sciencedirect.com
ScienceDirect
Spectrochimica Acta Part A 66 (2007) 135–142
SPECTROCHIMICA ACTA PART A
www.elsevier.com/locate/saa

Raman spectroscopic study of ancient South African domestic clay pottery

M.A. Legodi, D. de Waal *

Department Of Chemistry University of Pretoria, Pretoria 0002, South Africa

Received 14 October 2005; accepted 3 February 2006

Abstract

The technique of Raman spectroscopy was used to examine the composition of ancient African domestic clay pottery of South African origin. One sample from each of four archaeological sites including Rooiwal, Lydenburg, Makahane and Graskop was studied. Normal dispersive Raman spectroscopy was found to be the most effective analytical technique in this study. XRF, XRD and FT-IR spectroscopy were used as complementary techniques. All representative samples contained common features, which were characterised by kaolin ($Al_2Si_2O_5(OH)_5$), illite ($KAl_4(Si_7AlO_{20})(OH)_4$), feldspar (K- and $NaAlSi_3O_8$), quartz (α-SiO_2), hematite (α-Fe_2O_3), montmorillonite ($Mg_3(Si,Al)_4(OH)_2{\cdot}4.5H_2O[Mg]_{0.35}$), and calcium silicate ($CaSiO_3$). Gypsum ($CaSO_4{\cdot}2H_2O$) and calcium carbonates (most likely calcite, $CaCO_3$) were detected by Raman spectroscopy in Lydenburg, Makahane and Graskop shards. Amorphous carbon (with accompanying phosphates) was observed in the Raman spectra of Lydenburg, Rooiwal and Makahane shards, while rutile (TiO_2) appeared only in Makahane shard. The Raman spectra of Lydenburg and Rooiwal shards further showed the presence of anhydrite ($CaSO_4$). The results showed that South African potters used a mixture of clays as raw materials. The firing temperature for most samples did not exceed 800 °C, which suggests the use of open fire. The reddish brown and grayish black colours were likely due to hematite and amorphous carbon, respectively.

Keywords: South African; Pottery; Raman; Kaolin; Illite

1. Introduction

The technique of Raman spectroscopy was used to examine a series of African domestic clay pottery shards. Such a detailed examination of pottery could give valuable information on the characterisation of archaeological items by the identification of materials such as pigments, binders and clays used in the manufacturing process. The importance of this subject has already been demonstrated in the literature [1–3]. The chemical composition can be used to define the pottery of a particular area and people by determining the raw materials used. For very important artefacts the knowledge of the composition of raw materials and processing methods used will help in the reconstruction of such pieces. For instance, studies have shown that natural sources of Ca^{2+} in clay may be ash, bedrock clay bodies, shells (containing Ca particles), etc. while sources of P_2O_5 in clays are dung, blood, fats and lipids [4]. The bushmen are known to anoint their clay vessels with fat while still damp, then to smear them with gum after drying and to boil springbok blood in them after they were fired. The protein-based stem extraction product from animal bones and butcher's offal which is normally referred to as animal glue is a nitrogen-containing material. Animal glue is usually applied to pottery before colouring with metal-containing pigments [5].

There are two ways in which the pottery could be fired: in an open fire and in a kiln. The open firing methods have an upper limit of 800 °C [4]. The kilns were used for iron smelting and could reach a maximum temperature of 1230 °C.

Various techniques have been used to analyse pottery for defining non-local pottery; neutron activation, X-ray diffractometry (XRD), trace elemental analysis, spectroscopy, etc. by chemically and mineralogically characterising the clay paste [6]. However, the paste analysis is complicated by the diversity of clay minerals and trace elements in nature. Chemical analysis is applied in clay pottery for characterisation, as different clay deposits can be distinguished by their chemical composition. Optical emission spectroscopy is used for analysis of minor and/or trace elements [7]. The success of these approaches is

* Corresponding author. Tel.: +27 124203099; fax: +27 123625297.
E-mail address: danita.dewaal@up.ac.za (D. de Waal).

1386-1425/$ – see front matter © 2006 Elsevier B.V. All rights reserved.
doi:10.1016/j.saa.2006.02.059

constrained by data on regional and interregional distribution of clays and trace elements. Tempering (aplastic) agents in the pottery are often well suited for use as indicators of provenance and origin, even though they could be traded. The aplastics are often used to retain the shape of the pottery controlling the shrinkage during drying and firing [6]. Many tempering agents are not good indicators of source area, e.g. bone and shells, because they are common, but rock fragments and sand grain are better due to the fact that they may reflect geological source.

In this paper, we report on the results obtained by Raman spectroscopy during the determination of the main components of selected South African earthenware (low temperature fired clay pottery) objects in the form of domestic clay pottery shards. The purpose of the study was to characterise the samples on the basis of their chemical composition as obtained from their Raman spectra. This will help determine whether the same raw materials were used, and if so, whether the pottery samples were processed under the same conditions. It is intended that these results will help in revealing the potential of Raman spectroscopy as a tool in analysing earthenware pottery shards and their methods of production in South Africa.

2. Experimental

2.1. Samples

The samples originate from four areas in South Africa, namely, Lydenburg (Fig. 1), Makahane (Fig. 2), Graskop (Fig. 3) and Rooiwal (Fig. 4). The Makahane collection was obtained from an archaeological site just outside the Kruger National Park. The shards were found at the same location back in the 1930s. These were dated back to the 13th and 14th century, and most likely belonged to the Venda- and Pedi-speaking people who lived in that region. The Graskop collection was found at a place presently known as the Aventura Resort. Samples 1–6 were found in the Aventura Resort cave, while 7 and 8 were outside the cave, but in the vicinity. These have been dated to the 13th century. The people believed to have resided in the Aventura caves are the Swazi-speaking people. The Lydenburg collection, even though obtained from the same area, was not necessarily found at the same location. The date of these shards is the 14th century. The single shard, which was not dated was found in an area called Rooiwal, in Gauteng province, Republic of South Africa. The Graskop, Lydenburg and Makahane sites are situated within 40 km of each other in Mpumalanga province near the border of South Africa and Swaziland.

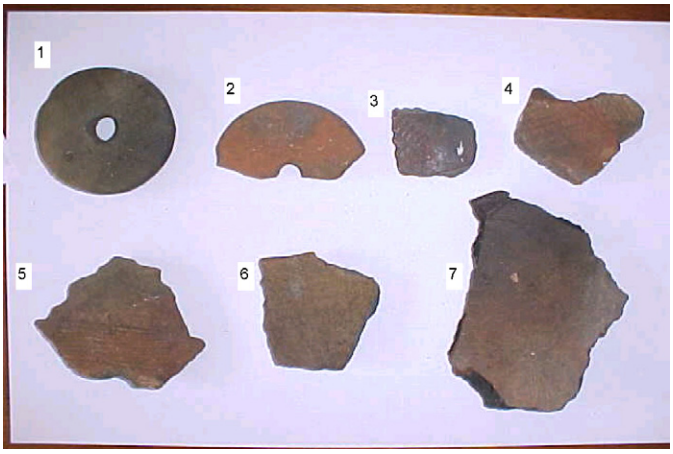

Fig. 2. Makahane shards: (1) black (no decorations); (2) orange-red surface and gray body with line (short and long) impressions; (3) orange-red outside and dark-brown inside (crossing line impressions); (4) orange-red with gray patches (with array of short line impressions); (5) reddish brown on one side and dark-brown on the other (with crooked line impressions); (6) yellowish brown on one side and reddish brown on the other (with short line impressions); (7) reddish brown and black on other areas (with short line impressions). (For interpretation of the references to color in this figure legend, the reader is referred to the web version of the article.)

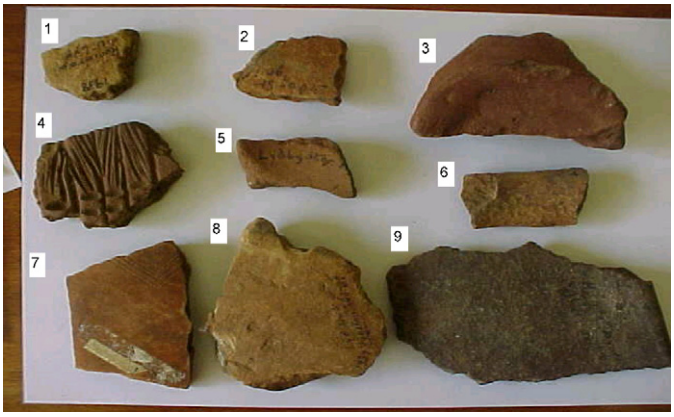

Fig. 1. Lydenburg shards: (1) dark red with impressions; (2) yellowish red with line impressions; (3) dark red with shape of pottery bottom (no decorations); (4) yellowish red with deep line impressions; (5) reddish brown with deep line impressions; (6) reddish brown with short parallel lines; (7) dark red with line impressions; (8) yellowish brown (no decorations); (9) reddish black (no decorations). (For interpretation of the references to color in this figure legend, the reader is referred to the web version of the article.)

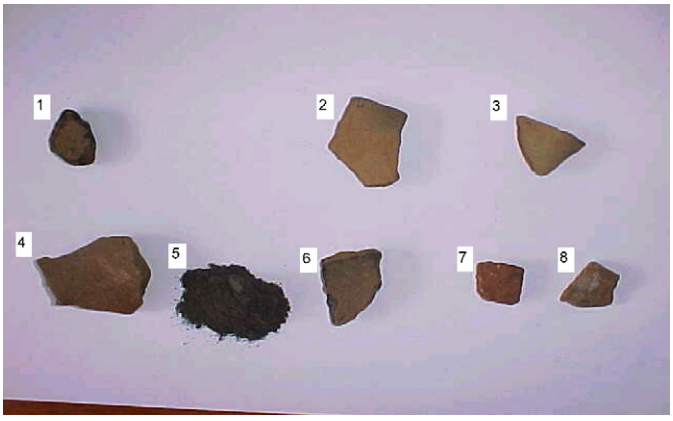

Fig. 3. Graskop shards: (1) light brown but black under surface (no decorations); (2) yellowish brown (no decorations); (3) yellowish brown (no decorations); (4) dark brown with deep line impressions; (5) light brown but black under surface (no decorations, but crushed); (6) light brown surface but black under surface (with short line decorations); (7) orange red with zig-zag impressions; (8) light brown with deep straight line impressions. (For interpretation of the references to color in this figure legend, the reader is referred to the web version of the article.)

Fig. 4. Rooiwal shard. Dark-brown on the outside and black burnt material in the inside. (For interpretation of the references to color in this figure legend, the reader is referred to the web version of the article.)

2.2. Instruments

2.2.1. Raman spectroscopy

Laser Raman spectra were collected at room temperature using a Dilor XY Raman spectrometer with a resolution of 2 cm^{-1}. Radiation at 514.5 nm from an Ar^+ Coherent Innova 300 laser was used to excite the samples. The laser power was set at 100 mW at the source. The recording time was set at between 30 and 180 s, with two accumulations per spectrum segment. An Olympus Mplan 100× objective on an Olympus BH-2 microscope was used to focus on the sample. The Raman spectra were analysed using Labspec v 2.04 software [8].

2.2.2. X-ray powder diffractometry

The X-ray diffraction (XRD) analyses were performed using a Cu Kα (1.5418 Å) source (40 kV, 40 mA) from a Siemens D-501, with a graphite secondary monochromator and a scintillation counter detector. The powdered sample was placed on a flat plastic plate, which was rotated at 30 rpm. The scans were performed at 25 °C in steps of 0.04°, with a recording time of 2 s for each step [9]. Where accurate 2θ values were required, Si was added as internal 2θ standard.

2.2.3. Infrared spectroscopy

The infrared spectra were recorded in the mid-infrared region (400–4000 cm^{-1}) in an evacuated chamber of Bruker 113v FT-IR spectrometer using KBr discs as matrices. A spectral resolution of 2 cm^{-1} was used and spectra were accumulated over 32 scans. The FT-IR spectroscopy was applied to all samples. Only 2 mg of each sample was mixed with 100 mg of KBr and pressed under 6 tonnes for 2 min in making the disk. At first (for Makahane sample no. 7, Graskop sample no. 5, Lydenburg sample no. 8 and Rooiwal sample) the samples were crushed and ground before making the KBr pellets.

The fitting of peaks and smoothing were done with OPUS 2000 software on the Bruker 113v over the working window, 400–4000 cm^{-1}.

2.2.4. X-ray fluorescence

An ARL 9400XP+ Wavelength-dispersive XRF Spectrometer with a Rh source was used for the X-ray fluorescence analyses of the samples. The XRF Spectrometer was calibrated with certified reference materials. The NBSGSC fundamental parameter program was used for matrix correction of major elements, as well as Cl, Co, Cr, V, Sc and S. The Rh Compton peak ratio method was used for the other trace elements. Samples were dried and fired at 1000 °C to determine the percentage loss on ignition; for the samples this was less than 2%. Major element analyses were carried out on fused beads, following the standard method used in the XRD and XRF laboratory of the University of Pretoria [10], as adapted from Bennett and Oliver [11]. A prefired sample of 1 and 6 g of lithium tetraborate flux was mixed in a 5% Au/Pt crucible and fused at 1000 °C in a muffle furnace, with occasional swirling. The glass disk was transferred into a preheated Pt/Au mould and the bottom surface was analysed. The trace element analyses were done on pressed powder pellets, using an adaptation of the method described by Watson [12], with a saturated Mowiol 40–88 solution as binder.

3. Results and discussion

The representative shards were Lydenburg sample no. 8, Makahane sample no. 7, Graskop sample no. 5 and the Rooiwal sample. The laser was focused in each recording on coloured areas visible on the object under the microscope. The predominant colours on the shards were black, orange, red and maroon scattered over the uncoloured background. This is normally an indication of the composite nature of clay products. A range of spectra was collected from different spots on each sample. The regions with similar colours (e.g. black) were not homogeneous and did not necessarily give similar spectra and composition. The spectra obtained for all samples were characterised mainly by the presence of aluminosilicates, inorganic phases and pigments [13,14].

All Raman bands together with their assignments obtained from various coloured areas on all representative samples are presented in Table 1. Typical Raman spectra of all samples recorded under microscopic conditions are shown in Figs. 5–8

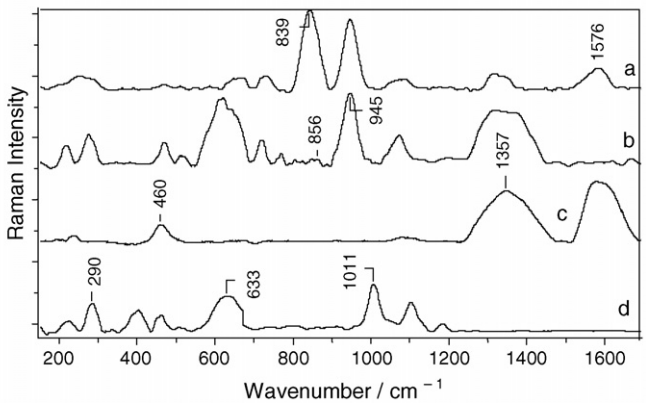

Fig. 5. Raman spectra obtained from Lydenburg shard no. 8.

Table 1
The Raman assignments of phases in the South African clay pottery

A Raman (cm^{-1})	B Raman (cm^{-1})	C Raman (cm^{-1})	D Raman (cm^{-1})	E	F	I
1576	1599		1605	Am. C[a]	C–C str	[41–43]
1358	1353		1349	Am. C	C–C str	[41–43]
1185			1175	Anhydrite	S–O str	[20,44]
1123			1125	Anhydrite	S–O str	[20,44]
1087	1082	1089		CO_3^{2-}	C–O str	[20,31,34,35]
1071	1055	1057		$CaSiO_3$	Si–O str	[13,46,45]
1011		1003		Gypsum	S–O str	[20,31,35]
	983	983		Feldspar	Si–O str	[26]
972	976			PO_4^{3-}	P–O str	[13,35]
			915	Montmor[b]	AlOH bend	[30]
856	895	863	860	$CaSiO_3$	Si–O str	[30,46]
839	821	809	836	Montmor	AlOH bend	[30]
771		793		Illite	Al–O–Si bend	[29]
729	760	746	759	CO_3^{2-}/kaolin	C–O/O–H bend	[19,31]
716	710	707	709	Illite	Al–O bend	[29]
680	685	689/671		Gypsum	S–O bend	[20,31,35]
660	660	665	650/667	Kaolin	Al–O–Si bend	[19]
633			627	Kaolin	Al–O str	[19]
	617			Rutile	Ti–O str	[20]
612		601	608	Hematite	Fe–O str	[14,16,17,20]
		538	556	Kaolin	Si–O–Al bend	[19]
509/520	511	511	504	Feldspar	Al–O–Si bend	[39]
472				Kaolin	Al–O–Si bend	[19]
460	461	464	464	Quartz/illite	Si–O–Si bend	[13,17,18,29]
	434			Rutile	Ti–O bend	[20]
405	402	403		Hematite	Fe–O bend	[14,17,20]
		400		$Ca_3(PO_4)_2$	P–O bend	[13]
	369	376	378	Quartz	Si–O bend	[18]
	333	324	358	Kaolin	O–H–O bend	[19]
290	285	288	280	Kaolin/hematite	O–H–O, Fe–O bend	[17–19]
275	278	276	278	CO_3^{2-}	C–O bend	[20,31]
246				Quartz	Si–O bend	[18]
235				Kaolin	O–H–O bend	[19]
218	222	222	220	Hematite	Fe–O bend	[20]
201			204	Kaolin	O–H–O bend	[19]

The wavenumbers are a summary of spectra obtained on all different shards in a particular collection. A, Lydenburg sample no. 8; B, Makahane sample no. 7; C, Graskop sample no. 5; D, Rooiwal sample; E, chemical phase; F, assignment; I, references.

[a] Amorphous carbon.

[b] Montmorillonite.

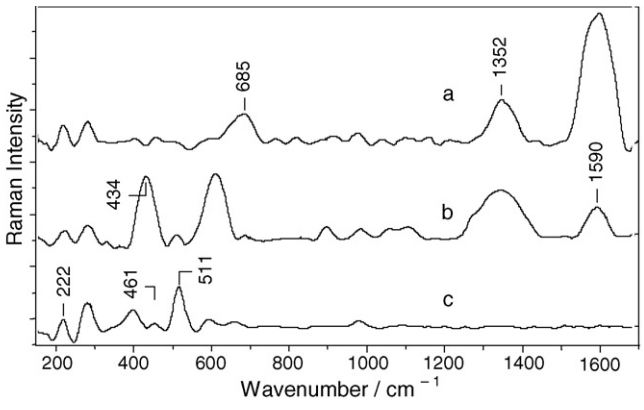

Fig. 6. Raman spectra obtained from Makahane shard no. 7.

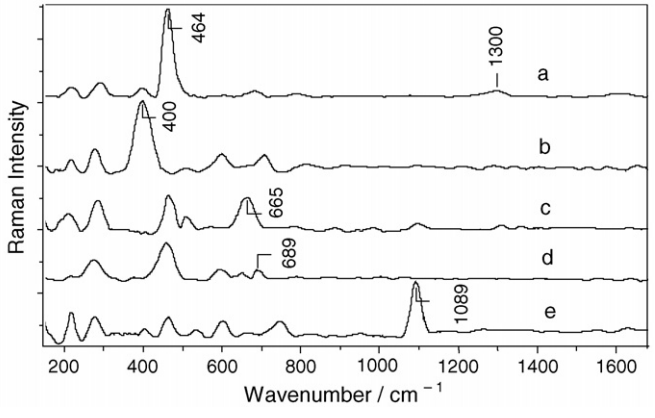

Fig. 7. Raman spectra obtained from Graskop shard no. 5.

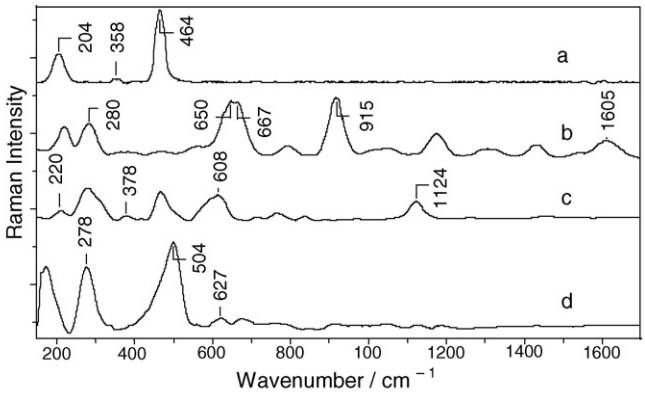

Fig. 8. Raman spectra obtained from Rooiwal shard.

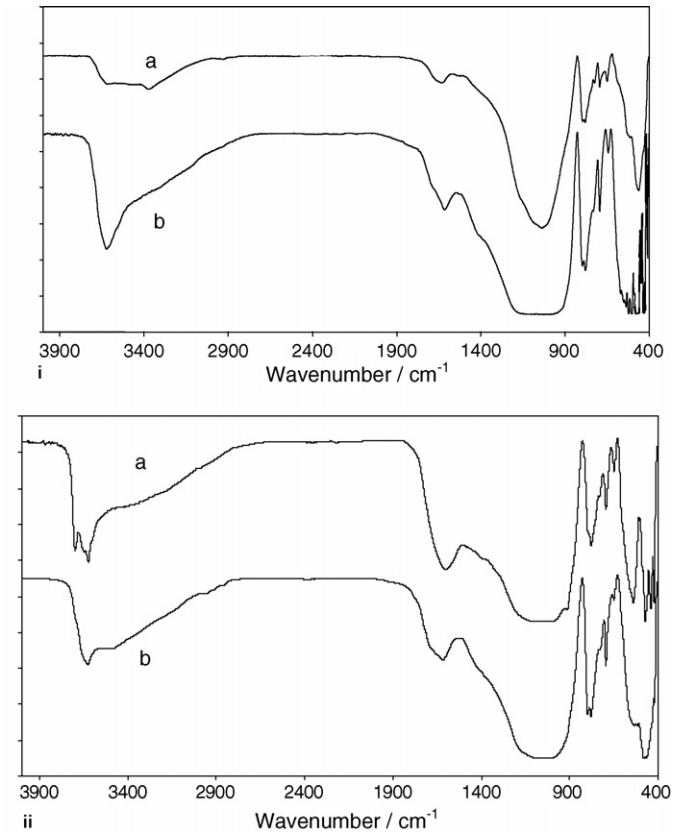

Fig. 9. (i) (a) FT-IR spectrum obtained from Makahane shard and (b) FT-IR spectrum obtained from Graskop shard. (ii) (a) FT-IR spectrum obtained from Rooiwal shard and (b) FT-IR spectrum obtained from Lydenburg shard.

for the wavenumber range 150–1700 cm^{-1}. The chemical phases detected by Raman spectroscopy in all representative samples include hematite, quartz, feldspar, kaolin, montmorillonite, illite and calcium silicate. Other phases observed in some samples are rutile, gypsum, phosphate, calcium carbonate, anhydrite, calcium silicate and amorphous carbon.

The bands around 220, 280 and 405 cm^{-1} are due to red iron(III) oxide [15–20], see Figs. 5 and 6 and Table 1. Due to the presence of the reddish areas throughout the sample and in the bulk of the body, this pigment could have been part of the starting material [21]. It also could have been added as a red pigment or in some other form, e.g. Fe_3O_4, $Fe(OH)_3$, etc., occurring naturally in clay [14,22], that was in turn converted into hematite, α-Fe_2O_3. The clay bodies and pastes used by African potters are normally brownish gray [22] in colour and various colours only develop during the process (particularly during firing). The reddish brown colour of most of the shards is due to relatively high iron oxide (α-Fe_2O_3) content. The XRF results show that the content of hematite (α-Fe_2O_3) is relatively high, $\geq$7 mass%. It has been reported that hematite is one of the most intense colouring materials. Only 1–1.5 mass% of hematite is required to give soil a reddish colour [23]. The presence of this compound is confirmed by XRD results.

The strongest Raman bands appearing around 460 cm^{-1} are due to quartz (see Figs. 7 and 8). The sandstones are most probably the natural source of quartz in this sample. These bands are normally very intense and narrow when quartz is in its free and isolated form, SiO_2 [18,13]. The presence of this band in its broadened form could be due to the slightly distorted crystal structure of quartz as it undergoes transformation during processing. Illite clay mineral also shows an intense band in the vicinity of 460 cm^{-1} and its presence will cause band overlap.

The strong intensity of the band around 460 cm^{-1} (in the Lydenburg, Graskop and Rooiwal shards) suggests high content of quartz. The FT-IR results (Fig. 9 and Table 2) also show intense absorption peaks normally associated with quartz (779 and 797 cm^{-1}) [24(a),25(a)].

The XRF and XRD results also suggest higher percentage of the quartz phase (Tables 3 and 4). The low intensity of this band (in the Makahane shard) may be an indication of the fused form of the quartz phase [18] or the breakdown in the skeletal structure of quartz as it reacts to form new phases.

The Raman spectroscopic analysis of all samples also shows the presence of kaolin clay mineral, indicated by the bands around 660 cm^{-1} [17–19]. The appearance of kaolin in the finished product suggests that the processing temperature was not high enough (i.e. $\leq$800 °C) to effect complete dissolution of this clay mineral [26]. The firing of African pottery is normally done in an open fire that reaches temperatures of around 800 °C [4]. The presence of kaolin is further confirmed by the FT-IR and XRD results (Tables 2 and 4, respectively).

Natural clay minerals often occur as mixtures [27,28]. In all samples, Raman spectroscopy showed features resembling those of illite clay mineral. The features associated with illite appear around 707 and 781 cm^{-1} [29–30]. The broad and intense band around 460 cm^{-1} could be due to the overlapping of the quartz and illite bands. The bands around 810 and 830 cm^{-1} in all representative samples are normally associated with those of montmorillonite clay mineral [30,32]. The presence of both clay minerals confirms that the firing temperatures were below 850 °C, because the skeletal structure of both illite and montmorillonite begin to break down around 850 °C [33]. FT-IR spectroscopy confirms the presence of illite and montmorillonite. The absorption bands of illite appear around 752 and 3620 cm^{-1} and that for montmorillonite around 3620 cm^{-1} (see Fig. 9(i) and Table 2).

Table 2
The IR assignments of phases in the South African clay pottery

A IR (cm^{-1})	B IR (cm^{-1})	C IR (cm^{-1})	D IR (cm^{-1})	E	F [17,19,24,48]
		3697		Kaolin	O–H str
		3654		Kaolin	O–H str
3626	3624	3624	3622	Kaolin/illite/Montmor[a]	O–H str
3429	3423	3410		Water	O–H str
1617	1622	1629	1629	Water	H–O–H bend
1080	1080	1096	1087	Amorph. Al–Si[b]	Al–O–Si str
1034	1036	1034	1035	Kaolin	Si–O–Si str
915		914	914	Kaolin	Al–O–H str
837		850	845	Illite/montmor	Al–O–H str
798	795	796	797	Quartz/kaolinite	Si–O bend
778	779	778	779	Quartz	Si–O–Si str
750	750	750	752	Illite	Al–O–Si bend
723	724	727	724	Feldspar/CO_3^{2-}	Al–O–Si str/C–O bend
695	695	694	695	Quartz/CO_3^{2-}	Si–O bend/C–O bend
652	650	645	648	Feldspar	Al–O–Si str
538	529	530	530	Kaolin/hematite	Al–O–Si/Fe–O bend
475	484	470	476	Kaolin/hematite	O–Si–O/Fe–O bend
	435	434		Kaolin	O–Si–O bend

The wavenumbers are a summary of spectra obtained for all different shards in a particular collection. A, Lydenburg sample no. 8; B, Makahane sample no. 7; C, Graskop sample no. 5; D, Rooiwal sample; E, chemical phase; F, assignment.
[a] Montmorillonite.
[b] Amorphous aluminosilicates.

Table 3
The XRF results of Graskop sample no. 5, Makahane sample no. 7, Lydenburg sample no. 8 and Rooiwal sample, given as normalised % concentration

Sample	SiO_2	Al_2O_3	Fe_2O_3	CaO	K_2O	TiO_2	MgO	P_2O_5	SO_3	Total
Graskop	51.9	28.3	13.9	0.72	2.42	1.00	0.18	0.14	0.14	98.70
Makahane	57.7	20.4	12.3	2.29	2.17	1.99	1.46	1.46	–	99.77
Lydenburg	64.0	23.8	6.93	0.92	0.99	1.56	0.88	0.007	0.253	99.34
Rooiwal	57.3	18.5	8.46	2.65	8.79	0.62	1.41	1.18	0.171	99.08

Note that heavy metals and other metals at low concentrations also occur but are not shown in this table.

The Raman spectra of all samples, except Rooiwal shard, further showed prominent features around 278 and 1087 cm^{-1}. These bands have previously been associated with calcite ($CaCO_3$) [18–20,31,34,35]. The presence of this phase further confirms the processing temperatures below 800 °C [36]. The natural sources of calcite include shells and limestone [36]. This means calcite occurs as an impurity in clays [22,37]. The XRF results suggest small amounts of calcite, below 1 mass%. Some calcite appears to have reacted with aluminosilicates to form feldspar, $(NaCa)Al(Si,Al)_3O_8$, as indicated by the XRD results. The pure calcium carbonate could not be detected by XRD, perhaps due to its low content or poor crystallinity [26]. It has been reported that calcium carbonate obtained from calcareous weathering crusts is non-crystalline [38(a)]. The FT-IR spectrum shows weak features previously associated with non-crystalline calcium carbonate at 695 and 724 cm^{-1} [24(b)].

Table 4
The XRD results on Graskop sample no. 5, Makahane sample no. 7, Lydenburg sample no. 8 and Rooiwal sample

Sample	Quartz	Feldspar	Kaolinite	Illite	Hematite
Graskop	√	√	√	√	√
Makahane	√	√	√	×	√
Lydenburg	√	√	√	√	√
Rooiwal	√	√	√	√	√

The presence of feldspar (albite) in all samples is shown by the Raman bands around 511 cm^{-1} [39], see Fig. 5 and Table 1. Absorption bands around 648 and 724 cm^{-1} manifest this phase. The identity of this feldspar is confirmed by XRD results, which further show the presence of another feldspar phase, microcline, Table 4. Albite and microcline are both known as alkali feldspar, Na and K end-member compositions, respectively, and have similar occurrence in rocks, such as granite, rhyolite, etc. [24(c),24(d)].

The intense broad bands around 1358 and 1576 cm^{-1} in the Lydenburg and Makahane shards suggest the presence of amorphous carbon [40–43]. The amorphous carbon is most likely bone black because of the corresponding peak around 970 cm^{-1}. When the bone collagen is calcined the organic matter results in carbon, while the inorganic matter forms phosphates. Therefore, the band occurring around 970 cm^{-1} is likely due to the phosphate ions [20]. The XRF results show very low content of phosphorus (Table 3) and no phosphorus compound could be detected by XRD analysis. The FT-IR spectrum showed no bands associated with phosphates perhaps due to their low con-

tent. The 1358 and 1576 cm^{-1} bands are assigned to the sp^3 and sp^2 bands of hybridised carbon [40–43], respectively, the so-called D and G bands. The ratio of intensities of these bands indicates the graphitic content of the amorphous carbon. From the relative intensities of these bands the sp^2 (G band) appear to be slightly stronger, suggesting more graphitic nature of the amorphous carbon for the Lydenburg shard. However, Fig. 5(b) shows only the D band, suggesting very low graphitic nature. It is difficult to conclude on the graphitic nature of the amorphous carbon in Makahane shard because the relative intensities of the D and G bands do not seem to follow any identifiable trend.

The Raman bands appearing around 1125 and 1175 cm^{-1} strongly suggest the presence of anhydrite ($CaSO_4$) [20,44] in Lydenburg and Rooiwal shards. This component could either have been part of the clay minerals or developed during the processing, e.g. from the dehydration of gypsum ($CaSO_4{\cdot}2H_2O$). The residual SO_3 detected by XRF may be due to oxidation of sulphur-containing compounds during firing. The XRD analysis expectedly showed no anhydrite because of its low content in the sample. Anhydrite is found as a massive rock of large extension and often occurs in natural clays [25(b)].

The Raman band that occurs around 617 cm^{-1} in the spectra of Makahane shard is characteristic of rutile (α-TiO_2) [18,20]. The relative amount of this phase as obtained from the XRF results is found to be ~2 mass%. However, it could not be detected by XRD analysis. The reason for this could be its low content or poor crystallinity. The titanium dioxide absorption spectrum shows very broad and weak bands in the region 400–1600 cm^{-1} [25(c)]. The presence of this phase suggests that the firing temperatures for Lydenburg and Makahane shards could have slightly exceeded 800 °C [18].

The presence of $CaSiO_3$ is suggested by the appearance of Raman bands around 860 and 1055 cm^{-1} [18,13,45,46] in all samples. Clays with high calcium carbonate content can form compact ceramic structures at lower firing temperatures because of the reactivity of carbonate. It easily reacts with quartz and other clay minerals to form $CaSiO_3$ [18,13]. The reaction of $CaCO_3$ often occurs at temperatures above 800 °C [36,47]. The $CaSiO_3$ phase is built of isolated $Si_3O_9^{6-}$ units between Ca^{2+} ions [18]. It is commonly associated with glassy aluminosilicates, even though it could occur in crystalline form. The presence of this phase suggests that the processing conditions were such that the carbonates were beginning to decompose into CaO and CO_2 most likely between 600 and 800 °C [26,47].

The Raman bands around 680 and 1007 cm^{-1} observed for Lydenburg, Makahane and Graskop shards are characteristic of gypsum ($CaSO_4{\cdot}2H_2O$) [20,35,36,46,48]. Gypsum is a common mineral widely distributed in sedimentary rocks and it frequently occurs interstratified with limestone and shales [38(b)].

The Raman spectrum (Fig. 7(b)) of the Graskop shard shows a distinct intense band around 400 cm^{-1}. This band occurs in the region for the E_g vibration mode of hematite. However, its strong intensity relative to the bands around 220 and 280 cm^{-1} makes its assignment uncertain. Table 5 gives a summary of all the chemical phases identified by Raman spectroscopy in all representative samples.

Table 5
The chemical phases identified by Raman spectroscopy in each representative sample

Compound	Lydenburg	Makahane	Graskop	Rooiwal
Kaolin	√	√	√	√
Hematite	√	√	√	√
Quartz	√	√	√	√
Feldspar	√	√	√	√
Carbonates	√	√	√	×
Montmorillonite	√	√	√	√
Illite	√	√	√	√
Gypsum	√	√	√	×
Anhydrite	√	×	×	√
$CaSiO_3$	√	√	√	√
Amorph. carbon	√	√	×	√
Phosphates	√	√	×	×
Rutile	×	√	×	×

4. Conclusion

Raman spectroscopy has been successfully used to determine the composition of African clay pottery shards from a selected number of South African archaeological sites (Lydenburg, Makahane, Graskop and Rooiwal). Despite the low Raman scattering effects of clay components and fluorescence commonly associated with this type of samples, important results were obtained in this study. A total of 13 chemical phases were identified by Raman spectroscopy in the samples investigated. The identification of so many chemical components in the low temperature fired clay products demonstrates the high sensitivity and applicability of Raman spectroscopy to these type of samples.

All representative shards (Lydenburg sample no. 8, Makahane sample no. 7, Graskop sample no. 5 and Rooiwal sample) from the four locations contained common features, which are characterised by kaolin, illite, quartz, feldspar, hematite, montmorillonite and $CaSiO_3$. The reason for this could be that the clay minerals and pottery making process did not vary significantly in the region that included the locations from which the samples were obtained. The potters could also have used common clay quarries.

The results confirmed that the samples under investigation were fired at lower temperatures, as indicated by the presence of clay minerals (kaolin, montmorillonite and illite). A minimum of two clay minerals was observed in each sample, which proves that the clay minerals in the locations investigated occur as mixtures. The presence of calcium carbonate in Lydenburg, Makahane and Graskop shards suggests that the pottery from which the shards were derived were fired at temperatures below 800 °C. The Makahane shard further shows the presence of rutile. This compound has been reported as a high temperature phase, which is formed between 800 and 1100 °C. The raw materials could also have been mixed with TiO_2 in rutile form. Therefore, it is likely that the firing temperature for Makahane shard reached some value above 800 °C. The pottery could have been fired at that high temperature for a short time, thus preserving the structures of calcium carbonate and clay minerals.

The compounds that gave the samples reddish brown and black colours are hematite and amorphous carbon, respectively.

Other compounds, which were observed in various samples, either occurred as impurities in the clay minerals (e.g. gypsum) or were formed during the firing process (e.g. anhydrite, calcium silicate and phosphates).

For the samples analysed, the results further showed that there is an overlapping of components between the sites and that no chemical species was unique to any one particular site. Due to its ability to detect various chemical species in low temperature fired clay products (as shown in this study), Raman spectroscopy can be useful in determining the raw materials used, processing conditions and discrimination based on unique chemical compounds.

Acknowledgements

The financial support by the National Research Foundation in Pretoria and the University of Pretoria is gratefully acknowledged. The authors would also like to thank Annette Weitz from the Centre for Indigenous studies for the supply of samples and historical information.

References

[1] J. Poblome, P. Degryse, W. Viaene, R. Ottenburgs, M. Waelkans, R. Degeest, J. Noud, J. Archaeol. Sci. 29 (2002) 873.
[2] R.J.H. Clark, Chem. Soc. Rev. 24 (1995) 187.
[3] R. Davey, D.J. Gardiner, B.W. Singer, M. Spoke, J. Raman Spectrosc. 25 (1994) 53.
[4] C.A. Bollang, J.C. Vogel, L. Jacobson, W.A. van der Westhuizen, C.G. Sampson, J. Archaeol. Sci. 20 (1983) 41.
[5] G.V. Robins, C. del Re, N.J. Sedey, A.G. Davis, J.A.A. Hawari, J. Archaeol. Sci. 10 (1983) 385.
[6] C.R. Ferring, T.K. Perttula, J. Archaeol. Sci. 14 (1987) 437.
[7] P.S. Peacock, J. Archaeol. Sci. 3 (1976) 271.
[8] Labspec, version 2.04, Distributed by Dilor SA & Universite' de Reims, France, 1997.
[9] S. Verryn, Details of XRD Procedure Used at the University of Pretoria, XRD Laboratory, Personal Written Communication, University of Pretoria, Pretoria, 2002.
[10] M. L. Loubser, (Typed) Report on XRF Analyses of Ceramics. mloubser@postino.up.ac.za, June 20, 2002.
[11] H. Bennet, G. Oliver, XRF Analysis of Ceramics, Minerals and Applied Materials Wiley, Chichester, 1997, p. 37.
[12] J.S. Watson, X-ray Spectrum 25 (1996) 173.
[13] P. Colomban, F. Treppoz, J. Raman Spectrosc. 32 (2001) 93.
[14] J. Zuo, C. Xu, C. Wang, Z. Yushi, J. Raman Spectrosc. 30 (1999) 1053.
[15] H.G.M. Edwards, C.J. Brooke, J.K.F. Tait, J. Raman Spectrosc. 28 (1997) 95.
[16] D. Crossley, Post-Medieval Archaeology in Britain, Leicester University Press, Leicester, 1990, p. 188.
[17] D. Bikiaris, S. Daniila, S. Sotiropoulou, O. Katsimbiri, E. Poulidou, P. Moutsatsou, Y. Chryssoulakis, Spectrochim. Acta Part A 56 (1999) 3.
[18] N.Q. Liem, G. Sagon, V.X. Quang, H. Van Tan, P. Colomban, J. Raman Spectrosc. 31 (2000) 933.
[19] R.L. Frost, P.M. Fredericks, J.R. Bartlett, Spectrochim. Acta Part A 49 (1993) 667.
[20] H.G.M. Edwards, E.M. Newton, J. Russ, J. Mol. Str. 550–551 (2000) 245.
[21] D. Hradil, T. Grygar, J. Hradilova, P. Bezdička, Appl. Clay Sci. 22 (2003) 223.
[22] G.W.A. Nyakairu, H. Kurzwell, C. Koeberl, J. Afri. Earth Sci. 35 (2000) 123.
[23] U. Schwertmann, in: J.M. Bigham, E.J. Ciolkosz (Eds.), Soil Color, vol. 31, Soil Science Society of American Special Publication, Madison, Wiscons, 1993, p. 51.
[24] (a) M.J. Wilson, Clay Mineralogy: Spectroscopic and Chemical Determinative Methods, Chapman and Hall, London, 1994, p. 52;
(b) M.J. Wilson, Clay Mineralogy: Spectroscopic and Chemical Determinative Methods, Chapman and Hall, London, 1994, p. 55;
(c) M.J. Wilson, Clay Mineralogy: Spectroscopic and Chemical Determinative Methods, Chapman and Hall, London, 1994, p. 33;
(d) M.J. Wilson, Clay Mineralogy: Spectroscopic and Chemical Determinative Methods, Chapman & Hall, London, 1994, p. 34.
[25] (a) H.W. van der Marel, H. Beutelspacher, Atlas of Infrared Spectroscopy of Clay Minerals and their Admixtures, Elsevier Scientific Publishing Company, Amsterdam, Oxford, New York, 1976, p. 234;
(b) H.W. van der Marel, H. Beutelspacher, Atlas of Infrared Spectroscopy of Clay Minerals and their Admixtures, Elsevier Scientific Publishing Company, Amsterdam, Oxford, New York, 1976, p. 249;
(c) H.W. van der Marel, H. Beutelspacher, Atlas of Infrared Spectroscopy of Clay Minerals and their Admixtures, Elsevier Scientific Publishing Company, Amsterdam, Oxford, New York, 1976, p. 259.
[26] J.M. Alia, H.G.M. Edwards, F.J. Garcia-Navaro, J. Parras-Armenteros, C.J. Sanchez-Jimenez, Talanta 50 (1999) 291.
[27] L. Jankovič, P. Komadel, J. Catal. 218 (2003) 227.
[28] F. Kooli, W. Jones, Clay Miner. 32 (1997) 633.
[29] W. Liu, Water Res. 35 (2001) 4111.
[30] R.L. Frost, L. Rintoul, Appl. Clay Sci. 11 (1996) 171.
[31] V.C. Farmer, in: H. Van Olphen, J.J. Fripiat (Eds.), Data Handbook for Clay Minerals and Other Non-metallic Minerals, Pergamon, Oxford, 1979, p. 307.
[32] R.L. Frost, J.T. Kloprogge, Spectrochim. Acta Part A 56 (2000) 2177.
[33] E. Ingerson, in: F. Bruce, Bohor (Eds.), High Temperature Phase Development in Illitic Clays, Proceedings of the 12th National Conference, Monograph No. 19, Pergamon, New York, 1971, p. 233.
[34] E.E. Coleyshaw, W.P. Griffith, R.J. Bowell, Spectrochim. Acta Part A 50 (1994) 1909.
[35] I.A. Degen, G.A. Newman, Spectrochim. Acta Part A 49 (1993) 859.
[36] M.M. Jordan, T. Sanfeliu, C. de la Fuente, Appl. Clay Sci. 20 (2001) 87.
[37] P. Valfre, Yixing Teapots for Europe, Edition Exotic Line, Janvier, China, 2000, p. 387.
[38] (a) C.S. Hurlbut Jr., C. Klein, Manual of Mineraology, 19th ed., John Wiley and Sons Inc., New York, 1971, p. 431;
(b) C.S. Hurlbut Jr., C. Klein, Manual of Mineraology, 19th ed., John Wiley and Sons Inc., New York, 1971, p. 322.
[39] R. Gout, E.H. Oelkers, J. Schott, A. Zwick, Geochim. Cosmochim. Acta 61 (1997) 3013.
[40] M. Tabbal, T. Christidis, S. Isber, M.A. El Khakani, P. Merel, M. Chaker, Thin Solid Films 453–454 (2004) 234.
[41] R.N. Tarrant, D.R. McKenzie, M.M.M. Bilek, Diamond Relat. Mater. 13 (2004) 1422.
[42] K. Lee, H. Sugimura, Y. Inoue, O. Takai, Diamond Relat. Mater. 13 (2004) 507.
[43] J.C. Orlianges, C. Champeaux, A. Catherinot, Th. Merle, B. Angleraud, Thin Solid Films 453–454 (2004) 285.
[44] C.H. Chio, S.K. Sharma, D.W. Muenow, Am. Miner. 89 (2004) 390.
[45] B. Mihailova, E. Dinolova, L. Konstantinov, J. Non-Crystal. Solids 191 (1995) 79.
[46] C.D. Yin, M. Okuno, H. Morikawa, F. Marumo, T. Yamanaka, J. Non-Crystal. Solids 80 (1986) 167.
[47] J.V. Owen, J. Archaeol. Sci. 24 (1997) 301.
[48] R.R. Shagidullin, A.V. Chernova, V.S. Vinogradova, F.S. Mukhametov, Atlas of IR Spectra of Organophosphorus Compounds (Interpreted Spectrograms), Kluwer Academic Publishers, Boston, 1990, p. 14.

CHAPTER 5

Raman analysis of red-brown and gray shards from 16th and 17th century Portuguese shipwrecks

The chapter contains an article published in "Crystal Engineering"

Available online at www.sciencedirect.com
SCIENCE DIRECT®

Crystal Engineering 6 (2003) 287–299

Crystal Engineering

www.elsevier.com/locate/cryseng

Raman analysis of red-brown and gray shards from 16th and 17th century Portuguese shipwrecks

M.A. Legodi, D. de Waal *

Department of Chemistry, University of Pretoria, Pretoria 0002, South Africa

Received 19 December 2003; accepted 10 April 2004

Abstract

The artifacts under investigation (three red clay shards, two gray clay shards and a red clay teapot) are from the J A Van Tilburg museum at the University of Pretoria (UP). The large red clay shard was recovered from the 1552 Portuguese shipwreck, São João, found in the region of Port Edward, South Africa. The other shards were recovered from the 1622 Portuguese shipwreck, the São João Baptista, which sank around Kenton-on-sea off the South African coast. The results from these are compared to those obtained from the analysis of a red-brown teapot. The oldest of this type of teapot was made in China during the second half of the 18th century. Raman spectroscopy has proven to be a useful tool for qualitative determination of the composition of these clay artifacts. The red clays were characterized by the presence of hematite, kaolin, quartz, amorphous carbon and aluminosilicates. The results of the clay teapot differed from those of red clay shards in that no quartz Raman bands were observed for the clay teapot. The gray clay shards were characterized mainly by the presence of quartz, kaolin, amorphous carbon and aluminosilicates. The presence of mullite in all samples could not be ascertained unambiguously using Raman spectroscopy. The pigments found in the investigated samples are hematite (α-Fe_2O_3) (for red samples) and amorphous carbon (for both red and gray samples).

Keywords: Raman; Shipwreck; Clay shard; South Africa; China

* Corresponding author. Tel.: +27-12-4203099; fax: +27-12-3625297.
E-mail address: danita.dewaal@up.ac.za (D. de Waal).

1463-0184/$ - see front matter
doi:10.1016/j.cryseng.2004.04.005

1. Introduction

The red iron oxides were widely used as pigments since antiquity because of their rich variety of shades and for the fact that they are not fugitive. Moreover, these pigments are highly variable in texture, lustre and hardness [1]. The red iron oxides (αFe_2O_3) are the most thermally stable of all iron oxide pigments [2]. They could be acquired during firing from siennas (FeOOH) or added to starting materials such as red ochre or synthetic hematite. These oxides also occur in soils and are normally mixed with a variety of clay minerals, e.g. kaolins.

The identification of pigments on artworks are important for conservation and restoration, characterization of materials, dating and authentication [3].

The most important clay minerals reportedly used in China since ancient times are the kaolin group minerals [4] and are also referred to as 1:1 phyllosilicates. They are layered silicates with the form 1:1 t–o (tetrahedral–octahedral) layered structures, and are triclinic [5]. Kaolin is a group of minerals with particles predominantly <2 μm in size, neutral and thus chemically stable. This group includes kaolinite, halloysite, nacrite and dickite all with the same chemical formula, $Al_2Si_2O_5(OH)_4$, but differing in structure and arrangement of aluminosilicate layers in the unit cell [4,5]. It is rare to find dickite and nacrite because these occur in small quantities in nature [6]. Kaolinite and halloysite are commercially significant and are used separately or as mixtures. These generally form the highest percentage of the clay used in making artifacts, because they are readily available in nature [6]. Kaolins are the major starting materials in the production of clay wares [7]. During firing at higher temperatures (above 1200 °C) these are transformed into mullite ($3SiO_2{\cdot}2Al_2O_3$) [8]. The presence of kaolins in the finished product suggests that the artifact was not fired at high enough temperatures to effect complete phase transformation [7].

Quartz (α-SiO_2) is normally part of raw materials used in clay pottery making. It occurs in the form of sand particles, pebbles or flint [9]. During high temperature firing, it is converted into tridymite or cristobalite depending on the form of quartz used [8]. For instance, cristobalite is formed when flint is fired at higher temperatures (1070 °C). To obtain vitrification of the silicium and flux present in the clay, very high temperatures are required around 1100–1300 °C [10]. These are the temperatures at which cristobalite and tridymite are formed from quartz. The observance of quartz peaks in the finished product and absence of its higher temperature phases (above) show that the object was not fired at high enough temperatures to transform its particles. Quartz peaks may be overshadowed by the broad bands of high content of amorphous aluminosilicates (e.g. glassy phase). The small amount and crystal size of quartz may make it difficult to detect its bands in the Raman spectrum [11,12].

As a non-destructive technique, Raman spectroscopy does not require any sample preparation [13]. Raman spectroscopy with its high reliability, sensitivity and specificity [14] has become the instrument of choice when analyzing archaeological artifacts and pigments on art works [15]. It probes those vibrational transitions involving polarizability changes.

Fig. 1. The ceramic artifacts analyzed (sample nos. 1–6). Sample no. 1 was recovered from the São João shipwreck, nos. 2–5 from São João Baptista shipwreck and no. 6 is a ceramic teapot originating from the 19th century China.

A number of artifacts kept in the Van Tilburg Museum at University of Pretoria were recovered from two shipwrecks off the South African coast. The Portuguese ships were from Asia en route to Europe. The artifacts under investigation included three red clay shards, two gray clay shards and a clay teapot shown in Fig. 1. The large red clay shard (no. 1) was recovered from the 1552 shipwreck, of the Portuguese ship called São João, which sank around Port Edward off the South African coast. The other shards were recovered from the 1622 Portuguese shipwreck, the São João, which sank around Kenton-on-sea off the South African coast. The clay teapot was made in China during the 18th century [10]. Due to the historic value of these samples, they need to be handled with care. Furthermore, the colouring materials for all samples seem to have been mixed entirely with the bulk material and not applied only on the surface.

The main objective of this study was to determine the composition of the above-mentioned clay artifacts and to investigate the presence and types of pigments (particularly the iron oxides) used for red and black colouring. The study will further contribute to the realization of Raman spectroscopy as a tool in the analyses of ceramic artifacts. The results obtained here will then be deposited to a database of ancient Chinese clay artifacts.

Table 1
List of the names, origins and descriptions of clay samples analyzed

Figure name	Origin	Description
Fig. 1, no. 1, large red clay	São João	Red with white tinge, small dents around body.
Fig. 1, no. 2 round red clay	São João Baptista	Red with white tinge, small dents around body.
Fig. 1, no. 3 small red clay	São João Baptista	Red with white tinge, small dents around body.
Fig. 1, no. 4 large gray clay	São João Baptista	Gray and black, small dents around the body.
Fig. 1, no. 5 small gray clay	São João Baptista	Gray and black, small dents around the body.
Fig. 1, no. 6 red clay pot	Chinese origin	Deep bright red.

2. Experimental

2.1. Samples

The samples analyzed are shown in Fig. 1 and described in Table 1.

2.2. Raman spectroscopy

The sample was placed on the stage of an Olympus confocal microscope and excited with 514.5 nm radiation from Coherent model Innova 300 argon ion laser. Scattered light was dispersed and recorded by means of a Dilor XY multichannel Raman spectrometer equipment with a liquid nitrogen-cooled charge-coupled detector. The spectral resolution was 3 cm^{-1}. The laser output power at the source was 100–150 mW. The wavenumber range of detection/analysis was from about 200 to 1700 cm^{-1} with 180 s collection time and three accumulations on each sub-region.

3. Results and discussion

When viewed under the microscope, each object appeared to have differently coloured regions. The predominant colours on the red shards were black, red and uncoloured; on the gray shards, black and uncoloured and on the teapot, red and uncoloured. This is normally an indication of the composite nature of clay products. A range of spectra were collected from different spots on each sample. The regions with similar colours (e.g. black) were still not homogeneous and did not give the same spectra nor compositions at all times. The spectra as described below were characterized mainly by the presence of quartz, aluminosilicates and pigments [14,15].

3.1. São João shipwreck sample

3.1.1. Large red shard

The red and black particles on the large red shard (no. 1) showed the presence of Raman bands at 226, 292, 407, 461, 603, 677, 737, 785, 967, 1021, 1058, 1124, 1163, 1325 and around 1600 cm^{-1} (Fig. 2a–d). The bands at 226(m), 292(s), 407(m)

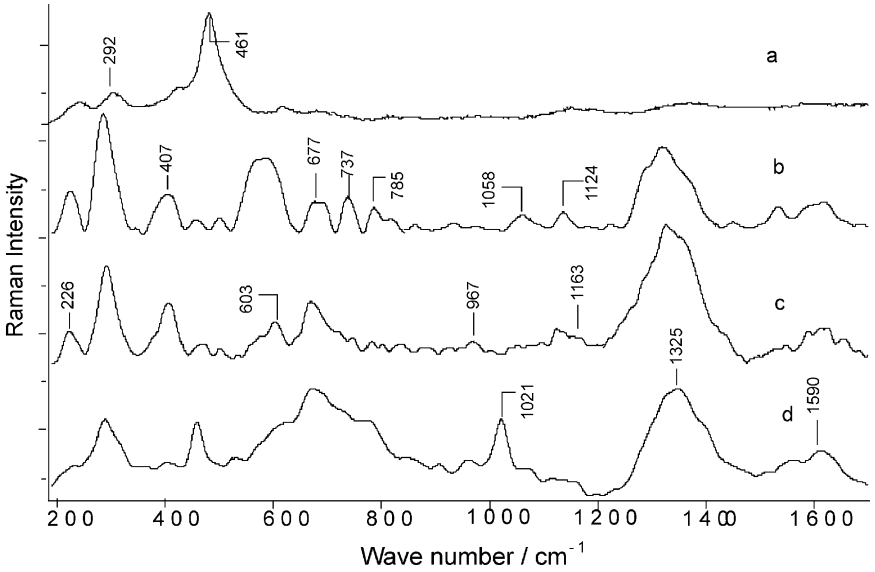

Fig. 2. Representative Raman spectra obtained on large red shard (sample no. 1). Typical components which could be identified were: a—hematite and quartz; b—hematite, kaolin, amorphous aluminosilicates and carbon; c—hematite, anhydrite, quartz and amorphous aluminosilicates and carbon; and d—anhydrite, amorphous aluminosilicates and carbon.

and 603(w) cm^{-1}, match closely those of red iron oxide (α-Fe_2O_3) [12,15,16]. These hematite characteristic bands were previously assigned to A_{1g} (226 cm^{-1}), E_g (292 cm^{-1}) and E_g (407 and 603 cm^{-1}) [16]. Also identified were kaolin bands due to Al–O symmetric stretching at 677 cm^{-1} [14,17], O–H bending vibration at 737 and 785 cm^{-1} and the Al–OH band at around 1124 cm^{-1} [17]. The broad bands in the range 1325–1600 cm^{-1} closely resembled those of amorphous carbon [15,18]. These bands are assigned to the sp^3 and sp^2 bands of the hybridized carbon, respectively, the so-called D and G bands [19–22]. A ratio of these bands indicates the graphitic content of the amorphous carbon. From the relative intensities of these bands in Fig. 2, it is clear that there is a significantly higher amount of D carbon in the large red shard. This means the amorphous carbon in the sample has a low graphitic content. The uncoloured areas gave high fluorescence background. The 677 cm^{-1} band was very broad and it appeared to comprise the Al–O–Si stretching band (characteristic of kaolins) which normally occurs around 658 cm^{-1} [15]. It is well known that some kaolin clay minerals, particularly kaolinite, show refractory characteristics [12]. Therefore, the detection of its structural O–H bending modes even after firing of the clay product shows that it was not completely decomposed. The appearance of a band resembling that of mullite (967 cm^{-1}, Fig. 1c) might mean that the firing occurred above 1200 °C. However, this band shows too low an intensity to be assigned with certainty. The assignment of this band could also be $\nu_1(A_g)$ mode of phosphate ion [3,23,24]. When this band appears together with

the amorphous carbon bands, it suggests that animal bones were used as part of the raw material. On calcinations, bone collagen forms carbon but the inorganic matrix forms phosphate ions with characteristic Raman bands in the region ~965 cm^{-1} [3,23]. This further implies that bone charcoal was used in the kiln as colourant. The sample also shows the strong presence of crystalline quartz characterized by the strong band at 461 cm^{-1}. The band at 1058 cm^{-1} could be due to the $\nu_1(A_{1g})$ mode of the carbonate ion [3,24] (Fig. 1a). The band at 1021 cm^{-1} is characteristic of $\nu_1(A_g)$ mode of the anhydrite ($CaSO_4$) [3,25]. The above assignments were confirmed by comparison of the observed spectra with reference data available for hematite, kaolin minerals and amorphous carbon [1,13–15, 16–18,26–29]. The identification of components in this shard is thus certain, except for mullite and the phosphate ion.

3.2. São João Baptista shipwreck samples

Two red shards (round, no. 2 and long, no. 3) and two gray shards (large, no. 4 and small, no. 5) from this wreck were investigated.

3.2.1. Round red clay shard

The results obtained for the black and red grains on the round shard showed features of hematite, kaolin, quartz, anhydrite ($CaSO_4$) and amorphous carbon (Fig. 3a–d) as assigned in Table 2. Generally, the spectra of the round red shard shows equal intensity bands at 1351 and 1596 cm^{-1}. This is an indication of a more or less equal amount of the sp^3 and sp^2 (amorphous and graphitic carbon characteristic, respectively) band characteristic in the amorphous carbon. This sample might contain mullite even though the associated band (954 cm^{-1}) shows a very low intensity and overlaps the broad bands which are typical of amorphous aluminosilicates. The other possible assignment for this band is phosphate ions [3,23].

3.2.2. Long red clay shard

The Raman spectra of the long clay shard (Fig. 4) also contained features of hematite, quartz, kaolin and amorphous carbon (Table 2). From Fig. 4, it is difficult to ascertain the true characteristics of the amorphous carbon, because some areas show low graphitic carbon (Fig. 4c) and others high graphitic carbon (Fig. 4a, b). Furthermore, the presence of mullite is again uncertain because of the low intensity of the band ascribed to it (958 cm^{-1}). The appearance of the 958 cm^{-1} band could also be due to phosphate ion which is closely linked to the amorphous carbon [3,23].

The Raman results showed similar composition for the two red shards (Figs. 3 and 4). The slight differences appeared to be brought about by the presence of additional bands at 1023 cm^{-1}. The broadening of 676 cm^{-1} band in Fig. 4 suggests that the crystalline kaolin is distorted to some extent. This band, at 676 cm^{-1}, together with the one at 1159 cm^{-1}, is rather broad which suggests the presence of amorphous aluminosilicates common in the fired clay products [12]. The band at 1023 cm^{-1} is narrower and high in intensity suggesting the presence of a highly crystalline substance. This feature together with the medium intensity band around

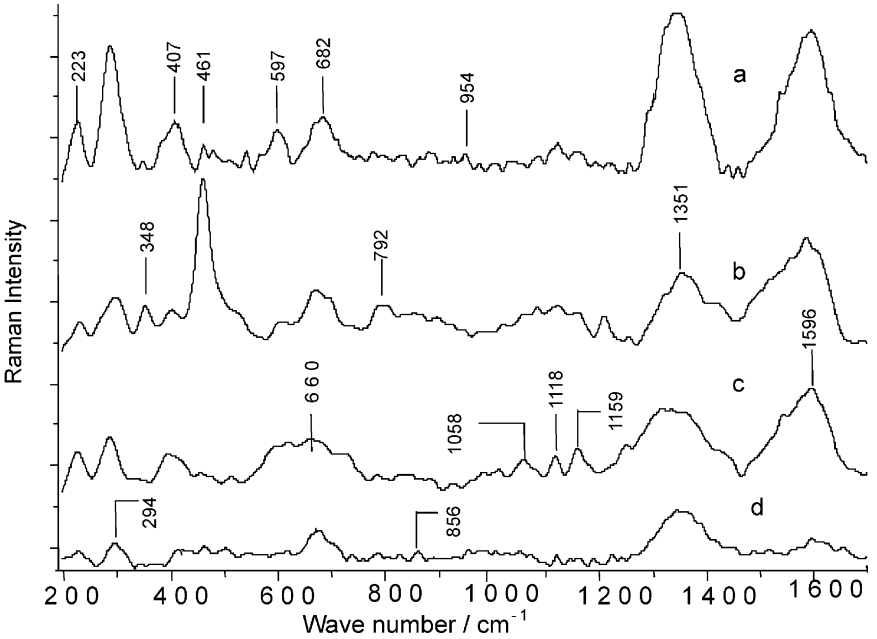

Fig. 3. Representative Raman spectra obtained from the round red shard (sample no. 2). Typical components which could be identified were: a—hematite, kaolin, quartz and amorphous carbon; b—hematite, kaolin, quartz and amorphous carbon; c—hematite, kaolin, amorphous carbon and aluminosilicates; and d—hematite, amorphous carbon and aluminosilicates.

1160 cm^{-1} is characteristic of the anhydrite ($CaSO_4$) [17,25]. The two red shards from the São João Baptista shipwreck show the presence of similar components. Although it is known that kaolin transforms into mullite at higher firing temperature (>1200 °C) [9], the feature around 960 cm^{-1} on these Raman spectra could not be assigned with certainty to mullite because of its weak intensity and the band broadening due to amorphous aluminosilicates. The band at 960 cm^{-1} could also be due to the phosphate ions resulting from the calcinations of animal bones.

3.2.3. *Large gray clay shard*

The Raman spectra of the black coloured grains observed on the large gray shard (Fig. 5) showed features of quartz (461 cm^{-1}) [12,17], kaolin (679, 1117 cm^{-1}) [14], amorphous aluminosilicate (502, ~960 cm^{-1}) [10,12,18] and amorphous carbon (1367, 1598 cm^{-1}) [15,17,18]. No red regions were observed here under the microscope. The presence of an aluminosilicate glassy phase was manifested by the appearance of broad Raman bands (Fig. 5a–c). In Fig. 5a, the relatively higher amount of G band (1598 cm^{-1}) points to the presence of graphitic carbon. The appearance of the band around 965 cm^{-1} suggested the presence of mullite, and this could mean that kaolin was used as part of the raw materials and that the firing temperature exceeded 1200 °C [7]. Alternatively, the 965 cm^{-1} band could be

Table 2
The Raman band assignments of phases in ancient Chinese clay artifacts. The following frequencies (cm^{-1}) are a summary of spectra obtained for all different grains/areas on a particular sample

Large red (cm^{-1})	Round red (cm^{-1})	Long red (cm^{-1})	Clay pot (cm^{-1})	Small gray (cm^{-1})	Large gray (cm^{-1})	Phase	Assignments	References
226m	223m	227w	225s			H	Fe–O (A_{1g})	[2,11,15,17]
					268w,b	CO_3^{2-}	C–O	[24,29]
292s	294s	295s	292m			H	Fe–O (E_g)	[2,11,15,17]
	348w		349w	334w	335w,b	Q	Si–O	[12]
407m	407m,b	407m	407w			H	Fe–O–Fe (E_g)	[2,11,15,17]
				417m		G	$\nu_2(A_g)$ S–O	[24]
461ss	461ss	459ss		463ss	461ss	Q	Si–O–Si	[4, 11, 13]
				492w,b	502b	Al–Si	Si–O ($Q^2 = SiO_2$)	[12,28]
					571			
603m	597m,b	609w	606w			H	Fe–O (E_g)	[2,11,15,17]
				621m,b		Al–Si	Si–O ($Q^2 = SiO_2$)	[12,28]
677m	682m,b	676s,b	676s	667m	679s,b	K	Si–O–Al	[11,14,20]
737m					743b	K	O–H	[14]
785w	792w,b	784m,b	800s,b		772w	K	O–H	[14]
		822m,b	823s,b			Al–Si	Si–O ($Q^2 = SiO_2$)	[12,28]
					878w,b	Al–Si	Si–O ($Q^2 = SiO_2$)	[12,28]
967vw	954vw	958vw		952vw	965m,b	M/PO_4^{3-}	Si–O/$\nu_1(A_g)$ P–O	[7,10,18,24]
				1007ss		G	$\nu_1(A_g)$ S–O	[3,25]
1021m		1023s			1013b	A	$\nu_1(A_g)$ S–O	[20]
1058m	1058m				1076b	CO_3^{2-}	$\nu_1(A_{1g})$ C–O	[3,24]
1124m	1118m	1128m,b		1121s	1117w	K	Si–O	[14]
1163w	1159m	1159s,b		1169s	1174vw	A and K	S–O and Si–O ($Q^1 = SiO_3$)	[14,26]
1325b	1351b	1356b	1353b	1358b	1367b	C	C	[15,18,19]
1590b	1596b	1585b	1589b	1596b	1598b	C	C	[15,18,26]

H, hematite; Q, quartz; K, kaolin; Al–Si, amorphous aluminosilicates; M, mullite; A, anhydrite ($CaSO_4$); G, gypsum; C, amorphous carbon; and Q^1 and Q^2, SiO_3 and SiO_2 silica tetrahedral unit with one and two bridging oxygens, respectively.
ss, very strong; s, strong; m, medium; w, weak; and b, broad.

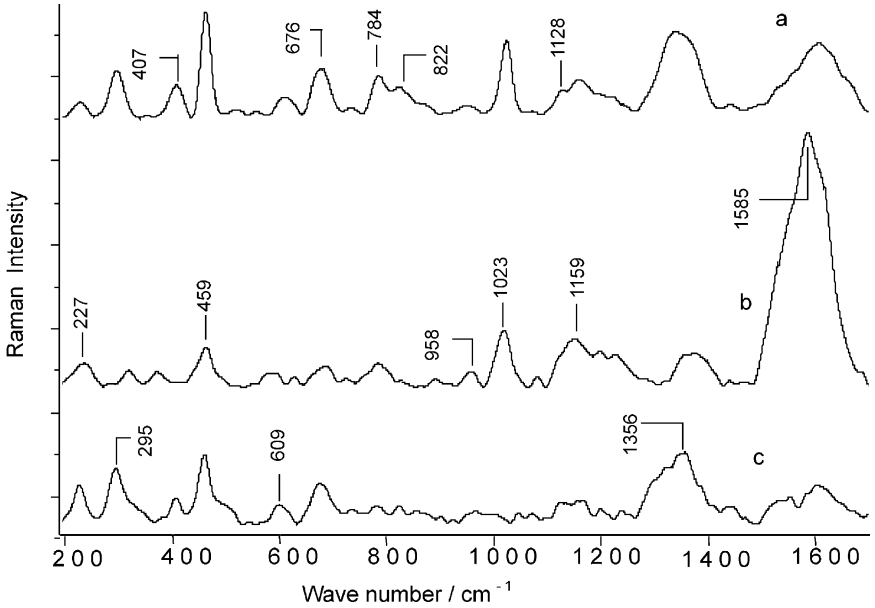

Fig. 4. Representative Raman spectra obtained on long red shard (sample no. 3). Typical components which could be identified were: a—hematite, quartz, kaolin, and amorphous carbon and aluminosilicates; b—kaolin, quartz, mullite, anhydrite, amorphous aluminosilicates and carbon; and c—hematite, quartz and amorphous carbon.

due to the phosphate ions that resulted from the calcinations of carbon source (possibly animal bones). Fig. 5a further shows a band around 1013 cm^{-1} (even though slightly lower) which is closest to the $\nu_1(A_g)$ mode in anhydrite ($CaSO_4$) [3,24]. The assignment of the band at 1076 cm^{-1} is uncertain. The authors suggest this band to be due to the $\nu_1(A_{1g})$ carbonate mode particularly when it is accompanied by the band at 268 cm^{-1} [3,23,29]. The band at 571 cm^{-1} could not be assigned.

3.2.4. *Small gray clay shard*

The Raman spectrum obtained from some black grains of the small clay shard (Fig. 6b) is dominated by broad features throughout the frequency range of analysis (200–1700 cm^{-1}). This suggested the presence of amorphous rather than crystalline aluminosilicates. However, the bands appearing above the broad features around 1120 cm^{-1} suggested that kaolin clay mineral was used as part of the raw materials [14]. The analysis of other black grains (Fig. 6a, b) confirms the presence of kaolin, indicated by bands at 667 and 1121 cm^{-1} [10: p. 129]. The intense and narrow band around 463 cm^{-1} (Fig. 6c) indicated the presence of crystalline quartz (α-SiO_2) [12]. No red grains were observed. The characteristic bands of amorphous carbon (1358, 1596 cm^{-1}) were also evident (Fig. 6a–c). In Fig. 6, the relatively higher amount of G band (1598 cm^{-1}) points to the presence of a significant amount of graphitic car-

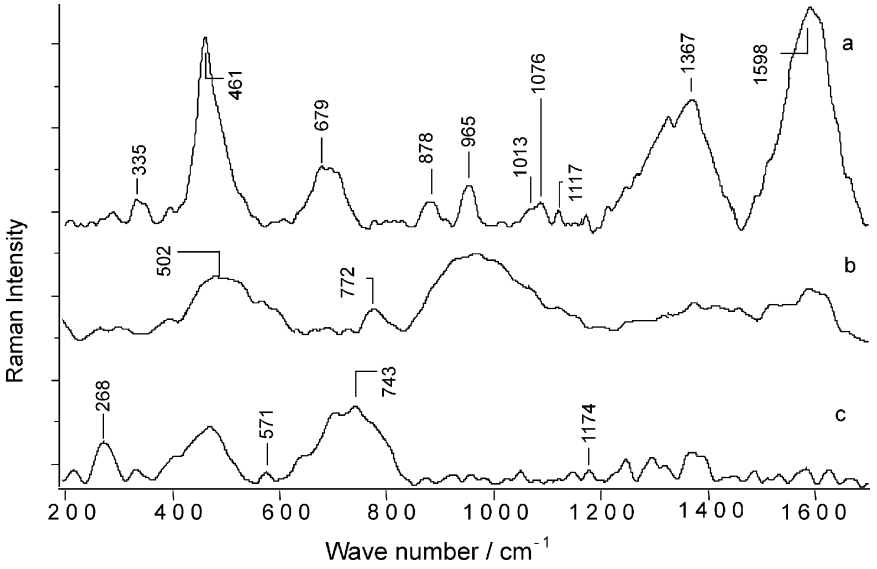

Fig. 5. Representative Raman spectra obtained on large gray shard (sample no. 4). Typical components which could be identified were: a—quartz, kaolin, mullite, anhydrite and amorphous carbon; b—amorphous aluminosilicates and kaolin; and c—kaolin and amorphous aluminosilicates.

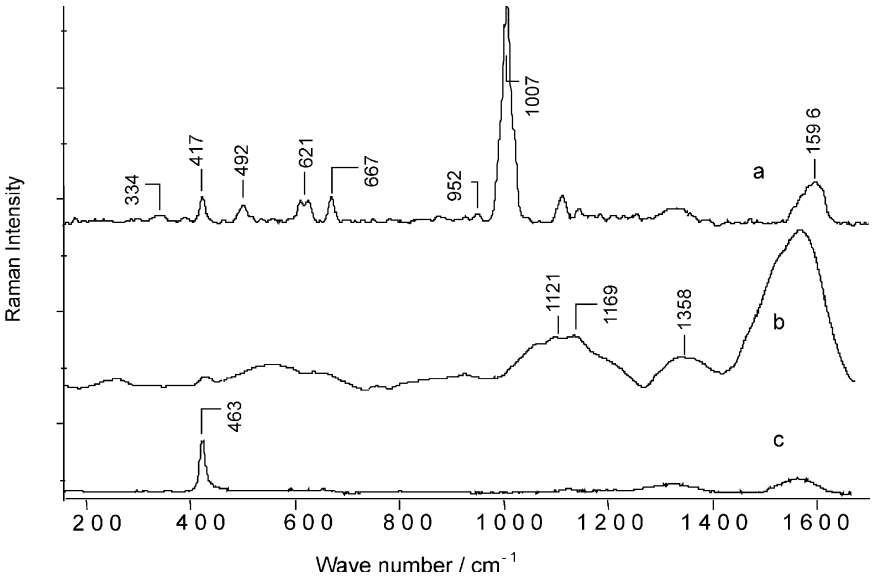

Fig. 6. Representative Raman spectra obtained on small gray shard (sample no. 5). Typical components which could be identified were: a—quartz, kaolin, mullite, anhydrite and amorphous carbon and aluminosilicates; b—kaolin, amorphous aluminosilicates and carbon; and c—quartz and amorphous carbon.

bon. The weak band appearing at 952 cm^{-1} (Fig. 6a) could be due to mullite or phosphate ions, but as a result of the weak intensity and broadening this assignment is uncertain. The most intense and narrow band appears at 1007 cm^{-1} in Fig. 6a. The bands in this region have previously been associated with the presence of $\nu_1(A_g)$ modes in gypsum ($CaSO_4 \cdot 2H_2O$) [3,25]. This assignment is further confirmed by the presence of $\nu_2(A_g)$ for gypsum at 417 cm^{-1} [24]. The Raman spectra of the uncoloured areas resulted in a high fluorescence background.

The Raman spectra of the above two gray clay shards showed no features of red iron oxides. The spectral features pointed to similar components for the two samples.

3.3. *Red clay pot of Chinese origin*

The object contained only red grains and uncoloured areas when viewed under the microscope. The spectra of the red grains showed features of hematite, kaolin, amorphous aluminosilicates and carbon (Fig. 7 and Table 1). The broadening of the bands appear to be due to the presence of amorphous aluminosilicate. The unusually lower intensity and broadening in the region of quartz could either be due to its low content or to its absence in free and crystalline form. The analysis on clear areas of the clay pot resulted in high fluorescence background.

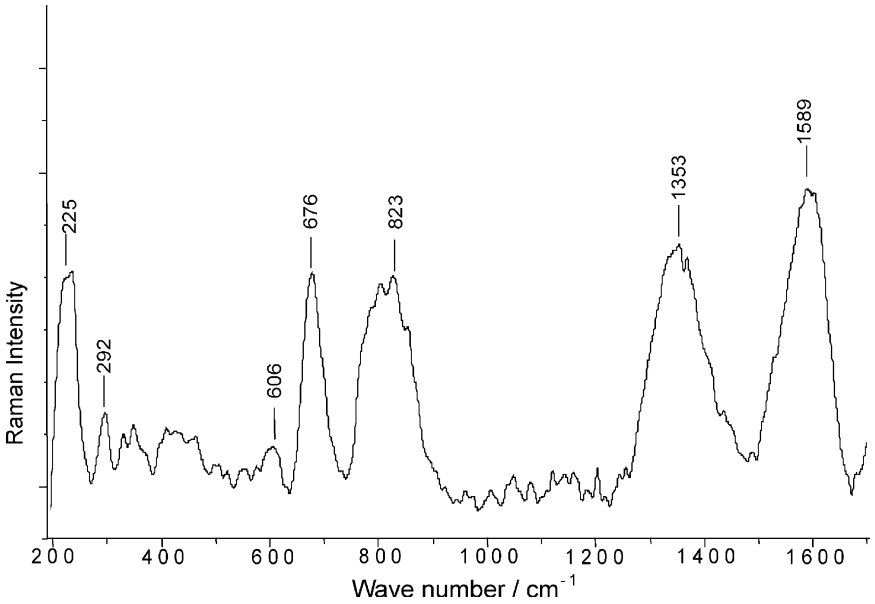

Fig. 7. Representative Raman spectrum obtained on the red clay pot (sample no. 6). Typical components identified were hematite, quartz, kaolin, amorphous aluminosilicates and carbon.

4. Conclusion

The three red clay shards (Fig. 1, sample nos. 1–3) have similar compositions characterized by the presence of kaolin, quartz, hematite, amorphous aluminosilicates and carbon. The spectrum from the red clay teapot (Fig. 1, sample no. 6) showed the presence of kaolin, hematite, amorphous aluminosilicates and carbon. The differences in the spectral features (including the absence of quartz bands in the clay teapot spectrum) of red clay shards and clay teapot are confirmed by the different visual appearances of the two sets of samples. The clay teapot appears to be more homogeneous than the red shards. The colouring materials (pigments) used on the red shards and clay teapot were hematite (red) and amorphous carbon (black). The gray clay shards (Fig. 1, sample nos. 4 and 5) showed the presence of kaolin, quartz, amorphous aluminosilicates and carbon. The colouring material or pigment detected on the gray shards was amorphous carbon with strong graphitic characteristics. The lack of iron oxides in the gray artifacts set them apart from the red artifacts.

There could be few reasons for the appearance of amorphous carbon in the finished (fired) clay products. Since clay artifacts are formed at higher temperatures, far above which carbon is likely to occur, the observed carbon could be originating from the firing (under reducing atmosphere) of some organic substance in the starting mixture or from colouring materials that could have been applied after the firing process [15]. It could also be that the raw material contained some carbon source (e.g. animal bones) which on firing in air resulted in amorphous carbon and phosphate ions. However, it is difficult to tell which method was used by simply looking at the samples.

All samples showed, in addition, the features resembling those of mullite, phosphates and carbonate ions, however, their presence could not be ascertained conclusively from the Raman spectroscopic results. The study has proven that differentiation (by Raman spectroscopy) between the present clay artifacts is based mainly on the colouring materials used. It follows that Raman spectroscopy can be used non-destructively to successfully identify crystalline and non-crystalline phases (including colouring materials) constituting the clay artifacts. In the present case, the only applicable technique was Raman spectroscopy because of its availability and non-destructive nature, as the samples used in this study were museum artifacts and could not be subjected to destructive techniques.

Acknowledgements

The financial support by the National Research Foundation in Pretoria and the University of Pretoria is gratefully acknowledged. The authors thank the J A van Tilburg museum curator Dr Valerie Esterhuizen for the supply of samples and historical information.

References

[1] R.J.H. Clark, M.L. Curri, J. Mol. Struct. 440 (1998) 105.
[2] C.S. Nurlbut Jr., C. Klein, Manual of Mineralogy, 19th ed., John Wiley & Sons Inc, New York, 1971.
[3] H.G.M. Edwards, E.M. Newton, J. Russ, J. Mol. Struct. 550–551 (2000) 245.
[4] L. Burgio, R.J.H. Clark, Spectrochim. Acta 57A (2001) 149.
[5] S.P. Best, R. Withnall, Endeavour 16 (1992) 66.
[6] M.J. Wilson, Clay Mineralogy: Spectroscopic and Chemical Determinative Methods, Chapman & Hall, London, 1994.
[7] N. Palmgren, W. Steger, N. Sundius, Sung Sherds, Almovist & Wilksell, Stockholm, 1963, pp. 380.
[8] P. Colomban, J. Mater. Sci. 24 (1989) 3011.
[9] N. Palmgren, W. Steger, N. Sundius, Sung Sherds, Almovist & Wilksell, Stockholm, 1963.
[10] P. Valfre, Yixing Teapots for Europe, Exotic line, Janvier 2000, (China).
[11] P. Colomban, G. Sagon, X. Faurel, J. Raman Spectrosc. 32 (2001) 351.
[12] D. Bikiaris, S. Daniila, S. Sotiropoulou, O. Katsimbiri, E. Poulidou, A.P. Moutsatsou, Y. Chryssoulakis, Spectrochim. Acta Part A 56 (1999) 3.
[13] N.Q. Liem, G. Sagon, V.X. Quang, H. Van Tan, P. Colomban, J. Raman Spectrosc. 31 (2000) 933.
[14] P. Colomban, F. Treppoz, J. Raman Spectrosc. 32 (2001) 93.
[15] J. Zuo, C. Xu, C. Wang, Z. Yushi, J. Raman Spectrosc. 30 (1999) 1053.
[16] L.A. De Faria, S.V. Silva, M.T. De Oliviera, J. Raman Spectrochim. 28 (1997) 873.
[17] R.L. Frost, P.M. Fredericks, J.R. Bartlett, Spectrochim. Acta 49A (5–6) (1993) 667.
[18] I.M. Bell, R.J.H. Clark, P.J. Gibbs, Spectrochim. Acta 53A (1997) 2159.
[19] M. Tabbal, T. Christidis, S. Isber, M.A. El Khakani, P. Mérel, M. Chaker, Thin Solid Films 453–454 (2004) 234.
[20] J.C. Orlianges, C. Champeaux, A. Catherinot, Th. Merle, B. Angleraud, Thin Solid Films 453–454 (2004) 285.
[21] K. Lee, H. Sugimura, Y. Inoue, O. Takai, Diamond Relat. Mater. 13 (3) (2004) 507.
[22] R.N. Tarrant, D.R. McKenzie, M.M.M. Bilek, Diamond Relat. Mater., in press.
[23] I.A. Degen, G.A. Newman, Spectrochim. Acta Part A 49 (5–6) (1993) 859.
[24] V.C. Farmer, Infrared spectroscopy, in: H. van Olphen, J.J. Fripiat (Eds.), Data Handbook for Clay Materials and Other Non-metallic Minerals, Pergamon, Oxford, 1979.
[25] C.H. Chio, S.K. Sharma, D.W. Muenow, Am. Miner. 89 (2004) 390.
[26] R.J.H. Clark, Chem. Soc. Rev. 24 (1995) 187.
[27] V.C. Farmer, The Infrared Spectra of Minerals, Mineralogical Society, London, 1975.
[28] E.C. Ziemath, M.A. Aegeter, J. Mater. Res. 9 (1994) 216.
[29] R. Burch, C. Passingham, G.M. Warnes, D.J. Rawlence, Spectrochim. Acta 46A (1990) 243.

Chapter 6

The preparation of magnetite, goethite, hematite and maghemite of pigment quality from mill scale iron waste

UNIVERSITEIT VAN PRETORIA
UNIVERSITY OF PRETORIA
YUNIBESITHI YA PRETORIA

Available online at www.sciencedirect.com
ScienceDirect

ELSEVIER

Dyes and Pigments 74 (2007) 161–168

DYES and PIGMENTS

www.elsevier.com/locate/dyepig

The preparation of magnetite, goethite, hematite and maghemite of pigment quality from mill scale iron waste

M.A. Legodi, D. de Waal*

Department of Chemistry, University of Pretoria, 0002 Pretoria, South Africa

Received 4 November 2005; accepted 23 January 2006
Available online 17 April 2006

Abstract

Mill scale iron waste has been used to prepare some iron oxide pigments via specific precursors. Magnetite and goethite were precipitated from their respective precursors in aqueous media. Various red shades of hematite were prepared by the calcinations of the precipitated goethite at temperatures ranging from 600 to 900 °C. Maghemite was obtained by thermal treatment of magnetite at 200 °C. The iron oxides were characterized by Raman spectroscopy, X-ray diffraction (XRD), surface area determination and scanning electron microscopy (SEM). They are generally composed of very small particles (mainly <0.1 μm) with high surface area. These particle properties suggest that the above pigments (prepared from mill scale) will show high tinting strength, quality hiding power and good oil absorption. Oil absorption is a property of the pigment that is closely related to the ease of dispersion.

Keywords: Mill scale; Raman; Iron oxides; Pigments; Precipitation

1. Introduction

Stainless steel finishing operations involve several cleaning processes, which eliminate dust, scale and metallic oxides [1]. Mill scale is a steel making by-product from steel hot rolling processes and is basically composed of iron oxides and metallic iron with variable oil and grease contents [2,3]. Its specific production is about 35–40 kg/t of hot rolled product [2]. The oil component in rolling mill scale makes the recycling difficult, and its direct re-use in sintering may lead to environmental pollution. Mill scale with high oil content is recycled after extracting the oil in a pretreatment stage. Coarse scale with a particle size of 0.5–5 mm and oil content of less than 1% can be returned to the sinter strand without any pretreatment. High oil content (>3%) results in increased emission of volatile organic compounds including dioxins and can lead to problems in waste gas purification systems, e.g. glow fires in electrostatic precipitators. Because of this mill scale needs to be pretreated before it can be re-used. Fine sludge mainly consists of very small-scale particles (0.1 mm). Since the fine particles adsorb oil to a very high degree (5–20%) this scale normally cannot be returned to the sinter strand without pretreatment [4]. The oil adsorption in the preceding line refers to the metallic mill scale and should not be confused with the oil absorption, pigment property, mentioned in the abstract and elsewhere in this paper. At MITTAL (former ISCOR), a steel manufacturing company in the Republic of South Africa, the bulk of mill scale waste is dumped in landfills. The continuous demand for more landfills and the leaching of some small percentages of heavy metals into soil and ground water, thus threatening the environment, highlight the need for more effective methods of waste disposal and productive utilisation of mill scale.

Production of iron oxide pigments is one of the possible ways of alleviating the problem facing the steel industry in RSA since mill scale has a high iron content in the form of oxides and metal. The use of iron waste in iron oxide preparations is vital because of the increasing demand for iron

* Corresponding author. Tel.: +27 1 242 030 99; fax: +27 123 625 297.
E-mail address: danita.dewaal@up.ac.za (D. de Waal).

0143-7208/$ - see front matter © 2006 Elsevier Ltd. All rights reserved.
doi:10.1016/j.dyepig.2006.01.038

oxide pigments driven by the increases in construction activities, current economic needs [5] in emerging markets and growing concern over the use of heavy metal-based pigments. The increasing importance of iron oxide pigments is also based on their non-toxicity, chemical stability, durability [6], wide variety of colours and low costs.

There are many studies in the literature that deal with different methods for the preparation of magnetite [7–11], hematite [12–15], maghemite [16–20] and goethite [21–23]. These are the iron oxides commonly used as pigments giving black, red, brown and yellow colours, respectively. Steel pickling chemical waste (SPW) has been thermally decomposed at various temperatures to give red iron oxide (hematite) [9,24,25]. The formation of mill scale (mainly FeO and Fe) can also be accompanied by the precipitation of corrosion product mixture, viz. Fe_3O_4, FeOOH, Fe_2O_3, etc. [26]. FeO is usually closest to the metal surface while Fe_2O_3 forms the outer layer [27]. Since corrosion products occur in a mixture and the overall mill scale is hardened and of poor colour, it is not of pigment value. Oulsnam and Erasmus [28] have succeeded in preparing magnetite from ferrous mill scale using a dry oxidation step. However, the particles of their product were too large and had to be ground (wet and dry) to <10 μm to improve the pigment qualities (colour, tinting strength, hiding power and oil absorption) [24,25]. Hematite was prepared by calcination of the obtained magnetite and its particles also had to be ground to sizes < 10 μm.

The present study was undertaken with the aim of preparing magnetite and goethite of pigment particle size < 10 μm via water-soluble mill scale-derived precursors. Furthermore, maghemite and hematite could then be prepared by thermal treatment of the obtained magnetite and goethite, respectively.

2. Experimental

2.1. Chemical preparation

2.1.1. Ferrous precursor

Conc. H_2SO_4 (analytical reagent, 300 ml) was added to 60 g of raw mill scale in a 600 ml glass beaker. The mixture when heated on a hot plate became turbid. The turbid mixture was further heated to dryness. The resulting muddy solid product was then used as the starting material for the preparation of magnetite and goethite. Preliminary investigations showed that the product was soluble in water (more readily in warm water) and a dark blue/green flaky sediment resulted when the aqueous solution was mixed with a base (e.g. NH_4OH or NaOH). This chemical behaviour is characteristic of the presence of $Fe(OH)_2$ in solution [21]. It indicates that the greater part of iron in the muddy solid product is in the Fe^{2+} form. The acidic environment was created in order to facilitate the conversion of iron oxides to ferrous or ferric ions in an aqueous solution [29].

2.1.2. Ferric precursor

Conc. H_2SO_4 (300 ml) was mixed with 30 g of raw mill scale in a 600 ml glass beaker. The mixture was then heated to dryness on a hot plate. The product, containing a fine white powder and dark solid particles, was cooled to room temperature and allowed to stand in open air for five days. During this time the product gradually turned into a yellowish fine white powder. No darker areas were observed. The fine powder was soluble in warm water and formed rust coloured sediment when a base, e.g. NH_4OH or NaOH, was added to its aqueous solution. This chemical behaviour is characteristic of the presence of $Fe(OH)_3$ [21]. Therefore, the greater part of iron in the fine yellowish white powder was in the form of Fe^{3+} [29].

Alternatively, 60 g of mill scale in 200 ml of conc. H_2SO_4 was digested on a hot plate at 100 °C for 30 min followed by the addition of 200 ml of 65% HNO_3. Further heating resulted in a cream white homogeneous solid substance, which was then heated to dryness. The cream white solid contained iron mainly in the Fe^{3+} form.

2.1.3. Magnetite (Fe_3O_4)

Magnetite was prepared by the method of Ueda et al. [8] with some modifications. Ferrous precursor (10 g) was dissolved in 120 ml of distilled water. To the filtered solution 130 ml of 25% NH_4OH solution was added, thus raising the pH to about 11–12. After ageing at room temperature for 20 h, the precipitate formed was collected by filtering. The precipitate was washed with 500 ml of distilled water and allowed to dry at room temperature. The black, magnetite product was qualitatively examined by Raman spectroscopy and confirmed by X-ray powder diffraction (XRD).

2.1.4. Maghemite (γ-Fe_2O_3)

The magnetite obtained above (Section 2.1.3) was heated in an oven at 200 °C for 3 h during which it turned light brown [30]. This product was identified by Raman spectroscopy and confirmed by XRD results to be maghemite.

2.1.5. Goethite (α-FeOOH)

This iron oxide polymorph was prepared using the method of Thiebeau et al. [23] with some modifications. Ferric precursor (20 g) was dissolved in 500 ml of distilled water. To the filtered solution 100 ml of 1 M $NaHCO_3$ solution was added which brought the pH to values between 5 and 7. The solution was held at 100 °C for 1 h and allowed to cool to room temperature. The resulting yellow precipitate was filtered off and washed with 300 ml of distilled water and allowed to dry in air. The product was identified by Raman spectroscopy and confirmed by XRD as goethite.

2.1.6. Hematite (α-Fe_2O_3)

The goethite obtained above, in Section 2.1.5, was calcined in the furnace at temperatures between 600 and 900 °C for 5 h. The colour of the resulting products gave the following shades of red as the temperature increased: orange-brown, brown-red, bright-red, maroon, purple and gray. The phase determination was carried out using Raman spectroscopy and XRD showed that the product was hematite.

The product particle characteristics (namely sizes, shapes and specific surface areas) were determined using scanning

electron microscopy (SEM) and BET single point surface area measurement.

2.2. Instruments

2.2.1. Raman spectroscopy

Laser Raman spectra were recorded at room temperature using a Dilor XY Raman spectrometer with a resolution of 2 cm^{-1}. Radiation at 514.5 nm from an Ar^{+} Coherent Innova 300 laser was used to excite the samples. The laser power was set at 100 mW at the source. The recording time was set between 30 and 180 s, with two accumulations per spectrum segment. An Olympus Mplan 100× objective on an Olympus BH-2 microscope was used to focus on the sample. The Raman spectra were analysed using Labspec v 2.04 software [31].

2.2.2. X-ray powder diffraction

The X-ray diffraction (XRD) analyses were performed using a Cu Kα (1.5418 Å) source (40 kV, 40 mA) from Siemens D-501, with a graphite secondary monochromator and a scintillation counter detector. The powdered sample was placed on a flat plastic plate, which was rotated at 30 rpm. The scans were performed at 25 °C in steps of 0.04°, with a recording time of 2 s for each step [32]. Where accurate 2θ values were required, Si was added as an internal 2θ standard.

2.2.3. X-ray fluorescence

An ARL 9400XP+ wavelength-dispersive XRF spectrometer with an Rh source was used for the X-ray fluorescence analyses of the samples. The XRF spectrometer was calibrated with certified reference materials. An NBSGSC fundamental parameter program was used for matrix correction of major elements, as well as Cl, Co, Cr, V, Sc and S. The Rh Compton peak ratio method was used for the other trace elements. Samples were dried and fired at 1000 °C to determine the percentage loss on ignition; for the samples this was less than 2%.

Table 1
XRF results of raw mill scale

Component	%Content
SiO_2	0.99
Al_2O_3	0.22
Fe as Fe_2O_3	103
MnO	0.800
MgO	640 ppm
CaO	660 ppm
P_2O_5	310 ppm
SO_3	0.25
Cl	260 ppm
Cr_2O_3	0.14
NiO	900 ppm
CuO	0.13
ZnO	130 ppm
ZrO_2	25 ppm
MnO_3	440 ppm
LOI	−6.3

The negative sign of the loss on ignition (LOI) value indicates that there were no volatiles in the sample.

Table 2
XRF results of ferrous and ferric mill scale precursors of iron oxides

Component	Ferrous mill scale (%)	Ferric mill scale (%)
SiO_2	0.12	2.47
Al_2O_3	0.11	2.20
Fe_2O_3	60.86	58.42
MnO	0.49	0.41
MgO	<0.01	0.64
CaO	0.08	0.09
P_2O_5	<0.01	<0.01
SO_3	38.33	35.35
Cl	<0.01	<0.01
Cr_2O_3	0.11	0.10
NiO	0.04	0.10
CuO	0.08	0.08
ZnO	0.03	<0.01
ZrO_2	<0.01	<0.01
MnO_3	<0.01	<0.01
LOI	58.34	58.85

Major element analyses were carried out on fused beads, following the standard method used in the XRD and XRF laboratory of the University of Pretoria [33], as adapted from Bennett and Oliver [34]. A pre-fired sample of 1 and 6 g of lithium tetraborate flux was mixed in a 5% Au/Pt crucible and fused at 1000 °C in a muffle furnace, with occasional swirling. The glass disk was transferred into a preheated Pt/Au mould and the bottom surface was analysed. The trace element analyses were done on pressed powder pellets, using an adaptation of the method described by Watson [35], with a saturated Mowiol 40–88 solution as binder.

2.2.4. Specific surface area (S_{BET}) determinations

Approximately 0.5 g of each sample was put into the sample container of the BET Single Point Surface Area instrument. Each sample was baked out for 30 min at 150 °C in a He/N_2 stream. The sample mass was determined after the drying process. The surface areas were determined using the standard single-point method. Samples were analysed in triplicate.

2.2.5. Scanning electron microscope (SEM)

The size and shape of the particles of iron oxide prepared in this study were monitored by the ISM 600F scanning electron microscope. Before observations, the powders were dispersed

Table 3
XRD phase results of ferrous precursor, ferric precursor, magnetite, goethite, hematite and maghemite

Sample	Phase
Ferrous mill scale	$FeSO_4 \cdot 2H_2O$, α-FeOOH, $3Fe_2O_3 \cdot 8SO_3 \cdot 2H_2O$, $FeOHSO_4$
Ferric mill scale	$FeSO_4 \cdot 2H_2O$, α-FeOOH, $3Fe_2O_3 \cdot 8SO_3 \cdot 2H_2O$, $FeOHSO_4$
Magnetite	$Fe_{2.894}O_4$
Goethite	α-FeOOH
Maghemite	γ-Fe_2O_3
Hematite	Fe_2O_3

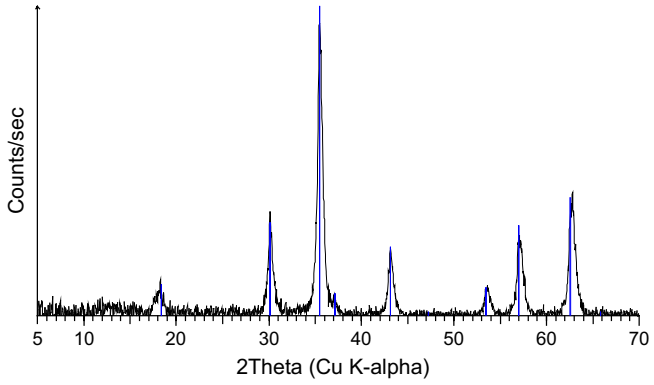

Fig. 1. X-ray powder diffractogram of magnetite obtained from mill scale.

in ethanol (100%) by ultrasonic waves. A drop of the dispersed sample was placed on a copper grid previously covered by a polymer film.

3. Results and discussion

3.1. Ferrous and ferric precursor

Tables 1 and 2 give the elemental compositions of ferrous and ferric mill scale as obtained from XRF analysis. The elemental compositions show that the percentage of iron increased significantly while the amounts of other elements decreased. This means that the acid digestion of raw mill scale increases the content of iron in the products formed. The high loss on ignition (LOI) value (over 50%) may be due to the high sulphate content, which was given off as SO_2 during the calcination that accompanied the elemental determinations.

The XRD analysis (Table 3) of both ferrous and ferric mill scale gave similar phases. The chemical behaviour of both the samples in aqueous medium shows that the ferrous mill scale contains more of ferrous compound ($FeSO_4 \cdot H_2O$) and less of ferric compounds ($3Fe_2O_3 \cdot 8SO_3 \cdot 2H_2O$, $FeOHSO_4$ and α-FeOOH) while ferric mill scale contained more of ferric

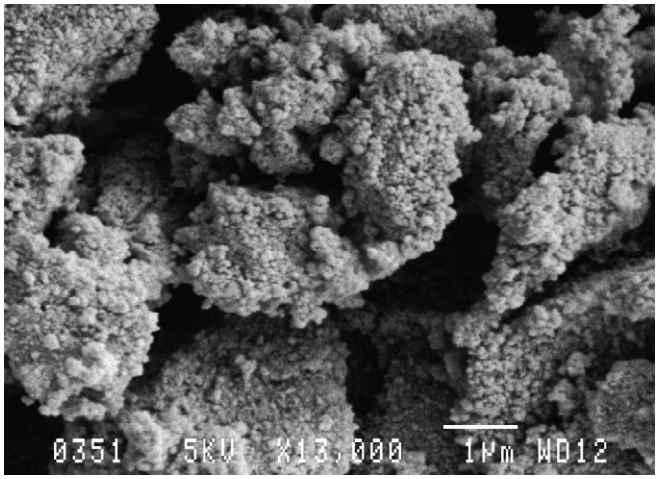

Fig. 2. SEM micrograph of magnetite obtained from mill scale.

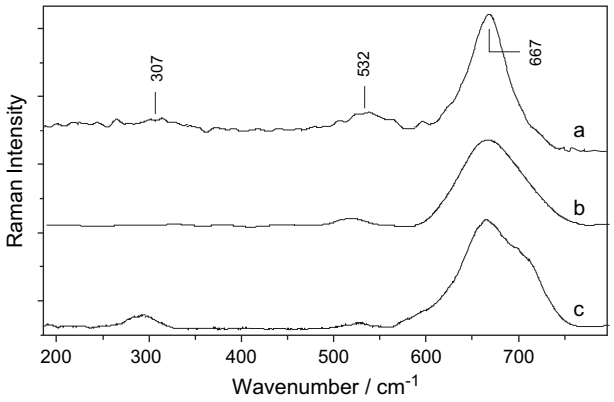

Fig. 3. Raman spectra of magnetite from various sources: (a) commercial magnetite; (b) magnetite from pure starting material and (c) magnetite obtained from mill scale.

compounds ($3Fe_2O_3 \cdot 8SO_3 \cdot 2H_2O$, $FeOHSO_4$ and α-FeOOH) and less of ferrous compounds ($FeSO_4 \cdot H_2O$).

3.2. Magnetite

The XRD analysis of the product showed largely the presence of magnetite phase. The slight broadening of the XRD lines (Fig. 1) can be interpreted in terms of poor crystallinity of the precipitated magnetite and small size of crystallites [36]. In fact the stoichiometry of this product as determined using XRD technique was $Fe_{2.894}O_4$. This suggests that the crystal structure is slightly distorted (leading to broadened XRD lines) due to the deficiency of Fe ions. The stoichiometry of magnetite with good black pigment quality should be as

Table 4
Raman wavenumbers and assignments of the prepared iron oxides

Compound	Experimental (cm^{-1})	Pure oxide (cm^{-1})	Assignment [21,30,38–40]
Magnetite	297	298	T_{2g} (Fe–O asym. bend)
	–	319	E_g (Fe–O sym. bend)
	523	540	T_{2g} (Fe–O asym. bend)
	666	668	A_{1g} (Fe–O sym. str)
Goethite	223	–	Fe–O sym. str
	297	299	Fe–OH sym. bend
	392	400	Fe–O–Fe/–OH sym. str
	484	–	Fe–OH asym. str
	564	550	Fe–OH asym. str
	674	–	Fe–O sym. str
Hematite	226	225	A_{1g} (Fe–O sym. str)
	–	247	E_g (Fe–O sym. bend)
	292	293	E_g (Fe–O sym. bend)
	406	412	E_g (Fe–O sym. bend)
	495	498	A_{1g} (Fe–O sym. str)
	600	613	E_g (Fe–O sym. bend)
	700	–	A_{1g} (Fe–O sym. str)
Maghemite	358	344	E_g (Fe–O sym. str)
	–	390	T_{2g} (Fe–O asym. bend)
	499	507	T_{2g} (Fe–O asym. bend)
	678	665	A_{1g} (sym. str)
	710	721	A_{1g} (sym. str)

Table 5
Prepared iron oxides and their corresponding particle sizes, shapes and surface area values

Compound	Shape	Size (μm)	Surface area (m^2g^{-1})
Magnetite	Pseudocubic	<0.1	90
Pure magnetite	Pseudocubic	<0.1	75
Goethite	Needle-like/acicular	<0.05	113
Pure goethite	Needle-like	<0.1	39
Maghemite	Irregular	<0.1	87
Pure maghemite	Pseudocubic	<1	20
Hematite	Pseudocubic	<0.05	~1
Pure hematite	Pseudocubic	<0.05	6.2

close as possible to the ideal one (Fe_3O_4) [28]. The magnetite stoichiometry obtained in this study is acceptably close. The correct stoichiometry ensures that there is little or no inclusion of other phases, e.g. hematite, into the synthetic magnetite to reduce the denseness of the black colour achieved.

Short time ageing resulted in a deep green precipitate, most likely green rust [8], which is expected to contain Fe^{2+}, Fe^{3+}, OH^- and SO_4^{2-} [12]. Observing the colour change from deep green to black with increase in ageing time easily followed the conversion from the green colloidal particles to spinel. The bulk of the solution was black after 5 h of ageing. However, a brown (rust colour) tinge was visible on the surface even after 8 h. This was perhaps due to the presence of an amount of unoxidized iron [27], FeOOH [25] or Fe_2O_3 detected in the ferrous precursor. By increasing the ageing time to 20 h the brown tinge disappeared and only very fine deep black colloidal particles were observed. The analysis of the product obtained after 20 h using SEM showed particles with pseudocubic shapes, Fig. 2.

This technique further showed that the product was composed of aggregates of minute particles of less than 1 μm in size. Such small particle size values indicate that the pigment will show high tinting strength [37]. The particles were regular and uniform suggesting that the pigment will show a quality hiding power [25,37]. Raman spectroscopy also confirmed the presence of magnetite (see Fig. 3, Table 4).

The surface area value of this product (90 m^2/g) is higher than that for standard products (commercial magnetite and magnetite obtained from pure starting material) as shown in Table 5. This could mean that the magnetite prepared in this study was highly porous. The surface area affects essentially the oil absorption ability of pigment such that the higher the surface area the greater is the oil absorption [37].

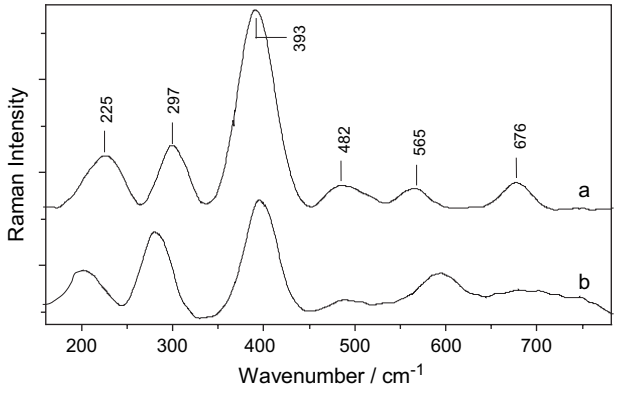

Fig. 4. Raman spectra of goethite from (a) pure starting material and (b) millscale.

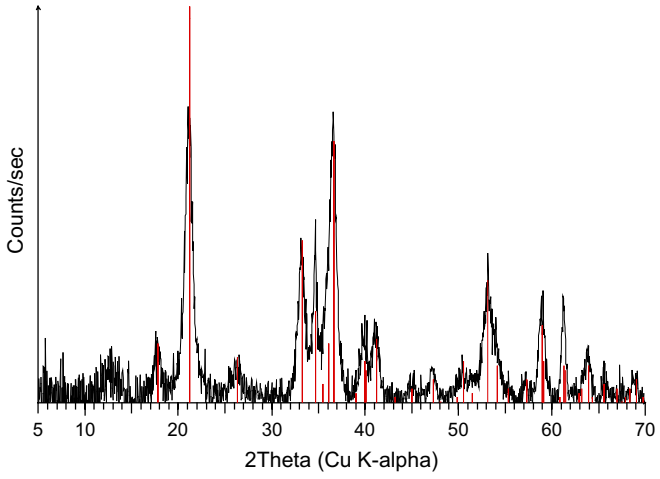

Fig. 5. X-ray powder diffractogram of goethite obtained from mill scale.

3.3. Goethite

The Raman spectroscopic analysis identified the phase of this product to be goethite, Table 4 and Fig. 4, as shown by the presence of the characteristic bands of goethite. Raman bands occurring at 223 and 674 cm^{-1} were assigned to the Fe–O A_{1g} mode and Fe–O stretching, respectively. Therefore, product showed the presence of small amounts of hematite impurity (223 cm^{-1}). The band around 483 cm^{-1} was not assigned. There is a strong possibility that the unassigned band is due to some impurities which are either amorphous or occur in small amounts only detectable by the Raman technique because of its microscopic nature. These impurities possibly interfere with the crystallinity of goethite.

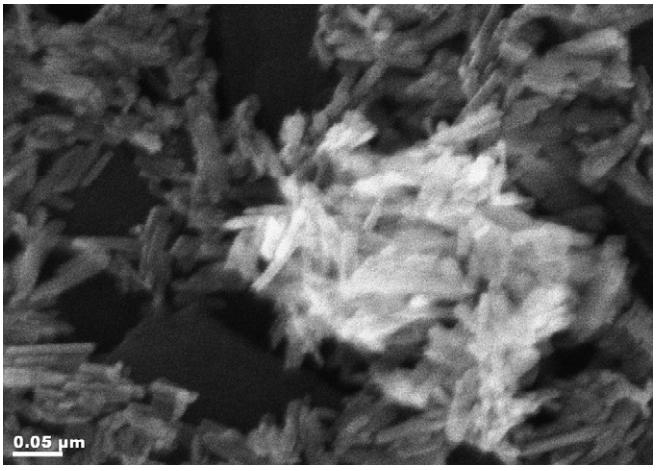

Fig. 6. SEM micrograph of goethite obtained from mill scale.

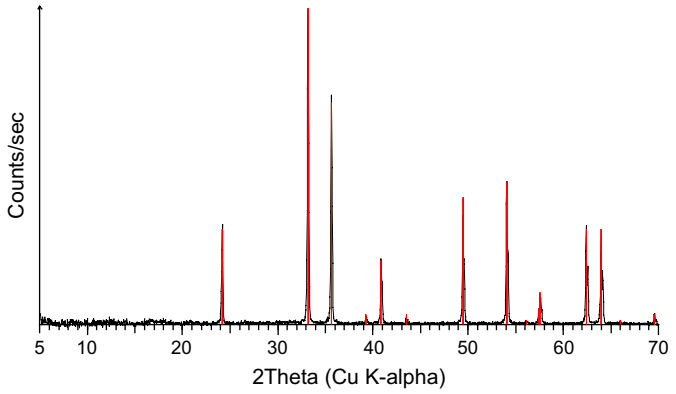

Fig. 7. X-ray powder diffractogram of hematite obtained from mill scale goethite at 750 °C.

The XRD analysis of the yellow powder showed goethite to be the main phase. The slight broadening of the XRD lines (Fig. 5) may be due to the poor crystallinity, impurities and small particle sizes. The hematite phase could not be detected by XRD analysis. The surface area value of goethite sample is far higher than that of the standard product (Table 5).

The SEM micrograph of goethite product (Fig. 6) showed that the particle size was less than 0.05 μm, a sign of high tinting strength [24]. The particles from bright yellow goethite were needle-like in shape and fairly regular. This indicates the quality hiding power that the pigment will show [25].

3.4. Hematite

The calcination of mill scale-derived goethite resulted in hematite phase as detected by X-ray diffraction. From the XRD lines (Fig. 7) it can be said that the product is fairly crystalline. This product seems to be relatively pure.

The Raman spectra also showed the presence of hematite characteristic bands in the region 200–700 cm^{-1} (Fig. 8, Table 4). Different shades of red colour were obtained, when thermal decomposition was carried out at different temperatures, including brownish-orange (650 °C for 3 h), brownish-red (700 °C for 5 h), bright-red (750 °C for 3 h), maroon/purple (800 °C for 5 h) and gray (900 °C for 5 h).

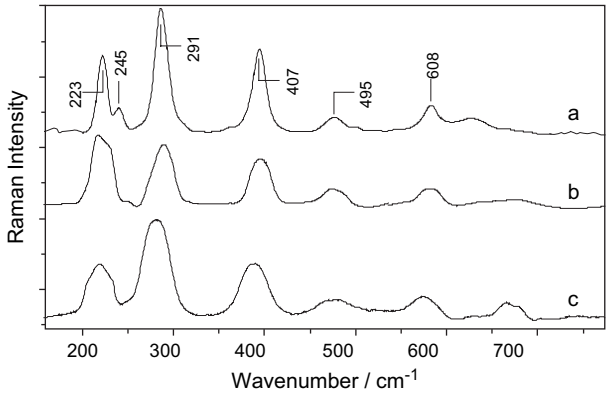

Fig. 8. Raman spectra of hematite from various sources: (a) commercial hematite; (b) hematite from pure starting material and (c) hematite from mill scale.

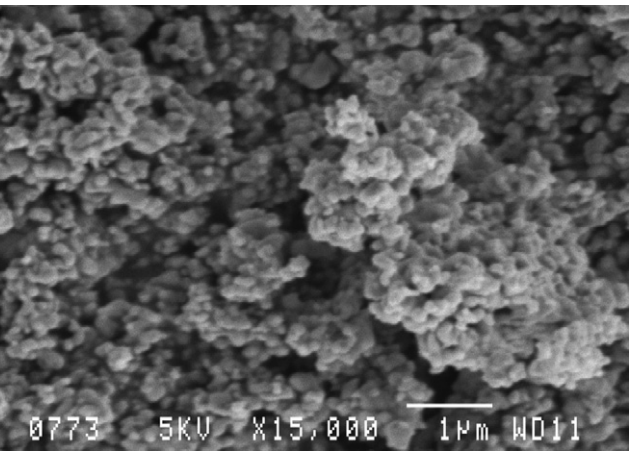

Fig. 9. SEM micrograph of hematite obtained from mill scale goethite at 750 °C.

SEM results of the product obtained at 750 °C showed very small particle sizes and uniform pseudocubic shapes (Fig. 9, Table 5). The hematite particles obtained at 750 °C were fairly regular and have surface area value comparable with that of the commercial product. Therefore, this pigment will show high tinting strength, good oil absorption ability and hiding power [24,25,37].

3.5. Maghemite

This product was identified by its broad Raman characteristic features around 358, 499 and 710 cm^{-1} (Table 4, Fig. 10) [38–40]. The XRD analysis (Fig. 11) also confirmed the presence of maghemite, even though not fully crystalline. The broad feature around 2θ value of 13 (Fig. 11) is due to the instrumental drift. The product may contain some small quantity of impurities (most likely magnetite and hematite). The surface area values are higher than those of the standard products. The particles were irregular and showed sizes below 1 μm (Fig. 12). Pigments with particle sizes below 10 μm

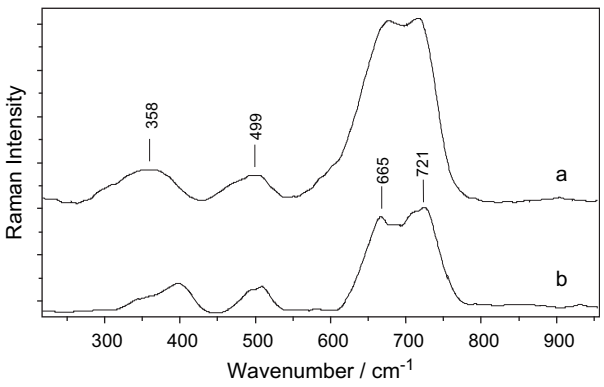

Fig. 10. Raman spectra of maghemite from (a) pure starting material and (b) mill scale.

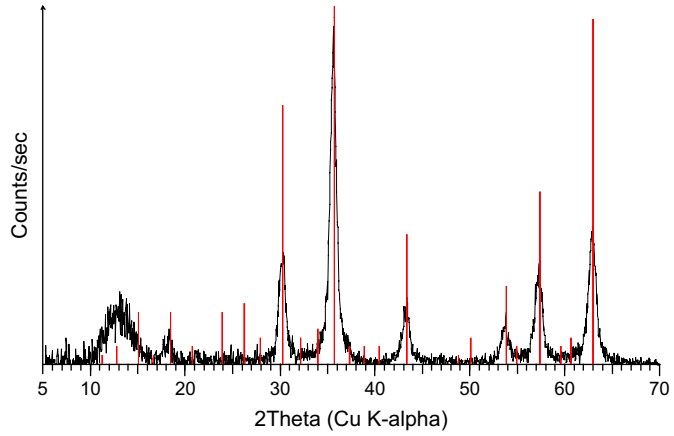

Fig. 11. X-ray powder diffractogram of maghemite obtained from mill scale magnetite at 200 °C.

normally show good pigment properties [28], including high tinting strength and oil absorption [24,25,37].

4. Conclusion

This study has shown that it is possible to prepare magnetite (black), hematite (red), goethite (yellow) and maghemite (brown) pigments of acceptable purity and with good morphological properties (i.e. particle size, shape, colour and surface area) from mill scale iron waste through simple and cost effective methods. The formation of iron oxide precursors (sulphate-containing compounds with iron as Fe^{2+} in one case and Fe^{3+} in another) has facilitated the precipitation of both magnetite and goethite in an aqueous medium. This has also led to the precipitation of pigments with particle sizes below 0.1 μm. The advantages of such small particle sizes are manifested by the good colour tones and intensity of magnetite (black) and goethite (yellow). Various shades of red colour were obtained depending on the temperature and duration of calcination of goethite. The thermal treatment of the obtained magnetite at 200 °C for 3 h resulted in maghemite. Generally, high surface area values obtained for all iron oxides prepared in this study when compared with standard products suggest that the pigments were highly porous. Due to the small particle sizes (<0.1 μm) of the iron oxides under study, the pigments prepared in this way will show good tinting strength, hiding powder and oil absorption.

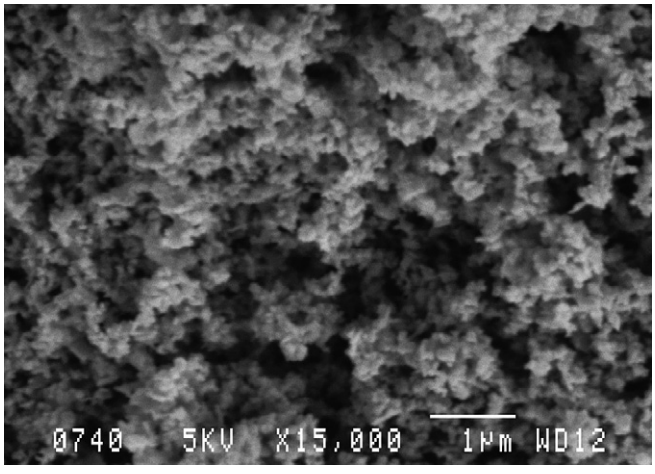

Fig. 12. SEM micrograph of maghemite obtained from mill scale magnetite at 200 °C.

Acknowledgement

The financial support by the National Research Foundation in Pretoria and the University of Pretoria is gratefully acknowledged. The authors thank the MITTAL STEEL, Pretoria, for the supply of mill scale iron waste.

References

[1] Lopez-Delgado A, Peña C, López V, López FA. Resour Conserv Recycl 2003;40:39–51 and references therein.
[2] International Iron and Steel Institute. The management of steel industry by-products and waste. Brussels Committee on Environmental Affairs; 1987.
[3] International Iron and Steel Institute. The management of plant ferruginous by-products. Brussels Committee on Environmental Affairs and Committee on Technology; 1994.
[4] Reference document on best available techniques in the ferrous metals processing industries. Spain: IPPC Directive European Commission, Institute for Prospective Technological Studies Seville, Directorate-General Joint Research Centre; October 2000.
[5] Solć Z, Trojan M, Brandova D, Kuchler M. J Therm Anal 1988;33:463–9.
[6] Allen RLM. Color chemistry. London: Thomas Nelson and Sons Ltd; 1971. p. 87.
[7] Sugimoto T, Muramatsu A, Sakata K, Shindo D. J Colloid Interface Sci 1993;158:420–8.
[8] Ueda M, Shimada S, Inaga M. J Eur Ceram Soc 1996;16:685–6 and references therein.
[9] Tamaura Y, Ito K, Katsura T. J Chem Soc Dalton Trans 1983;1983:189–94.
[10] Bate G. In: Wohlfarth EP, editor. Ferromagnetic materials, vol. II. North-Holland; 1980. p. 406.
[11] Leskelä T, Leskelä M, Niinisto L. Thermochim Acta 1984;72:229–37.
[12] Ismail HM, Gadenhead DA, Zaki MI. J Colloid Interface Sci 1996;183:320–8.
[13] Ismail HM, Zaki MI, Hussein GA, Magar MN. Powder Technol 1990;63:87–96.
[14] Bailey JK, Brinker CJ, Mecartney ML. J Colloid Interface Sci 1993;157:1–13.
[15] Itoh H, Sugimoto T. J Colloid Interface Sci 2003;265:283–95.
[16] Rao V, Sashimohan AL, Biswas AB. J Mater Sci 1974;9:430–3.
[17] Ravindranathan P, Patil KC. J Mater Sci Lett 1986;5:221–2.
[18] Narasimhan BRV, Prabhakar S, Manohar P, Gnanam FD. Mater Lett 2002;52:295–300 and references therein.
[19] Luo H, Zeng H. J Therm Anal 1995;45:185–91.
[20] Nunez NO, Morales MP, Tatraj P, Serna CJ. J Mater Chem 2000;10:2561–5.
[21] Nauer G, Strecha P, Brinda-Konopik N, Liptay G. J Therm Anal 1985;30:813–25 and references therein.
[22] Kalinskaya TV, Krasotkin IS, Lobanova LB. J Appl Chem USSR 1979;520:955–8.
[23] Thiebeau RJ, Brown CW, Heidersback RH. Appl Spectrosc 1978;32:532–5 and references therein.
[24] Ismail HM, Fouad NE, Zaki MI, Magar MN. Powder Technol 1992;70:183–8.
[25] Fouad NE, Ismail HM, Zaki MI. J Mater Sci Lett 1998;17:27–9.

[26] Škvara F, Kaštanek F, Pavelkova I, Šolcova O, Maleterova Y, Scheider P. J Hazard Mater 2002;89:67–81.
[27] Coburn SK, editor. Corrosion source book. Metals Park, OH: American Society For Metals; 1984. p. 12–3.
[28] Oulsnam BT, Erasmus D. US Patent 5,738,717,1998.
[29] Li Yuang-Shen. Waste Manag 1999;19:495–502.
[30] de Faria DLA, Silva SV, de Oliviera MT. J Raman Spectrosc 1997;28:873–8 and references therein.
[31] Labspec, version 2.04, Distributed by Dilor SA & Universite' de Reims, France; 1997.
[32] Verryn S. Details of XRD procedure used at the University of Pretoria XRD laboratory, personal written communication, University of Pretoria, Pretoria; 2002.
[33] Loubser ML. (Typed) Report on XRF analyses of ceramics, mloubser@postino.up.ac.za; 20 June 2002.
[34] Bennet H, Oliver G. XRF analysis of ceramics, minerals and applied materials. Chichester: Wiley; 1997. p. 37.
[35] Watson JS. X-ray spectrom 1996;25:173–4.
[36] Musić S, Orehovec Z, Popović S, Czakó-Nagy I. J Mater Sci 1994;29:1991–8.
[37] Turner GPA. Introduction to paint chemistry and principles of paint technology. 2nd ed. London: Chapman and Hall; 1980. p. 95–107.
[38] Dunnwald J, Otto A. Corros Sci 1989;29:1167–76.
[39] Kieser JT, Brown CW, Heidersbach RH. Corros Sci 1983;23:251–9.
[40] Boucherit N, Hugot-Le Goff A, Joiret S. Corros Sci 1991;32:497–507.

Erratum to "The preparation of magnetite, goethite, hematite and maghemite of pigment quality from mill scale iron waste", Dyes and Pigments 2007;74:161 – 168

M.A. Legodi and D. de Waal

The authors would like to acknowledge that the idea used in the introduction of this article is related to the published material (in article F. A. López, M. I. Martin, C. Pérez, A. López-Delgado and F.J. Aguacil, Removal of copper ions from aqueous solutions by a steel-making by-product, Water Research 2003;37:3883-3890). The contested material in our article, even though similar, is not an exact copy of that in López et al. related article (see above). We therefore, acknowledge inadvertent omission of the above reference (López et al.) in our article and wish to express our sincere apology for this.

Therefore, the first part of the introduction section, containing the corrected material and a corresponding partial list of references would read as follows:

"Stainless steel finishing operations involve several cleaning processes, which remove dust, scale, iron oxides and hydroxides [1,2]. Mill scale is a steel making by-product from steel hot rolling processes and is basically composed of iron oxides and metallic iron with variable oil and grease contents [3–5]. Its specific production is about 35–40 kg/t of hot rolled product [3, 4]. The oil component in rolling mill scale makes the recycling difficult, and its direct re-use in sintering may lead to environmental pollution. Mill scale with high oil content is recycled after extracting the oil in a pretreatment stage. Coarse scale with a particle size of 0.5–5 mm and oil content of less than 1% can be returned to the sinter strand without any pretreatment. High oil content (>3%) results in increased emissions of volatile organic compounds including dioxins and can lead to problems in waste gas purification systems, e.g. glow fires in electrostatic precipitators. Because of this mill scale needs to be pretreated before it can be re-used. Fine sludge mainly consists of very small-scale particles (0.1 mm). Since the fine particles adsorb oil to a very high degree (5–20%) this scale cannot normally be returned to the sinter strand without pretreatment [3, 6]. The oil adsorption in the preceding line refers to the metallic mill scale and should not be confused with the oil absorption, pigment property, mentioned in the abstract and elsewhere in this paper. At MITTAL STEEL (former ISCOR), a steel manufacturing company in the Republic of South Africa, the bulk of mill scale waste is dumped in landfills. The continuous demand for more landfills and the leaching of some small percentages of heavy metals into soil and ground water, thus threatening the environment, highlights the need for more effective methods of waste disposal and productive utilization of mill scale.

References

1. A. Lopez-Delgado, C. Peña, V. López and F. A. López, Resources, Conserv and Recycl 2003;40:39-51.
2. A. López -Delgado, J. L. Martin de Vidales, E. Vila and F. A. López, J Alloys Comp 1998;281:312-317.
3. F. A. López, M. I. Martin, C. Pérez, A. López-Delgado and F. J. Aguacil, Water Res 2003;37:3883-3890.
4. International Iron and Steel Institute. The Management of steel industry by-products and waste. Brussels Committee on Environmental Affairs 1987.
5. International Iron and Steel Institute. The Management of plant ferruginous by-products. Brussels Committee on Environmental Affairs and committee on Technology, 1994.
6. Reference Document on Best Available Techniques in the Ferrous Metals Processing Industries, IPPC Directive European Commission. Institute for Prospective Technological Studies Seville, Spain: Directorate-General Joint Research Centre, December 2001. "

Chapter 7

Overall conclusion

Characterisation of materials (the core of the current study) is a continually growing and an important component of science in general. It is mainly used to determine the properties (chemical and physical), causes of certain behaviours (e.g. reactivity), design of materials with specific properties, composition (identity and amounts of chemical constituents) of materials, etc. Many different techniques and test methods have been developed to investigate specific aspects of materials. Therefore, the capabilities, relevance, strengths and weaknesses in various techniques have to be considered carefully before deciding on the techniques for analysis. This chapter presents the systematic way followed in selecting the primary technique applied to samples in the current study by outlining four major types of instrumental analysis, namely, elemental analysis, phase analysis, surface characterization and non-destructive testing. For each type of instrumental analysis some related, common and useful techniques are discussed in terms of their advantages and disadvantages (i.e. applicability to the samples studied). The last section outlines the major conclusions drawn from the investigation of the samples in the current study and the future work.

7.1 Elemental analysis

The first step in the characterisation of materials is elemental analysis. There are techniques that give information on elemental composition of samples such as X-ray fluorescence spectroscopy (XRF), particle induced X-ray emission (PIXE), inductively coupled plasma (ICP), neutron activation analysis (NAA), atomic absorption (AA), X-ray photoelectron spectroscopy (XPS), etc. The techniques discussed in this section are X-ray fluorescence spectroscopy (XRF), particle induced X-ray emission (PIXE), inductively coupled plasma (ICP) and neutron activation analysis (NAA).

7.1.1. X-ray fluorescence spectroscopy (XRF)

X-ray fluorescence is the process of emission of X-rays. A sample is normally irradiated with X-rays, which are either absorbed by atoms or scattered in the material. During absorption the energy is absorbed to the innermost electron. However, if the energy is high enough electrons are knocked off from the inner energy levels/shells. The relaxation of the atoms to their stable conditions is accompanied by the return of electrons from the outer shells to the inner shells giving off characteristic X-rays in the process. Since each element has a unique set of shells, each element produces X-rays at a unique set of energy. XRF measures the elemental composition of a sample [1]. The XRF analysis method is in itself non-destructive, but sample preparation is required. Large sample sizes (> 2 g) are required. The advantages of XRF include rapid analysis, spectral coverage of most elements, good precision and accuracy [2]. Energy dispersive XRF has been used mainly for assessment of surface heavy metal contamination [3, 4].

7.1.2. Particle induced X-ray emission (PIXE)

In PIXE, the sample is irradiated with a beam of α-particles (or protons). One electron of an atom-core orbital is ejected on impact. As the electrons reorganises themselves to fill the vacancies created by the ejection, X-rays of characteristic energy are emitted [5]. For instance, if an electron is ejected from the K shell, the K–emission spectrum can contain several bands (due to the dropping of electrons from other different higher energy levels to fill the K shell vacancies), which are denoted with Greek letters. The energy of these X-rays, which is proportional to the amount of energy separating the two orbitals, is characteristic of the emitting element [1]. PIXE's sensitivity is highest for Fe and neighbouring elements with similar Z number (~ 20). For heavy elements, e.g. selenium (Se) or cadmium (Cd), PIXE analysis is not so convenient. The analysis of elements with atomic number lower than 15 can be done best with particle induced gamma-ray emission (PIGE) method [6].

7.1.3. Laser induced breakdown spectroscopy (LIBS)

LIBS measurements consists of spectral and time resolved analysis of the atomic and ionic emission lines generated at the surface of a sample after focusing with an intense nanosecond laser pulse [7]. It gives the emission lines, which are spectral signatures of each element [8]. The relative intensities can be used for the quantitative determination. No sample pretreatment is required. LIBS gives rapid qualitative and possibly *in situ* analysis [9]. LIBS has, however, not yet overcome the experimentation stage to become a routine methodology because of different experimental configurations reported in the literature. Under optimal experimental conditions LIBS is minimally destructive resulting in the formation of a small crater with typical diameters around 40 μm and depth of no more than 10 μm [9, 10]. The spatial resolution of LIBS is superior to that of XRF [10]. The fact that a single laser pulse measurement is complete in less than a second, offers an unparalleled speed to the technique.

Various researchers have applied LIBS to the investigation of artworks and archaeological objects. LIBS has been used to study, qualitatively and quantitatively, the decorative films applied to artworks, such as glazed pottery [11], painted plaster [12], archaeological ceramics and metal artifacts [13], pigments artworks such as in easel and oil paintings [10, 14, 15] and in ancient manuscripts [10]. The application of LIBS provides rapid, *in situ*, depth profile and practically non-destructive determination of pigments in painted artworks [15]. The results obtained using LIBS have been used, among other things, to elucidate manufacturing processes of artwork, its actual degree of conservation and presence of residual surface decorations [11].

7.1.4. Inductively coupled plasma (ICP)

Atmospheric pressure inductively coupled plasmas are flame-like electrical discharges used for speciation, elemental and isotopic ratio analysis [16]. Argon ICPs are remarkable vaporisation-atomisation-excitation-ionisation sources for atomic emission and mass spectrometry. In ICP, plasma is used to excite elemental electrons, which produce photons

(in the form of energy spectrum) unique to that element. ICP is a multi-element method that is suitable for the determination of many elements under the same or different working conditions. There are two common types, which are inductively coupled plasma optical emission spectroscopy (ICP-OES) and inductively coupled plasma mass spectroscopy (ICP-MS). They are both used for bulk elemental analysis of any material or substance, with the exception of H, O, N, F, Cl and Br. It detects elemental concentrations in the range of parts/million or trillion with the aid of a calibration curve [17, 18]. ICP-OES requires dissolution procedures, are time consuming and can induce loss of some volatile elements (e.g. As, Pb, Se, Sb and Zn) [19].

7.1.5. Neutron activation analysis (NAA)

NAA was traditionally applied to cosmochemical and geochemical problems [20]. The detectors may either be high-resolution Ge(Li) γ-rays (high energy photon) detectors for trace elements [21, 22] or low energy photon detectors (LEPD) [23]. NAA is a multi-element method for analysis of a wide variety of silicate rocks [21]. The detection limit is 0.1 – 100 ppm [21], with moderate accuracy and precision for a number of trace elements [22]. Sample preparation (grinding, mixing with polyethylene wax or graphite and pelletisation) is required [23]. The use of NAA is relatively costly and time consuming [19].

Elemental characterisation is a method of choice for materials obtained from metallurgical processes, because these processes often involve the formation of metallic objects from a single or few specific elements. For instance, techniques such as ICP-MS and ICP-OES have been used to characterise bullet lead alloys [24, 25]. The results of which helped to determine the purity and origins of the samples concerned [26]. Other techniques such as PIXE are often applied to objects made from various precious metals to determine the composition, homogeneity in depth and at the surface [27]. Such studies often reveal, for instance, the original goldsmith techniques, which include the gilding process of ornaments and artifacts.

In the case of more complex materials, such as cement and clay based objects (see sections 1.2 and 2.1), their physical properties, e.g. wettability, particle size, etc., influence material properties. Wettability can be defined as a process in which a liquid covers part or the whole surface of a solid phase. Wettability of cement depends on the free surface energy of adsorption of a methyl group, ΔG_{CH2} (commonly denoted as γ_s^d, dispersive component of the surface energy at solid-vapour interface), and water to cement (W/C) ratio [28 - 30]. The higher the W/C ratio, the more pronounced is the initial decrease of γ_s^d. The higher the W/C, the higher the interacting sites at the surface [29]. The technique used to measure γ_s^d is contact angle measurement [29, 30]. The contact angle is greater than zero when the liquid covers only a part of the solid phase and equals zero when the whole surface of a solid phase is covered [31]. The contact angle measurement technique measures the angle formed between the liquid drop interface and the solid surface at the point of three-phase contact (the contact point) [32].

The particle size of the constituent components of the cement influences the properties such as strength and setting times, etc [33]. One of the common techniques used to measure the particle size is photon correlation spectroscopy also referred to as dynamic light scattering (DLS). It involves the measurement of Brownian motion and relates this to the particle size, through a mathematical equation [34]. The important basis for the Brownian motion is that small particles move quicker and larger ones move more slowly.

In other cases, such as the design of materials with specific properties, additional information is needed to characterise such materials. The knowledge of elemental composition is not sufficient in the evaluation of characteristics such as colour, hardness, durability and reactivity. For instance, the colour of the pigment is determined by specific compounds, particle size, dispersing media, etc. [35a]. The durability of the material may be defined as the resistance to the environment in which the material will be exposed [35b]. This property can only be evaluated from the results of specific tests carried out, e.g. weathering tests, lightfastness tests, curing in water and heat treatment, in terms of

pigments and cement or concrete [35b, 36]. Hardness is another property of the material mainly evaluated by specific standard tests, such as Barcol Hardness [37].

The reactivity of a material can also be described in terms of chemical stability. Materials such as pigments are usually tested for chemical stability during which the pigment is exposed (for a set time) to chemical environment in which it will be used and the effects are then evaluated [35b]. The reactivity of other materials such as cement and fly ash is evaluated by exposing the material to the environment of application, e.g. water vapour and carbon dioxide in air, and then determining the heat of hydration (related to the amount of water taken up) and the content of calcium hydroxide (related to the measure of carbon dioxide that reacted with lime, CaO, an important component in the such samples) [38].

The elemental information plays a very limited part in the characterisation of materials. It is sufficient in the determination of purity of objects made from pure metals or even alloys. However, its application to the evaluation of physical, some chemical and unique properties does not yield useful results, even though, in some cases, the elements present may indirectly influence the desired properties.

7.2. Chemical phase analysis

At an advanced level of material characterisation it is important to determine in what form (chemical phases) various elements occur in a sample of interest. The techniques available for phase analysis are X-ray diffraction (XRD), Raman spectroscopy, extended X-ray absorption fine structure (EXAFS), etc. The techniques discussed in this section are XRD and Raman spectroscopy.

7.2.1 X-ray diffration (XRD)

XRD is a qualitative and quantitative analytical technique for analysis of various crystalline compounds present in solid and powder materials [39]. This technique uses the phenomenon of X-ray diffraction by the sample crystal to reveal the details of the structure at

the atomic level. The identity of the sample is determined by comparing its diffraction pattern to that of a known compound in the database. The shapes of the peaks give an indication of the degree of crystallinity [40]. Highly crystalline materials give narrow peaks, while poorly crystalline materials and very small crystals give broad XRD peaks and are thus difficult to identify. The sample size has to be above 2 g and be in powder or crystal form. The XRD spectrum of the crystalline silicon oxide (quartz, α-SiO_2) normally shows a very narrow intense characteristic peak around 2θ value of 27^o (Si(111) peak) [41]. Due to high crystallinity and corresponding isolated narrow and intense XRD peak of quartz, this substance is often used as an internal standard for XRD quantitative analysis. The relative content is determined from the peak intensities.

7.2.2. Raman spectroscopy

The basic principles and theory of Raman spectroscopy are given in chapter 3. This technique was instrumental in characterisation of iron oxide polymorphs, some of which have the same chemical formulas but different structures, because of its sensitivity to chemical phases based on structural variations. Details are provided in section 2.3 and chapter 6. Liem et al. [42] also showed that Raman spectroscopy can distinguish between various phases of silicon oxide with same chemical formulas but different structure [42].

7.3. Surface characterisation

The next step to follow (after phase determination) in the characterisation of materials is to measure the texture of the sample to determine properties such as the particle size, faults, domain structure, etc. Applicable techniques include light microscopy, scanning electron microscopy (SEM), atomic force microscopy (AFM), etc. The particle size is important in some materials because it often influences the properties of the materials [43]. For instance, particles in the nano scale size range can cross the fenestration in the epithelial lining (in e.g. liver) and are generally taken up efficiently by the cells [44]. Therefore, nanoparticles can be used for drug delivery systems [45].

Faults in materials may include damage such as cracks, pores, etc. The presence of cracks on materials may be the source of material failure or influence the performance thereof. The introduction of faults in construction materials (e.g. concrete, matrix composites) may be beneficial and sufficient to fully relax the energy (tension) [46].

Domain structures results when a material undergoes phase separation, in a length of few tens of nanometers, due to the intrinsic incompatibility between two different segments (e.g. hard and soft) [47]. The presence of domain structures is a primary source of hysteresis and cycling softening [48].

7.3.1. Light microscopy

Light microscopy normally uses a polarising optical microscope with reflected and transmitted light together with a mercury lamp and filters. Therefore, the objects as small as a few micrometers can be observed while sample degradation is rare. However, sample preparation is required [49, 50].

7.3.2. Scanning electron microscopy (SEM)

SEM is an optical technique that uses high-energy electrons to bombard the surface of a specimen. When the electrons collide with the atoms of the specimen they dislodge electrons from these atoms as radiated secondary electron. The secondary electrons are collected at the detector, usually a phosphorescent screen, where a secondary electron image of the atoms of the specimen is formed [51]. The main results of SEM are particle size (and in some instruments size distribution) and morphology (texture and shape) [52]. The sample has to be in solid form and only a few milligrams are required. Sample preparation involves coating with a thin layer of carbon or gold to create a conducting surface for samples, because most surfaces often accumulate electrons/charge during the electron bombardment. The recovery of the sample in its original form is not possible after analysis. Both amorphous and crystalline samples can be analysed using SEM.

7.3.3. Atomic force microscopy (AFM)

AFM is also an optical technique. It measures surface properties through an interaction between the probe (a commercial micro-fabricated tip) and the surfaces, while moving across the sample recording the x, y and z coordinates [53]. The probe is a tip on the end of cantilever, which bends in response to the force between the tip and the sample. The instrument can operate in a contact mode (where the probe is in contact with sample analysed) or in a non-contact mode (where the probe does not touch the sample surface) [53]. AFM does not require sample preparation and can be operated in air or liquids [54]. It also gives information on particle size, morphology and 3-dimensional images [53, 55]. It has higher spatial resolution than that of SEM [56, 57].

7.4. Non-destructive testing

This is the type of analysis during which the physical and chemical integrity of the sample cannot be altered. Therefore, no sample preparation or modification whatsoever, is allowed. Examples of samples that require non-destructive testing are valuable objects, manufactured articles (e.g. silicon chips), objects of art, archaeological and other unique samples.

The main reasons for non-destructive testing may be the need for preservation, reconstruction, authentication, study of properties and technologies as well as *in situ* analysis (e.g. of blood, skin and brain in medical applications). The samples currently under study are clay-based archaeological objects and related iron oxide pigments. Therefore, information on chemical phases needs to be obtained non-destructively.

The elemental results will be useful to some limited extent and more information will still be required if the forms of the constituent components are to be ascertained. The only elemental techniques that are non-destructive are laser-based, such as PIXE. However, not

all elements can be detected by PIXE. LIBS is another technique which, in most applications may be viewed as non-destructive, but it is technically not non-destructive.

The surface characterisation properties that were important in the current study relate to the particle size and shape. These properties influence mainly the colour of the objects and pigments themselves. However, all surface techniques mentioned above require sample preparation and therefore were not suitable for non-destructive analysis of archaeological samples. SEM was applied only to the synthesised iron oxides for particle size and shape determination.

Techniques that give information on phases non-destructively are essential in the current study, as explained above. XRD is one of the most robust techniques in the determination of chemical phases but it is destructive and cannot detect amorphous phases and small crystallites. Therefore, Raman spectroscopy may be the alternative because it detects amorphous and crystalline phases non-destructively, has *in situ* capabilities, show high sensitivity and specificity (see section 1.2.3). Therefore, Raman spectroscopy with the use of known or literature assignments has been selected and successfully applied to the characterisation of components in earthenware archaeological objects and pigments obtained from iron waste materials.

7.5. Application of Raman spectroscopy

7.5.1. Earthenware archaeological objects

The determination of chemical components in earthenware archaeological objects of Chinese and South African origin confirmed the effectiveness of Raman spectroscopy in the analysis of these objects. Some chemical components identified were crystalline aluminosilicates, non-crystalline aluminosilicates, inorganic minerals and pigments. Crystalline clay minerals identified in South African objects were kaolins, illite and montmorillonite, and appeared to have been mixed, either intentionally or unintentionally. The Chinese clay objects contained mainly kaolins. The non-crystalline aluminisilicates

identified in samples from the two origins were mullite, anhydrite, feldspar and calcium silicates ($CaSiO_3$). Other inorganic compounds, namely, quartz, rutile, gypsum, phosphates and calcium carbonate, were also detected by Raman spectroscopy. Some pigments such as hematitie (red-brown in colour) and amorphous carbon (gray and black in colour) were also identified in both Chinese and South African objects.

The processing conditions were deduced from the above chemical components identified in respective samples. The processing temperatures of Lydenburg, Graskop and Rooiwal were below 800 ^oC and those for Makahane reached some temperatures between 800 ^oC and 1100 ^oC. The corresponding processing temperatures for the Chinese samples were above 800 ^oC. The chemical components identified further suggested that the objects were most likely fired in an open fire. All the samples appear to have been processed under oxidative atmosphere.

Clay objects from different origins have been distinguished. It has been shown that Raman spectroscopic results can be used to deduce the raw materials and processing conditions used in the production of earthenware objects. The pigments that lend colour to the objects have also been identified. The use of Raman spectroscopy further showed that earthenware objects from different origins have different chemical components. The chemical components obtained also revealed differences and similarities between processing conditions used by corresponding potters in making the objects. It has also been found that different potters in the same vicinity tended to use similar raw materials (either obtained from the same source or mixed in a similar fashion) and processing conditions, as indicated by the overlapping chemical components from different origins. The results further revealed that the most likely firing mode was an open fire.

7.5.2. Iron oxide pigments

The present study proved that chemical substances (containing mainly sulphates of Fe^{2+} and Fe^{3+}) derived from mill scale iron waste can be used as the raw materials for the

preparation of good quality magnetite and goethite. Magnetite and goethite were in turn thermally converted to maghemite and hematite, respectively.

The characterisation of the products was successfully carried out using Raman spectroscopy, the results of which were confirmed by XRD, FT-IR and in some cases XRF spectroscopy. Raman spectroscopy revealed reduced crystallinity made apparent by shifting or broadening of characteristic bands. This was also observed in the XRD results. The results obtained further revealed that the methods applied in preparing various iron oxides were generally specific and gave only the intended product, except in the case of goethite synthesis. The goethite product was contaminated with some traces of the hematite polymorph detectable only by Raman spectroscopy. In general the products were of high purity, as indicated by very low levels of contamination in cases where it was detected.

In the end the complete chemical characterisation of earthenware archaeological objects should entail the qualitative analysis of aluminosilicates (crystalline or non-crystalline), other inorganic compounds and pigments, all of which are the main components (either added as raw materials or evolved during processing). The techniques applied for this purpose should show capabilities of rapid measurement, high sensitivity, specificity, non-destructive analysis, free of sample preparation, *in situ* analysis, detection of crystalline and amorphous phases and give unambiguous results.

The present study has met the above requirements. The study has succeeded in identifying a number of aluminosilicates (various clay minerals, feldspars and silicates), other inorganic compounds (e.g. titanium dioxide, calcium carbonate and phosphates) and pigments (various iron oxides and amorphous carbon) the results of which laid a fair basis for chemical characterisation of the samples involved. The investigation of both the Chinese and South African samples and the results thereof confirmed the relevance and appropriateness of Raman spectroscopic application to the earthenware archaeological objects in general.

The analysis of iron oxides from iron waste (i.e. mill scale, which normally contains other substances besides iron and its related compounds) in a way presented a practical scenario of the analysis of multi-components of crystalline and non-crystalline compounds in a single sample as is common with earthenware archaeological objects. The results obtained further confirmed the sensitivity, *in situ* capability and specificity of Raman spectroscopy. The mill scale iron oxide results further added credit to the quality of the results obtained for earthenware archaeological objects (particularly for iron oxides identified therein).

Therefore, it can be concluded that the Raman spectroscopy has been found to be the relevant and appropriate technique for the full characterisation of earthenware archaeological objects (and their related iron oxide pigments) of Chinese and South African origin.

7.5.3. Future work

For earthenware archaeological objects the future work will involve the quantitative analysis of chemical components as identified by Raman spectroscopy. The most appropriate tool for such multi-component samples is chemometrics (i.e. multivariate analysis). The determination of the amount of each chemical component will form a sound basis for the reconstruction of these clay objects. The raw materials for the clay objects may be obtained from the quarries (if known) in the vicinity of each collection or prepared from pure components as identified by Raman spectroscopy. The pottery thus formed will provide further evidence and a more accurate level of appropriateness of Raman spectroscopic application to these types of samples. The combination of infrared and Raman spectroscopy in the non-destructive investigation of clay objects in this study could reveal even more valuable information. This can only be achieved by analysing same areas/spots on the sample. The newly emerging focusing accessories that can be simultaneously linked to both infrared and Raman spectroscopy could be very useful.

For iron oxide pigments the future work will involve the determination of the actual pigment properties of magnetite, goethite, hematite and maghemite prepared from mill scale. These

properties include tinting strength, hiding power, oil absorption, colour strength, choice of stabiliser and its compatibility with the pigment. Furthermore the causes of discolourisation of iron oxides (magnetite being the worst affected) with time could be investigated. Such a study will also clarify the mechanism of pigments discolourisation at the same time providing insight into how the process can be slowed down or stopped completely. This investigation would limit the use of stabilisers and subsequently the costs of iron oxide pigments will decrease.

7.6. References

1. R. Jenkins, Anal. Chem. Part A **56**, 1099 (1984).
2 X. Hou and B. T. Jones, Microchem. J. **66**, 155 (2000).
3. G. A. Rano, R. E. Enwall, W. H. Cole, C. A. Kuharic and G. S. Duggan, Environ. Sci. Res. **42**, 155 (1991).
4. P. J. Potts, P. C. Webb, O. Williamsons-Thorpe and R. Kilworth, Analyst **12**, 1253 (1995).
5. M. Bertrand, G. Weber and B. Schoeffs, Trends Anal. Chem. **22**, 254 (2003).
6. A. K. Kiss et al J. Radioanal. Nucl. Chem. **89**, 123 (1985).
7. V. Lazic, R. Barbini, F. Colao, R. Fantoni, A. Palucci, Spectrochim. Acta Part B **56**, 807 (2001).
8. D. A. Rusak, B. C. Castle, B. W. Smith and J. D. Wineforder, Crit. Rev. Anal. Chem. **27**, 257 (1992).
9. E. Tognoni, V. Palleschi, M. Corsi and G. Cristoforetti, Spectrochim. Acta Part B **57**, 1115 (2002).
10. D. Anglos Appl. Spectrosc. **55**, 186A (2001).
11. F. Colao, R. Fanti, V. Lazic and V. Spizzichino, Spectrochim. Acta Part B **57**, 1219 (2002).
12. A. Prysbaert, K. Melessanaki and D. Anglos, J. Archaeol. Sci. **33**, 1095 (2006).
13. K. Melessanaki, M. Mteo, S. C. Ferrence, P. P. Betancourt and D. Anglos, Appl. Surf. Sci. **197**, 198 (2002).

14. L. Burgio, R. J. H. Clark, T. Stratoudaki, M. Doulgeldis and D. Anglos, Appl. Spectrosc. **54**, 463 (2000).
15. D. Aglos, S. Curtis and C. Fotakis, Appl. Spectrosc. **51**, 1025 (1997).
16. H. Watenabe, M. Aihara and M. Kiboku, Bunseki Kagaku **39**, 61 (1990).
17. M. J. Tominson, L. Lin and J. A. Caruso, Analyst **120**, 583 (1995).
18. C. B'Hymer and J. A. Caruso. J. Chromatogr. Part A **1114**, 1(2004).
19. O. Dogan and M. Kobya, J. Quant. Spectrosc. Radiat. Transfer **101**, 146 (2006).
20. J. Hertogen in P. J. Elving, V. Krivan and I. M. Kolthoff (eds), Treatise on analytical chemistry, Vol. 14, 2nd edns., Wiley, New York p. 713 (1986).
21. G. E. Gordon. K. Randle, G. G. Goles, J. B. Corliss, M. H. Buson and S. S. Oxley, Geochim. Cosmochim. Acta **32**, 369 (1968).
22. J. Hertogen and R. Gijbels, Anal. Chim. Acta **56**, 61 (1971).
23. R. Gijbels , Inorg. Chim. Acta **140**, 295 (1987).
24. R. O. Keto, J. Forensic Sci. **44**, 1020 (1999).
25. E. Randich, W. Dverfeldt, W. McLendon and W. Tobin, Forensic Sci. Int. **127**, 174 (2002).
26. J. L. Ruvalcaba-Sil and G. Demortier, Instr. Methods Phys. Res. Section B **113**, 275 (1996).
27. J. L. Ruvalcaba-Sil and G. Demortier, Instr. Methods Phys. Res. Section B **130**, 297 (1997).
28. A. W. Momber, J. Adhesion 78, **203** (2002).
29. K. Benzarti, C. Perruchot and M. M. Chehimi, Colloid Surface Part A **286**, 78 (2006).
30. J. Lawrence, Mater. Sci. Eng. Part A **356**, 162 (2003).
31. A. Gijbels, Int. J. Heat Mass Transfer **48**, 4829 (2005).
32. T. D. Blake, J. Colloid and Interf. Sci. **299**, 1 (2006).
33. C. Liu, H. Shau, F. Chen and H. Zheng, Biomaterials **27**, 5003 (2006).
34. K. Kita-Tokarczyk, J. Grumelard, T. Haefele and W. Meier, Polymer **46**, 3540 (2005).
35. J. A. Kroschwitz and M. Howegrant, *Pigments to powders handling.* In: Encyclopedia of chemical technology, 4th ed, John Wiley & sons, New York, Vol. 19, a: p. 26, b: p. 8 (1996).
36. F. P. Togal and J. P. Castro-Gomes, Constr. Build. Mater. **20**, 1079 (2006).

37. A. C. Berg, L. C. Bank, M. G. Oliva and J. S. Russell, Constr. and Build. Mater. **20**, 515 (2006).
38. M. R. Jones, A. McCarthy and A. P. P. G. Booth, Fuel **185**, 2250 (2006).
39. K. Norrish and R. M. Taylor, Clay Miner. **5**, 98 (1962).
40. C. P. Nicolaides, N. P. Sincadu and M. S. Scurrell, Catal. Today **71**, 429 (2002).
41. V. Kapaklis, C. Politts, P. Poulopoulos and P. Schweiss, Mater. Sci. Eng. **124 – 125**, 475 (2005).
42. N. Q. Liem, G. Sagon, V. X. Quang, H. Van Tan and P. Colomban, J. Raman Spectrosc. **31**, 933 (2000).
43. W. H, Hunter, Jr. JOM 13 – 18 (2004).
44. K. Bugunia-kubik and M. Sugisaka, BioSystems **65**, 123 (2002).
45. K. Dillen and W. Weyenberg, J. Vandervoort and A. Ludwig, Pharm. Biopharm **58**, 539 (2004).
46. A. Pandolfi, S. Conti and M. Ortiz, J. Mech. Phys. Solids **33**, 1505 (2006).
47. H. J. Qi and M. C. Boyce, Mech. Mater. **37**, 817 (2005).
48. Z. Petrovic and J. Ferguson, Prog. Polym. Sci. **16**, 625 (1991).
49. J. E. Gillot, Can. J. Earth Sci. **1**, 121 (1964).
50. L. Tong and M. Tang, Cer. Concr. Res. **21**, 361 (1991).
51. J. H. Butler, D. C. Joy, G. F. Bradley and S. J. Krause, Polymer **36**, 1781 (1995).
52. H. Shu, W. Yu, Y. Zhao and X. Liu, J. Food Eng. **76**, 664 (2006).
53. R. Pereira, Biochem. Pharm. **62**, 975 (2001).
54. S. Anabousi, M. Laue, C. Lelu, U. Bakowsky and C. Ehrhardt, Eur. J. Pharm. Biopharm. **60**, 295 (2005).
55. M. Oliva, C. Caramella, I. Diez-Perez, P. C. Gorostiza, F. Lastra, I. Oliva and E. L. Marino, Int. J. Pharm. **242**, 291 (2002).
56. L. Mu and S. S. Feng, J. Control. Release **76**, 239 (2001).
57. S.-S. Feng and G. Fluang, J. Control. Release **71**, 53 (2001).

Appendix

This section outlines the status of the core chapters (chapters 4 – 6) in the international peer review journals.

1. Chapter 4: Raman spectroscopic study of ancient South African domestic clay pottery.
Status: Published article - Spectrochimica Acta, Part A
Reference: M. A. Legodi and D. de Waal Spectrochim. Acta Part A **66**, 135 (2007).

2. Chapter 5: Raman analysis of red-brown and gray shards from 16th and 17th century Portuguese shipwrecks.
Status: Published article - Crystal Engineering
Reference: M. A. Legodi and D. de Waal, Cryst. Eng. **6**, 287 (2003).

3. Chapter 6: The preparation of magnetite, goethite, hematite and maghemite of quality from mill scale iron waste.
Status: Published article - Dyes and Pigments
Reference: M. A. Legodi and D. de Waal, Dyes and Pigments **74**, 161 (2007).